MEASUREMENTS BEFORE FATIGUE TESTING

Spec. 1 - page 2

Number of cycles before measurements : 3 cycles

F_{min}(kN)	F_{max}(kN)	R_S	T (°C)	Frequencies (Hz)	Extrapol. Hot Spot Strainrange *
0	84	0		10	2230

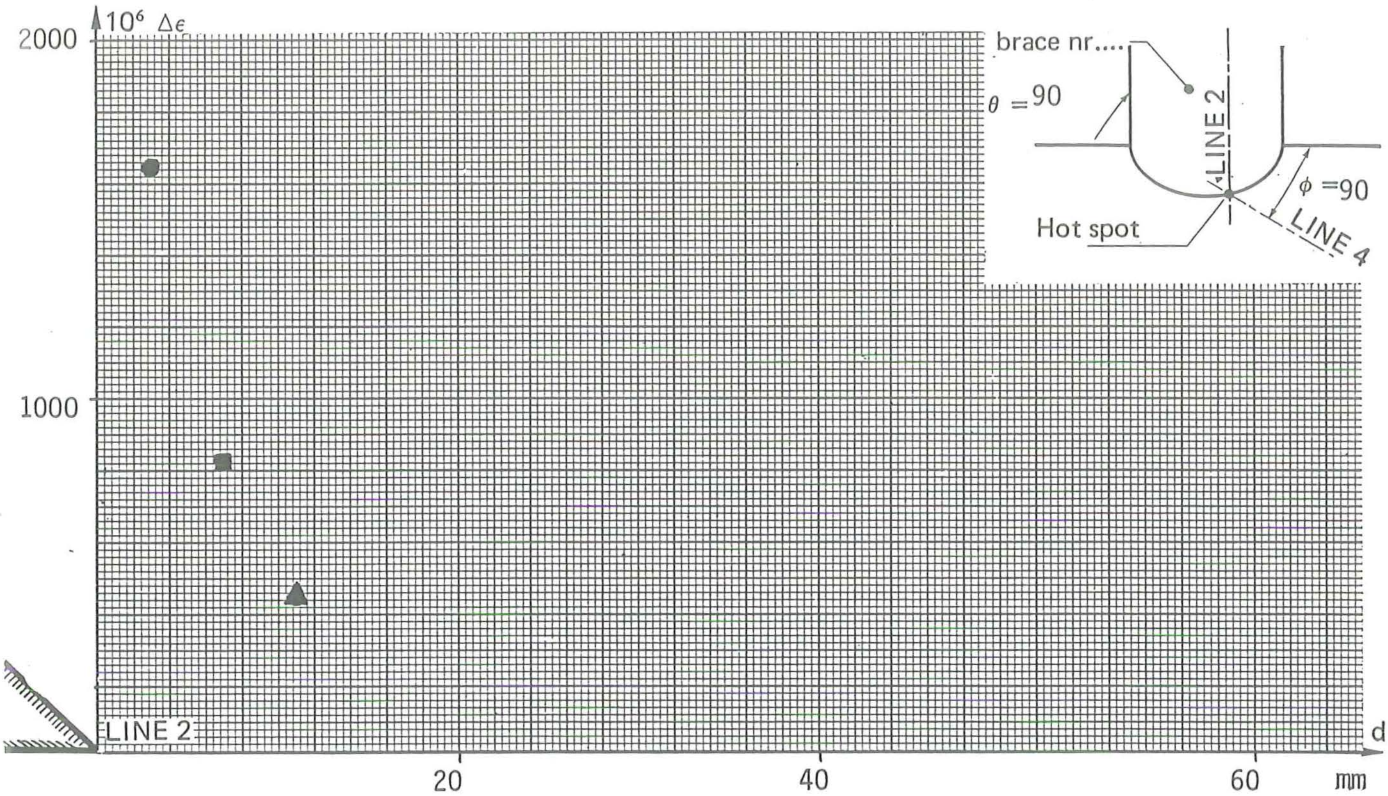

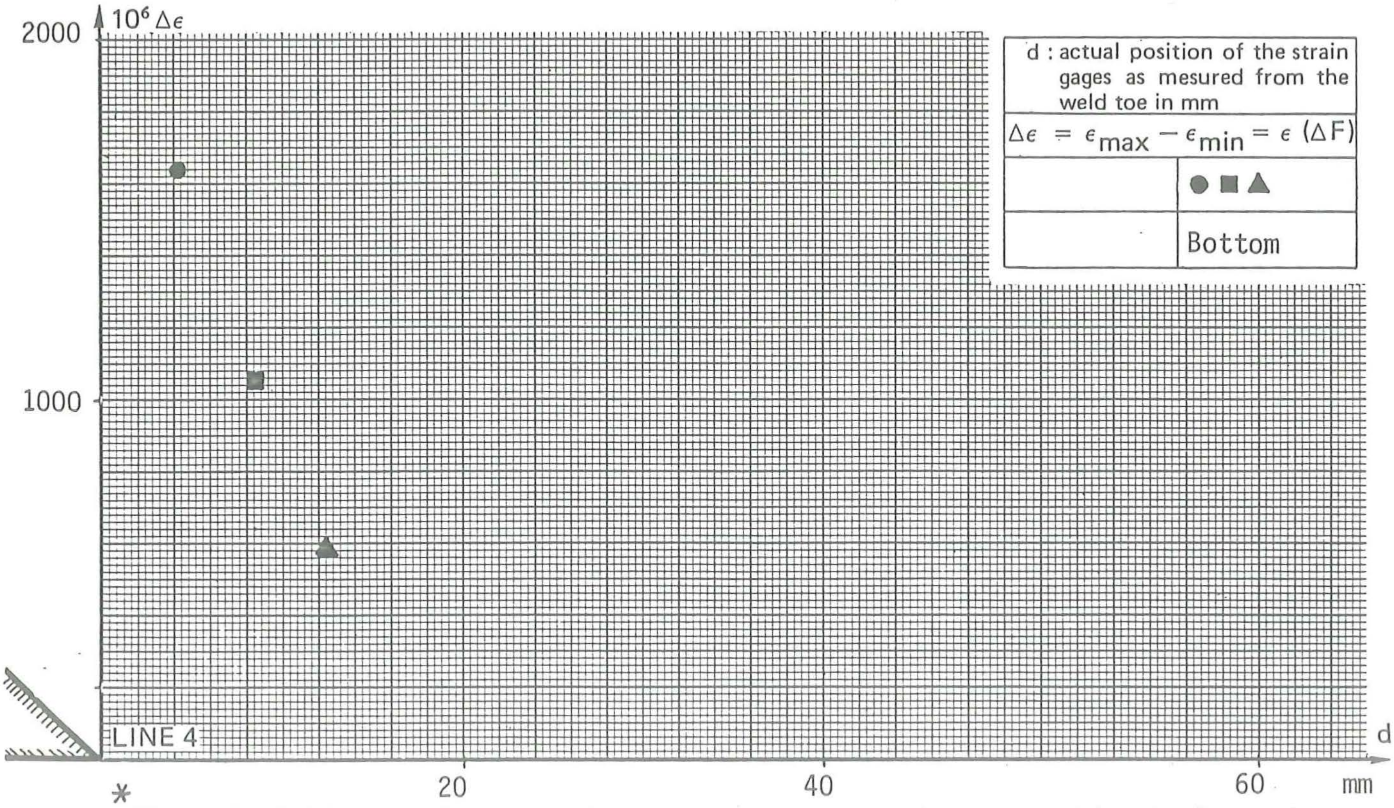

* The calculation has been based on the average SNCF 's of the identical specimens

OFFSHORE TUBULAR JOINT TEST DATA SHEET

ECSC Pg. F7

Type	T - joint
Loading	Axial
Laboratory	TNO - IBBC
Specimen nr.	1

GEOMETRY ~~actual~~ values in mm	outside diameter	wall thickness
	D 168.3	T 6.3
	d_1 88.9	t_1 3.2
	d_2	t_2

SKETCH	geometry, dimensions, loads boundary conditions

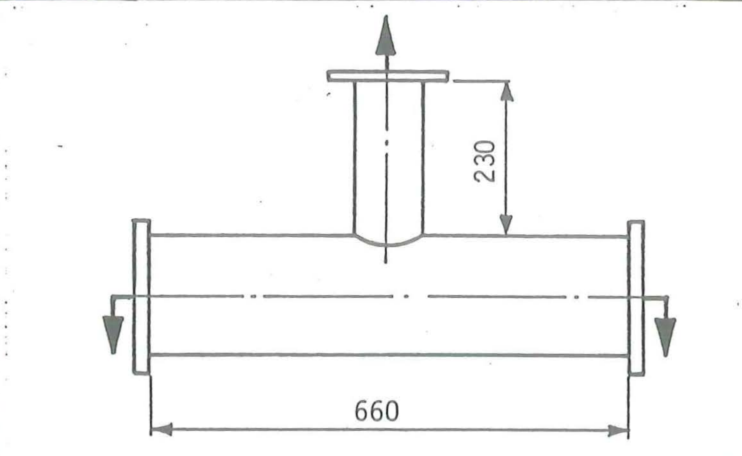

Post weld stress relief H.T. ~~Yes~~ No

ACTUAL PROPERTIES OF CRACKED MEMBER

BASE METAL	Grade : 50 C			STD : BS 4350						
	C %	Si %	Mn %	S %	P %	Al %				
	0.22	0.30	1.25	0.012	0.019					

WELDING	Welding process : MMAW , Current : AC Filler materials : – ~~ISO~~ – AWS – .... : E 7016 Electrode diameter (mm) : 2.5

WELD BEAD GEOMETRY AT THE HOT SPOT applied STD : ASME VIII

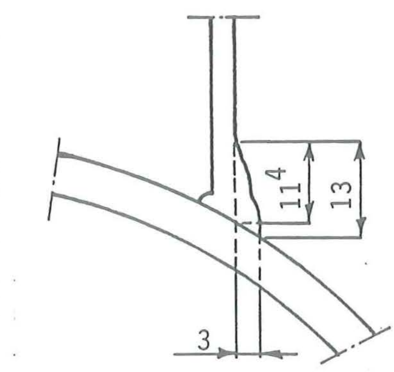

WELDING PROCEDURE	
Position	5G
Nr of runs	2
Energy (kj/m)	
preheat. temp. (° C)	65
postheat. temp. (° C)	none

POST WELDING TREATMENT

~~Heat treatment – tig or plasma dressing~~

~~Shoot peening – grinding~~

WELD METAL DEPOSIT	C %	Si %	Mn %	S %	P %	Ni %					

TENSILE PROPERTIES	Base metal	weld metal
Yield strength σ_y (N/mm²)	426	
Tensile strength σ_u (N/mm²)	563	

Other properties see page 4

Appendix 3-II

Test data sheets

0/24509	T.N.O. I.B.B.C.	TUBEPROGRAM EEG-SMOZ	T.H. STEVINLAB.	TEST. 39-40 (A)

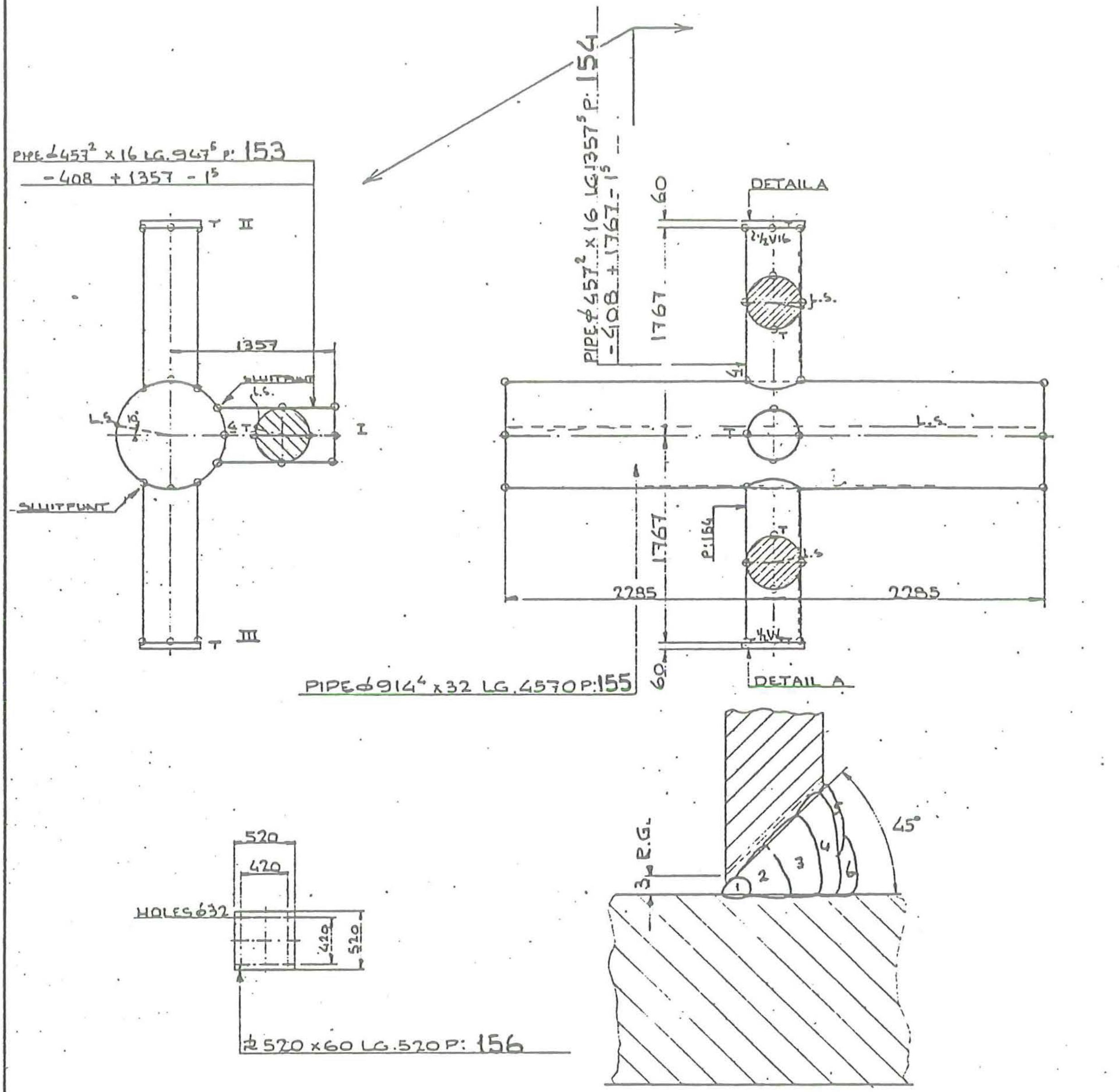

DETAIL "A"

WELDDETAIL

STAMP HEATNR. NEAR L.S. AT THE END OF THE PIPE.

MATERIAL QUALITY: B = 9055 / C = 500395

CONNECTION: PIPE ⌀457² x 16 TO PIPE ⌀914⁴ x 32

METHOD OF WELDING: MANUAL | PREHEAT: 100°C

U.S. RESEARCH ACCORDING TO ASME VIII | POSITION: 5G | WELDERNAME: FRANKEN / LIDO

PASSNUMBER	ELECTRODE		AMP.	TEMP.	I	II	III	SYMBOLS
1	BH 100	2½	85	100°	57	46	44	o : LOCATION ℄ ON PIPE-CIRCUMFERENCE
2	BH 100	3¼	110 - 130	100°	47	52	43	∩ : LOCATION TACKWELD
3	BH 100	4	140 - 160	100°	29	25	24	___ : LOCATION REPAIRWELD
4	BH 100	4	140 - 160	100°	32	29	27	.... : LOCATION ARCSTRIKE OUTSIDE W. SEAM
5	BH 100	3¼	110 - 130	100°	27	27	21	L.S. : LONGITUDINAL SEAM. (10° BESIDE ℄)
6	BH 100	3¼	110 - 130	100°	31	32	28	T. TOP
								B: BRACING C: CHORD

DE GROOT CONSTRUCTIE B.V. - ZWIJNDRECHT

0/24509	T.N.O. I.B.B.C.	TUBEPROGRAM EEG-SMOZ	T.H. STEVINLAB.	TEST 36-38 (A)

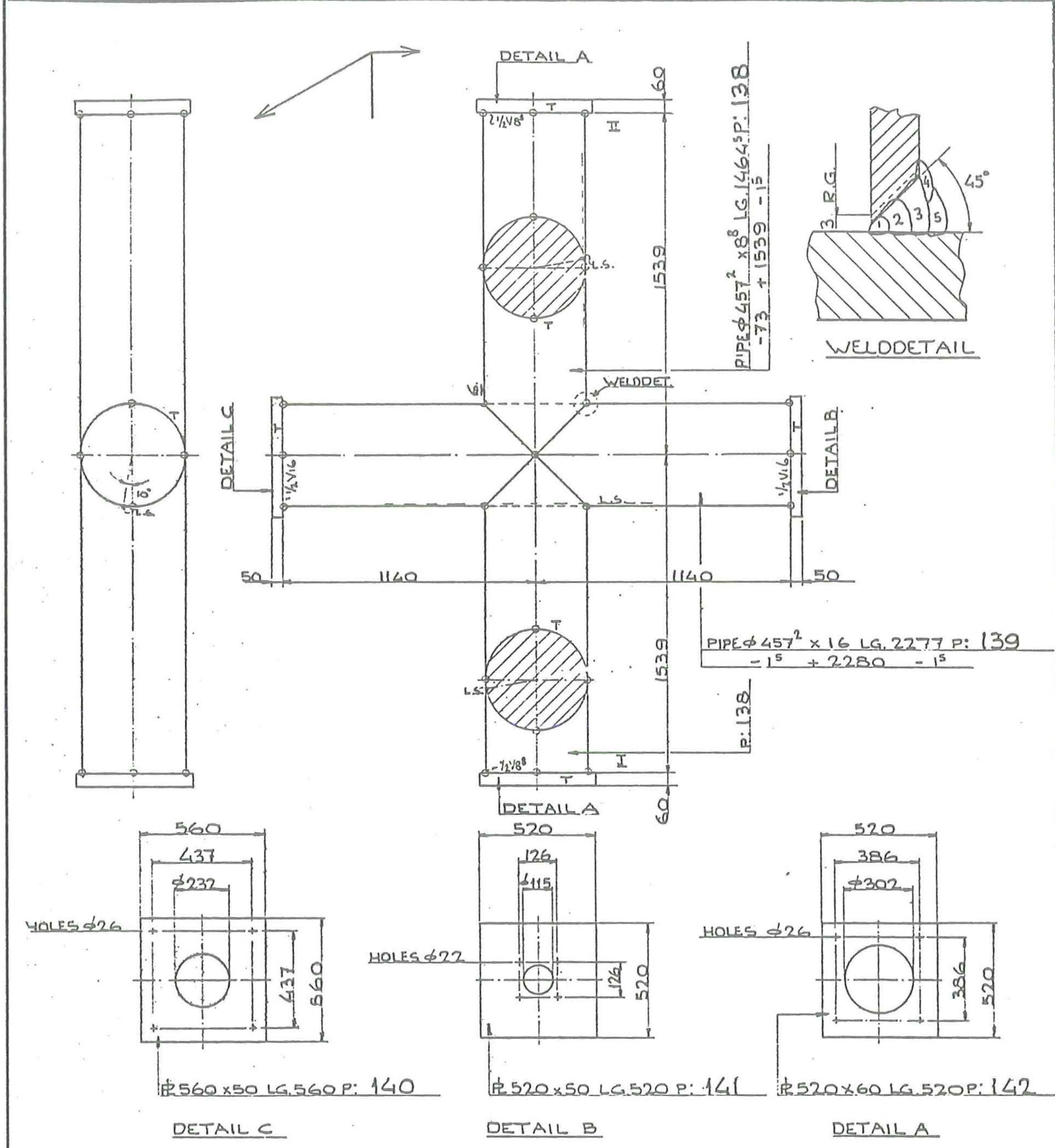

STAMP HEATNR. NEAR L.S. AT THE END OF THE PIPE
MATERIAL QUALITY : B = E291 /C = 9055
CONNECTION: PIPE ⌀ 457² x 8⁸ TO PIPE ⌀ 457² x 16
METHOD OF WELDING: MANUAL | PREHEAT: 65° C
U.S. RESEARCH ACCORDING TO ASME VIII | POSITION: 5G | WELDERNAME: FRANKEN-UDO

PASSNUMBER	ELECTRODE	AMP.	TEMP.	I	II	SYMBOLS
1	BH 100 2½	85	65°	46	52	o : LOCATION ℄ ON PIPE - CIRCUMFERENCE
2	BH 100 3¼	110 - 130	65°	28	27	⌒ : LOCATION TACK WELD
3	BH 100 3¼	110 - 130	65°	36	33	— : LOCATION REPAIRWELD
4	BH 100 3¼	110 - 130	65°	21	23	... : LOCATION ARC STRIKE OUTSIDE W.SEAM
5	BH 100 3¼	110 - 130	65°	38	36	L.S. : LONGITUDINAL SEAM (10° BESIDE ℄)
						T : TOP
						B = BRACING C = CHORD

DE GROOT CONSTRUCTIE B.V. - ZWIJNDRECHT

0/24509	T.N.O. I.B.B.C.	TUBEPROGRAM EEG-SMOZ	T.H. STEVINLAB.	TEST. 34-35 (A)

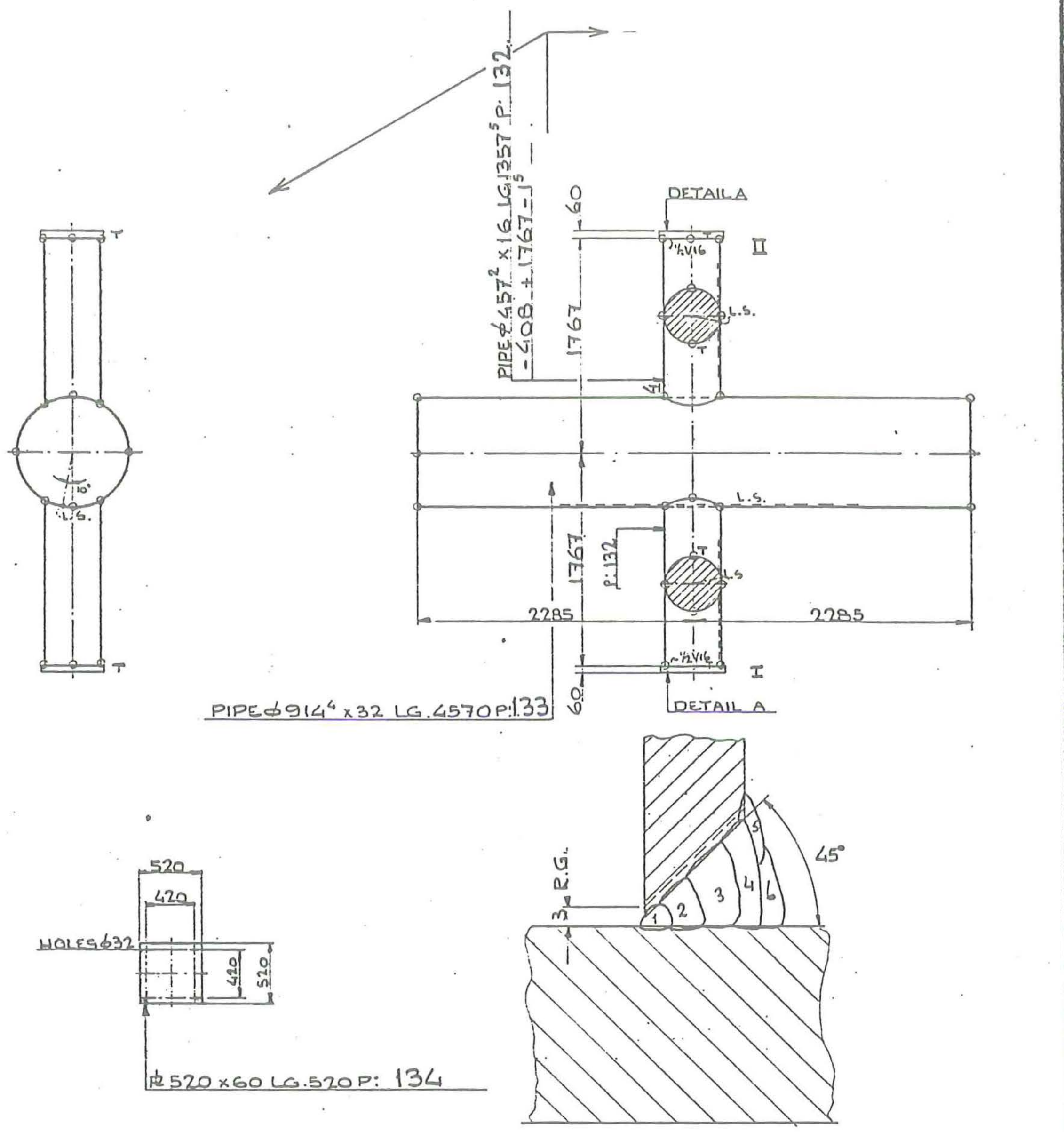

DETAIL "A"

WELDDETAIL

STAMP HEATNR. NEAR L.S. AT THE END OF THE PIPE.	
MATERIAL QUALITY: B = 9055	/C = 500395
CONNECTION: PIPE ⌀457² x16 TO PIPE ⌀914⁴ x32	
METHOD OF WELDING: MANUAL	PREHEAT: 100°C

U.S. RESEARCH ACCORDING TO ASME VIII

PASSNUMBER	ELECTRODE		AMP.	TEMP.	POSITION: 5G I	II	WELDERNAME: FRANKEN - UDO
							SYMBOLS
1	BH100	2½	85	100°	49	43	o : LOCATION ℄ ON PIPE-CIRCUMFERENCE
2	BH100	3¼	110 - 130	100°	39	42	∩ : LOCATION TACKWELD
3	BH100	4	130 - 160	100°	30	29	__ : LOCATION REPAIRWELD
4	BH100	4	130 - 160	100°	30	26	.... : LOCATION ARCSTRIKE OUTSIDE W. SEAM
5	BH100	3¼	110 - 130	100°	29	27	L.S. : LONGITUDINAL SEAM. (10° BESIDE ℄)
6	BH100	3¼	110 - 130	100°	36	32	T. : TOP
							B = BRACING C = CHORD

DE GROOT CONSTRUCTIE B.V. - ZWIJNDRECHT

0/24509	T.N.O. I.B.B.C.	TUBEPROGRAM EEG-SMOZ	T.H. STEVINLAB.	TEST 31_33 (A)

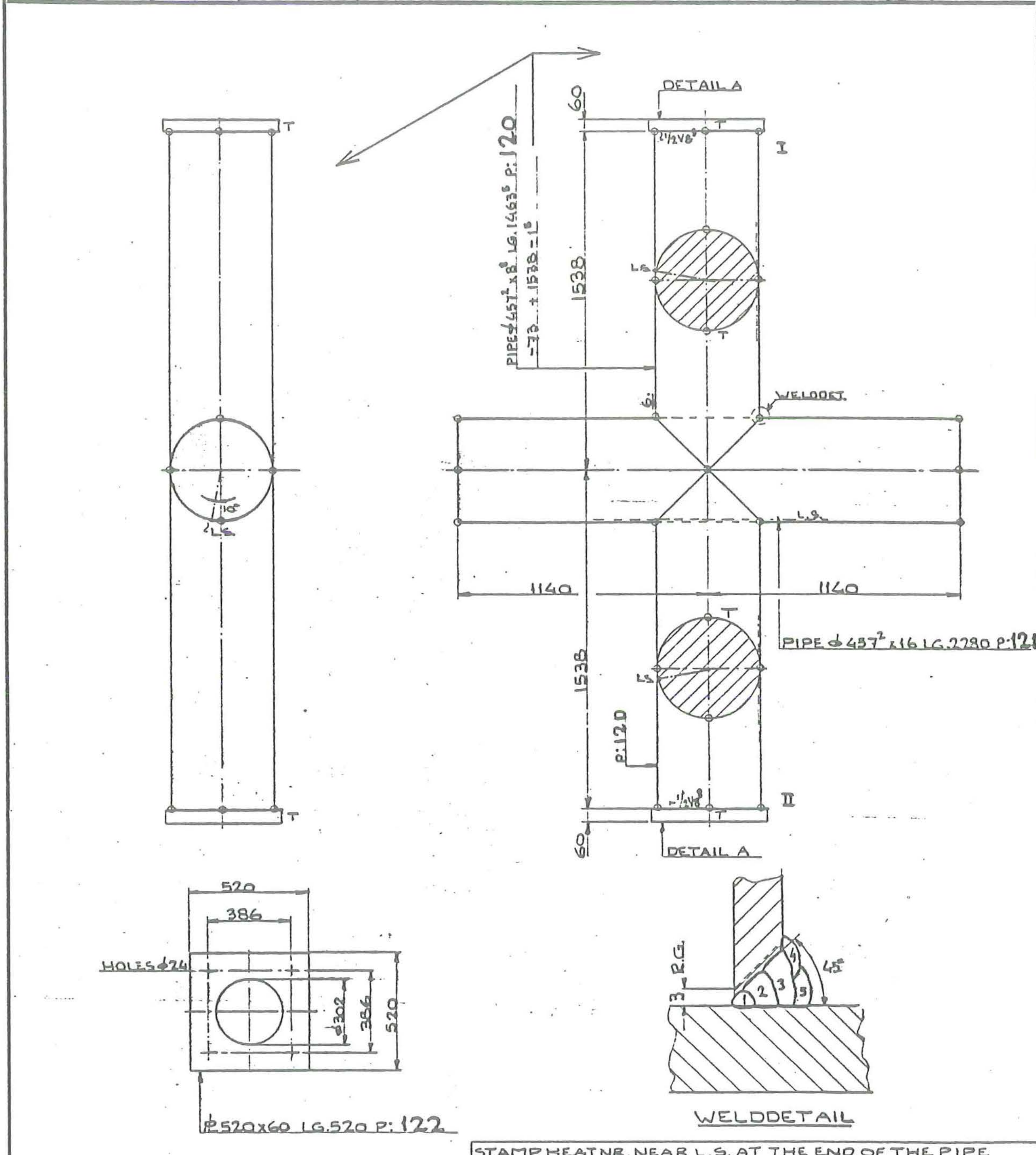

STAMP HEATNR. NEAR L.S. AT THE END OF THE PIPE	
MATERIAL QUALITY: B, E290 /C=9055	
CONNECTION: PIPE ϕ457² x8⁸ TO PIPE ϕ457² x16	
METHOD OF WELDING: MANUAL	PREHEAT: 65°C

U.S. RESEARCH ACCORDING TO ASME VIII				POSITION: 5G		WELDERNAME: FRANKEN-UDO
PASSNUMBER	ELECTRODE		AMP.	TEMP.	I	II	SYMBOLS
1	BH 100	2½	85	65°	43	46	o : LOCATION ℄ ON PIPE-CIRCUMFERENCE
2	BH 100	3¼	110 - 130	65°	29	26	∩ : LOCATION TACKWELD
3	BH 100	3¼	110 - 130	65°	37	35	__ : LOCATION REPAIRWELD
4	BH 100	3¼	110 - 130	65°	26	25	.... : LOCATION ARCSTRIKE OUTSIDE W.SEAM
5	BH 100	3¼	110 - 130	65°	18	19	L.S. : LONGITUDINAL SEAM (10° BESIDE ℄)
							T : TOP
							B = BRACE C = CHORD

DE GROOT CONSTRUCTIE B.V. - ZWIJNDRECHT

0/24509	T.N.O. I.B.B.C.	TUBEPROGRAM EEG-SMOZ	T.H. STEVINLAB.	TEST 27-29 (A)

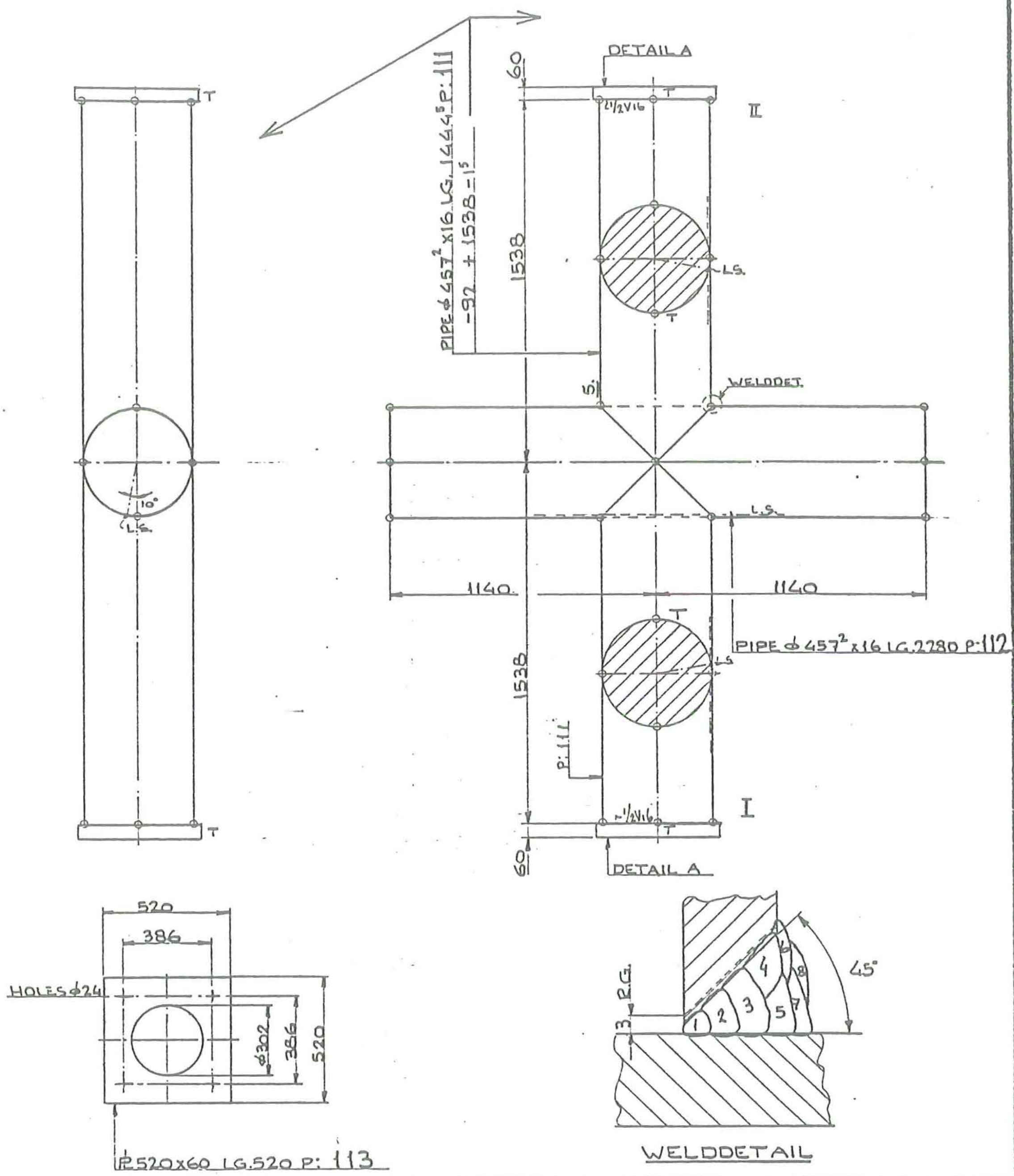

STAMP HEATNR. NEAR L.S. AT THE END OF THE PIPE	
MATERIAL QUALITY : B = 9055 /C = 9055	
CONNECTION: PIPE ϕ 457² x16 TO PIPE ϕ 457² x16	
METHOD OF WELDING: MANUAL	PREHEAT: 65°C

U.S. RESEARCH ACCORDING TO ASME VIII				POSITION: 5G		WELDERNAME: FRANKEN / UDO
PASSNUMBER	ELECTRODE	AMP.	TEMP.	I	II	SYMBOLS
1	BH100 2½	85	65°	51	63	o : LOCATION ℄ ON PIPE - CIRCUMFERENCE
2	BH100 3¼	110 - 130	65°	37	40	∩ : LOCATION TACKWELD
3	BH100 3¼	110 - 130	65°	34	39	__ : LOCATION REPAIRWELD
4	BH100 4	140 - 160	65°	28	31	.... : LOCATION ARCSTRIKE OUTSIDE W. SEAM
5	BH100 4	140 - 160	65°	31	34	L.S.: LONGITUDINAL SEAM (10° BESIDE ℄)
6	BH100 3¼	110 - 130	65°	23	26	T. : TOP
7	BH100 3¼	110 - 130	65°	35	37	B = BRACING C = CHORD
8	BH100 3¼	110 - 130	65°	22	21	

DE GROOT CONSTRUCTIE B.V. - ZWIJNDRECHT

0/24509	T.N.O. I.B.B.C.	TUBEPROGRAM EEG-SMOZ	T.H. STEVINLAB	TEST 24.26 (A)

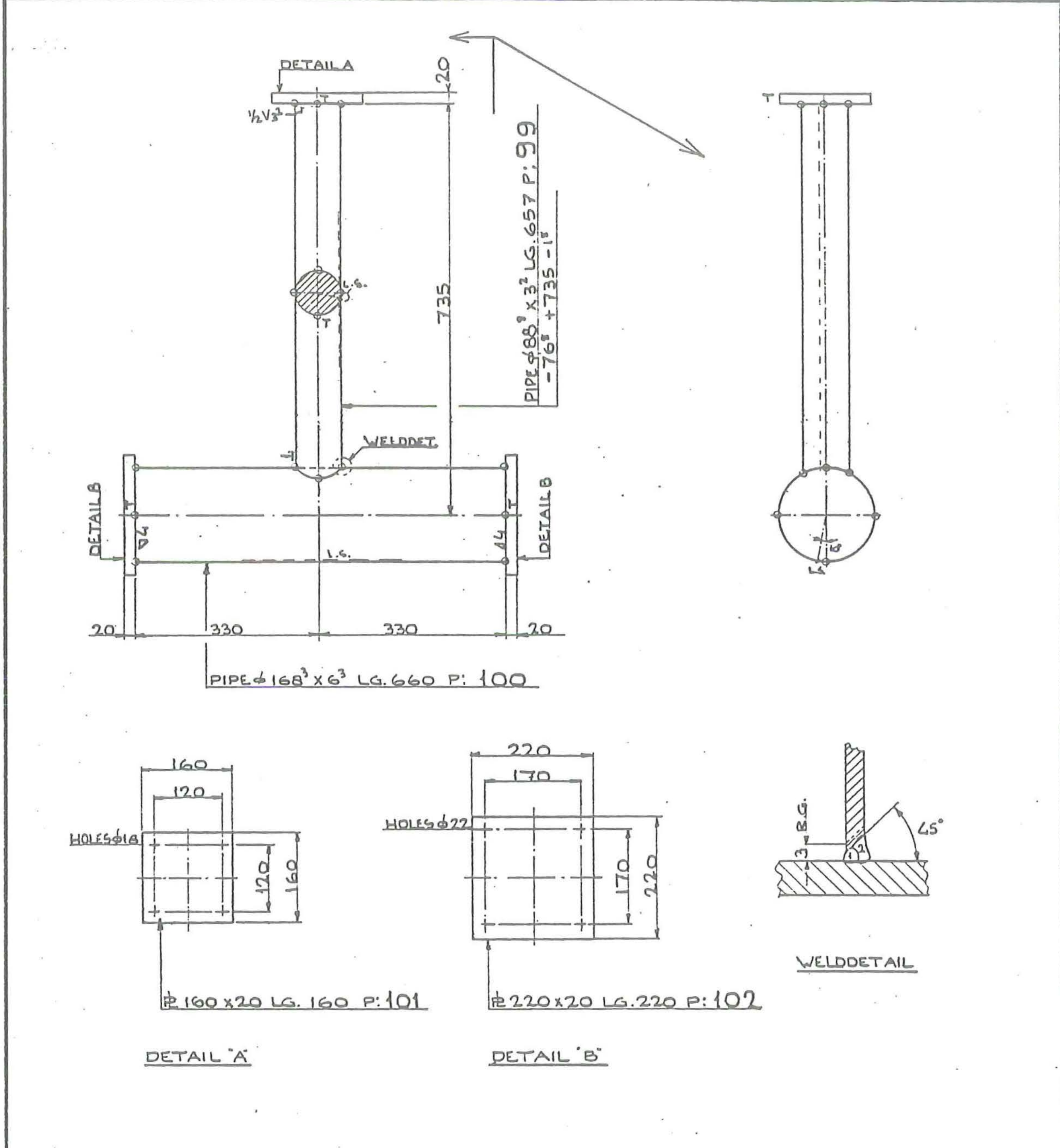

STAMP HEATNR. NEAR L.S. AT THE END OF THE PIPE

MATERIAL QUALITY: B: ST. 52-3   C: VH 0204

CONNECTION: PIPE φ88⁹ x 3² TO PIPE φ168³ x 6³

METHOD OF WELDING: MANUAL | PREHEAT: 65°C

U.S. RESEARCH ACCORDING TO ASME VIII

POSITION: 5G | WELDERNAME: FRANKEN

PASSNUMBER	ELECTRODE	AMP.	TEMP.	REMARKS	SYMBOLS
1	BH 100 2½	75	65°	6	: LOCATION ℄ ON PIPE-CIRCUMFERENCE
2	BH 100 2½	85	65°	6	: LOCATION TACKWELD
					: LOCATION REPAIRWELD
					: LOCATION ARCSTRIKE OUTSIDE W. SEAM
					L.S. : LONGITUDINAL SEAM (10° BESIDE ℄)
					T. : TOP
					B = BRACING C: CHORD

DE GROOT CONSTRUCTIE B.V. - ZWIJNDRECHT

0/24509	T.N.O. I.B.B.C.	TUBEPROGRAM EEG-SMOZ	T.H. STEVINLAB.	TEST 22-23 (A)

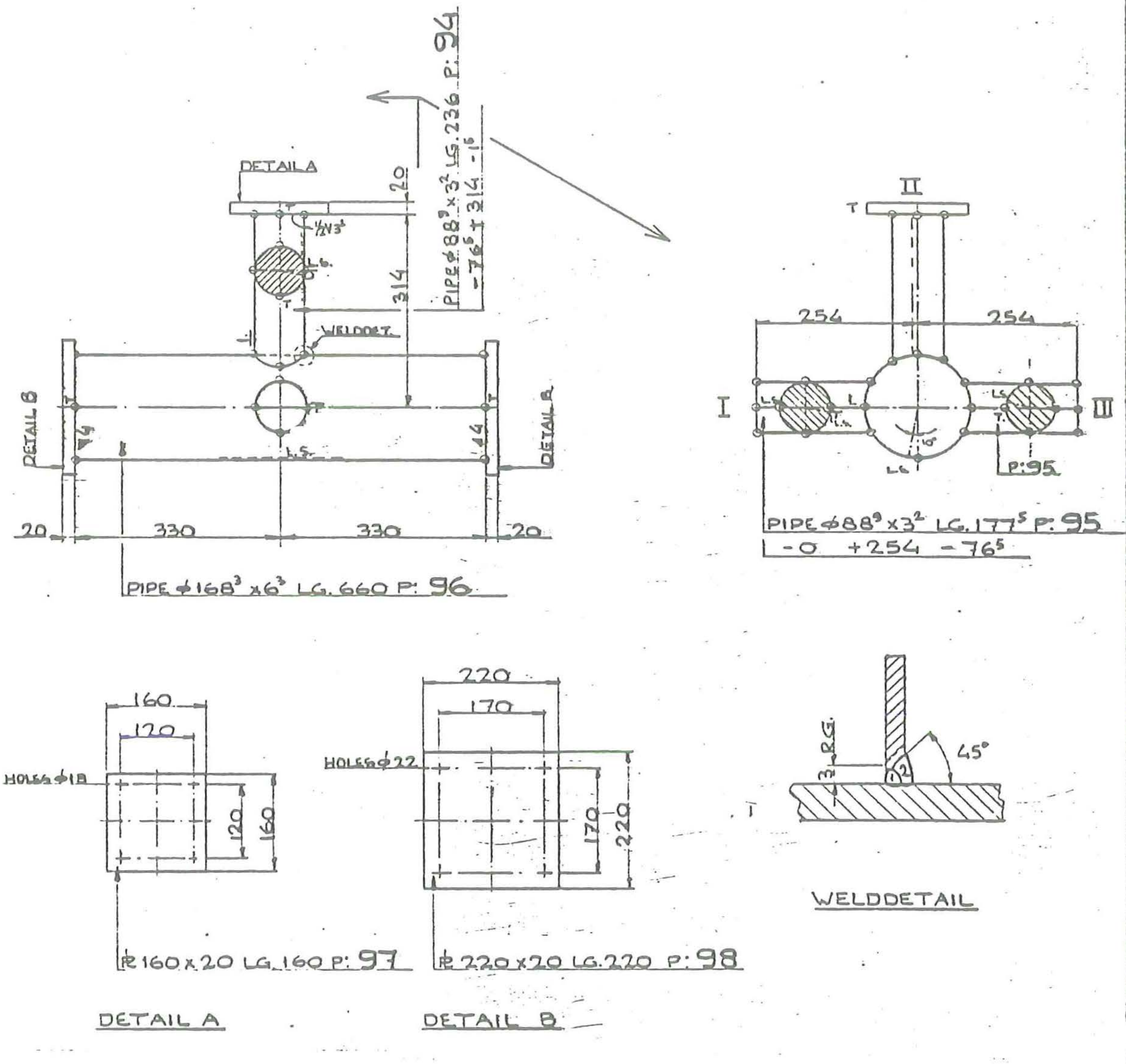

STAMP HEATNR. NEAR L.S. AT THE END OF THE PIPE
MATERIAL QUALITY : B = ST. 52-3 /C. VH0204
CONNECTION: PIPE ϕ88⁹ x 3² TO PIPE ϕ168³ x 6³
METHOD OF WELDING: MANUAL | PREHEAT: 65°

U.S. RESEARCH ACCORDING TO ASME VIII

POSITION: 5G | WELDERNAME: UDO

PASSNUMBER	ELECTRODE	AMP.	TEMP.	I	II	III
1	BH100 2½	70	65°	6	6	6
2	BH100 2½	85	65°	7	7	7

SYMBOLS

- o : LOCATION ℄ ON PIPE-CIRCUMFERENCE
- ∩ : LOCATION TACKWELD
- __ : LOCATION REPAIRWELD
- _._ : LOCATION ARCSTRIKE OUTSIDE W. SEAM
- L.S. : LONGITUDINAL SEAM (10° BESIDE ℄)
- T : TOP
- B : BRACING C : CHORD

DE GROOT CONSTRUCTIE B.V. - ZWIJNDRECHT

0/24509	T.N.O. I.B.B.C.	TUBEPROGRAM EEG-SMOZ	T.H. STEVINLAB	TEST 20-21 (A)

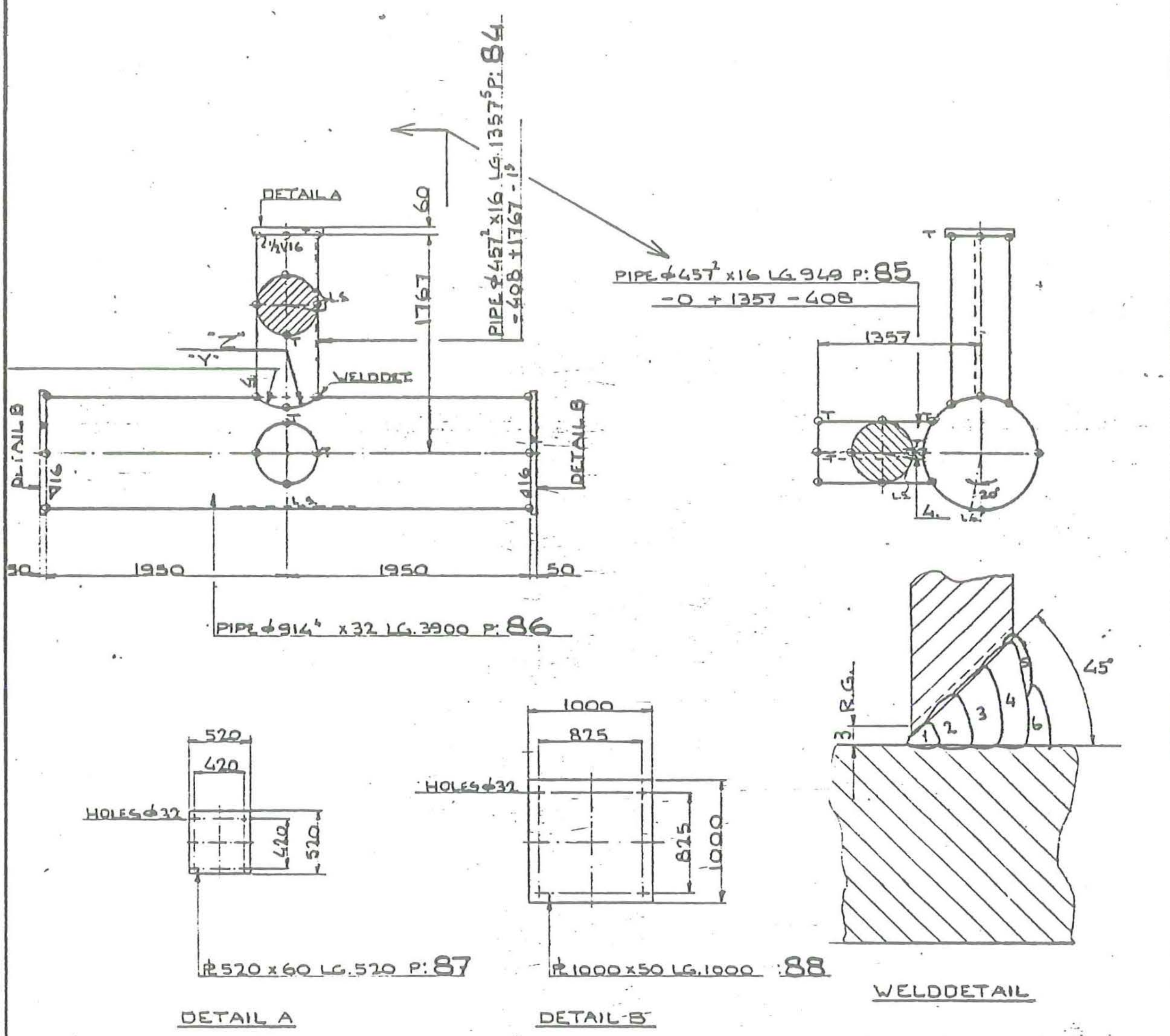

STAMP HEATNR. NEAR L.S. AT THE END OF THE PIPE	
MATERIAL QUALITY: B.9055	/C: 500395
CONNECTION: PIPE ⌀457² x16 TO PIPE ⌀914⁴ x32	
METHOD OF WELDING: MANUAL	PREHEAT: 100°C
POSITION: 5G	WELDERNAME: FRANKEN - UDO

U.S. RESEARCH ACCORDING TO ASME VIII

PASSNUMBER	ELECTRODE		AMP.	TEMP.	REMARKS P84	P85	SYMBOLS
1	BH 100	2½	85	100°	47	53	o : LOCATION ℄ ON PIPE CIRCUMFERENCE
2	BH 100	3¼	110 - 130	100°	43	43	⌒ : LOCATION TACKWELD
3	BH 100	4	140 - 160	100°	24	32	_ : LOCATION REPAIRWELD
4	BH 100	4	140 - 160	100°	19	19	___ : LOCATION ARCSTRIKE OUTSIDE W.SEAM
5	BH 100	3¼	110 - 130	100°	29	27	L.S. : LONGITUDINAL SEAM (10° BESIDE ℄)
6	BH 100	3¼	110 - 130	100°	37	29	T : TOP
							B. BRACING C. CHORD

DE GROOT CONSTRUCTIE B.V. - ZWIJNDRECHT

0/24509	T.N.O. I.B.B.C.	TUBEPROGRAM EEG-SMOZ	T.H. STEVINLAB.	TEST 18-19 (A)

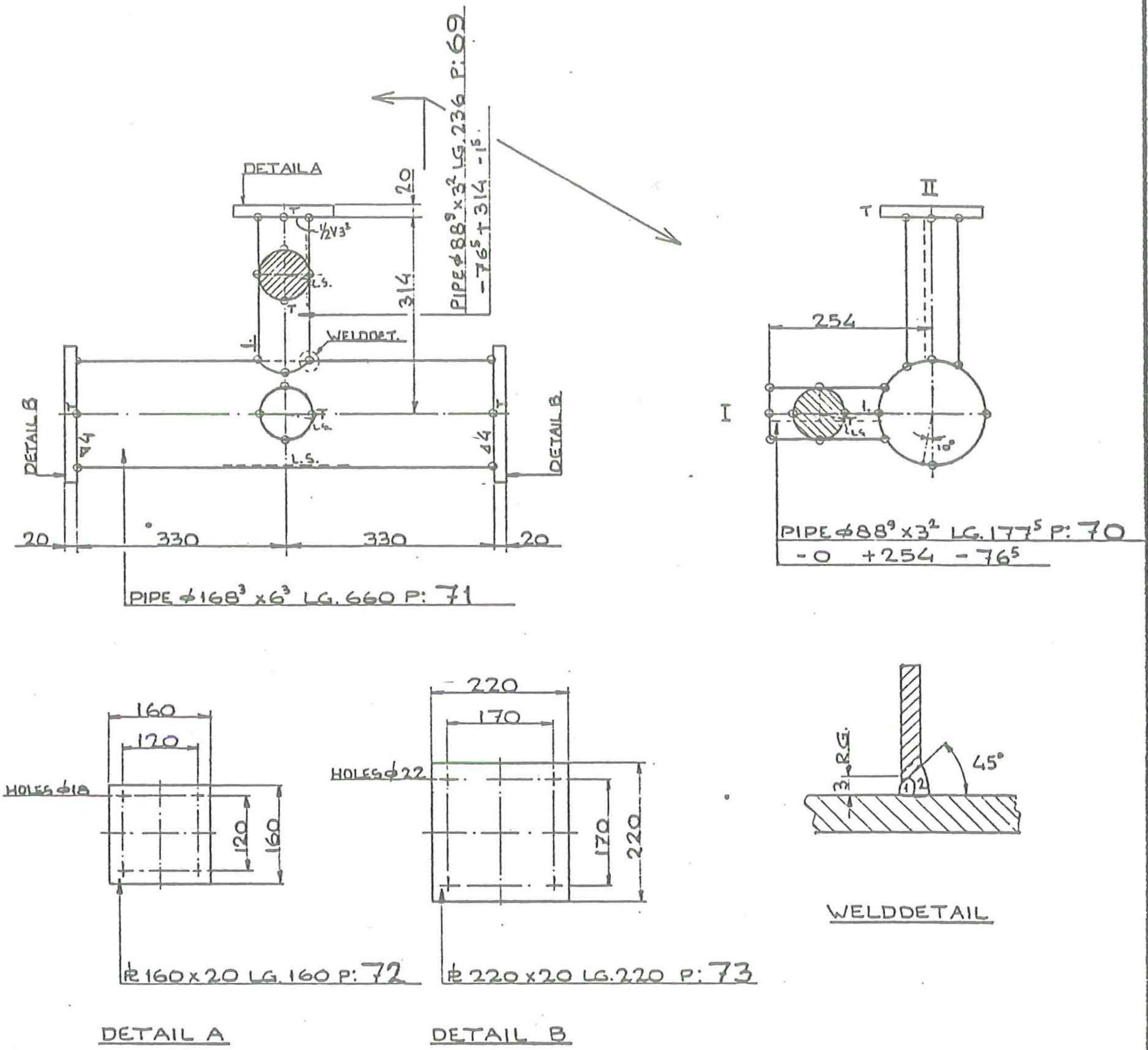

STAMP HEATNR. NEAR L.S. AT THE END OF THE PIPE
MATERIAL QUALITY : B = ST. 52-3 / C = VH 0204
CONNECTION: PIPE ⌀88⁹ x 3² TO PIPE ⌀168³ x 6³
METHOD OF WELDING: MANUAL | PREHEAT: 65°
POSITION: 5G | WELDERNAME: FRANKEN

U.S. RESEARCH ACCORDING TO ASME VIII

PASSNUMBER	ELECTRODE	AMP.	TEMP.	I	II	SYMBOLS
1	BH 100 2½	70	65°	6	6	o : LOCATION ℄ ON PIPE-CIRCUMFERENCE
2	BH 100 2½	85	65°	7	7	⌒ : LOCATION TACKWELD
						__ : LOCATION REPAIRWELD
						_ _ : LOCATION ARCSTRIKE OUTSIDE W. SEAM
						L.S. : LONGITUDINAL SEAM (10° BESIDE ℄)
						T. : TOP
						B = BRACING C = CHORD

DE GROOT CONSTRUCTIE B.V. - ZWIJNDRECHT

0/24509	T.N.O. I.B.B.C.	TUBEPROGRAM EEG-SMOZ	T.H. STEVINLAB.	TEST 13-17 (A)

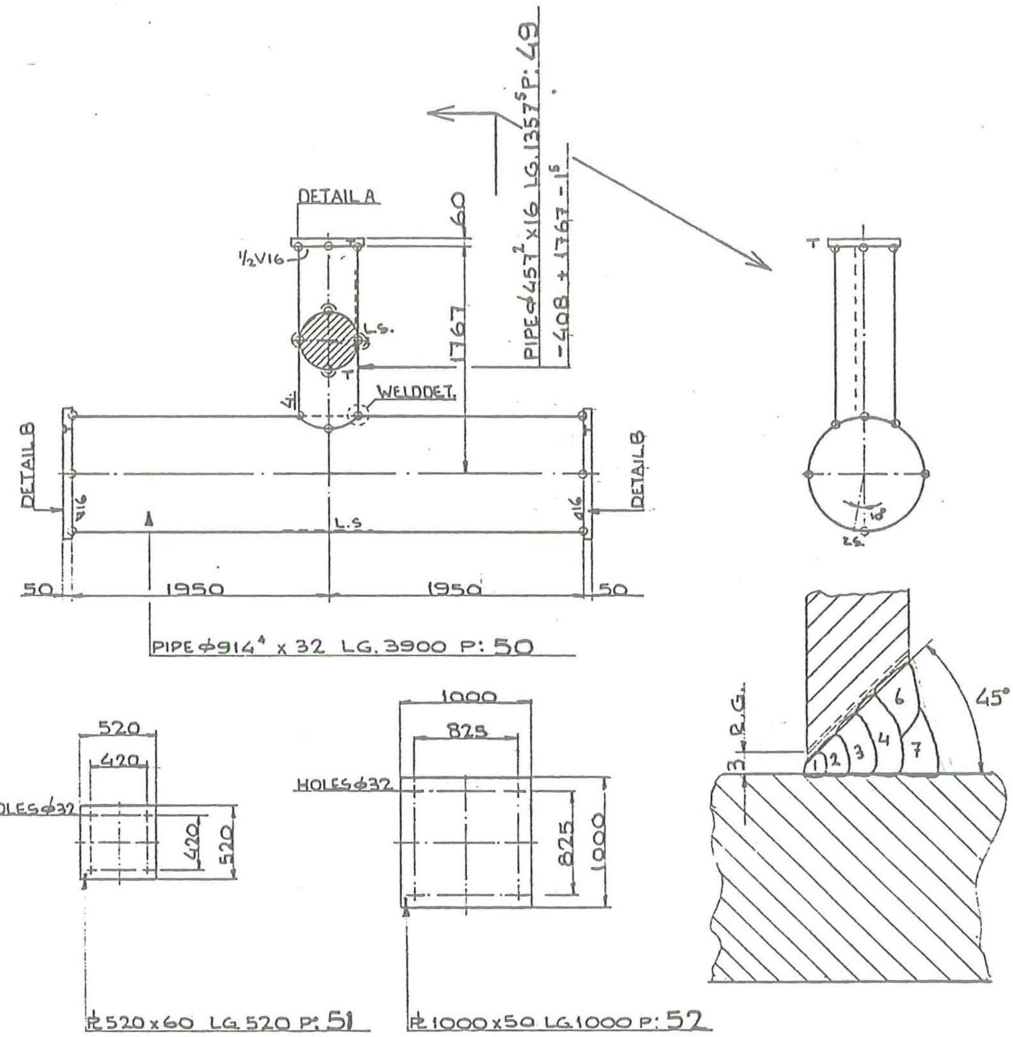

DETAIL A

DETAIL B

WELDDETAIL

STAMP HEATNR. NEAR L.S. AT THE END OF THE PIPE	
MATERIAL QUALITY: B: 9055 /C: 500395	
CONNECTION: PIPE ϕ457² x16 TO PIPE ϕ914⁴ x32	
METHOD OF WELDING: MANUAL	PREHEAT: 100°C
POSITION: 5G	WELDER NAME: FRANKEN / UDO

U.S. RESEARCH ACCORDING TO ASME VIII

PASSNUMBER	ELECTRODE	AMP.	TEMP.	REMARKS	SYMBOLS
1	BH100 2½	85	100°	33 ELECTRODES	o :LOCATION ℄ ON PIPE-CIRCUMFERENCE
2	BH100 3¼	130	100°	21 "	∩ :LOCATION TACK WELD
3	BH100 3¼	120-140	100°	35 "	__ :LOCATION REPAIRWELD
4	BH100 4	150-165	100°	28 "	.... :LOCATION ARCSTRIKE OUTSIDE W. SEAM
5	BH100 4	150-165	100°	9 " (BOVEN)	L.S. :LONGITUDINAL SEAM (10° BESIDE ℄)
6	BH100 3¼	110-130	100°	20 "	T. :TOP
7	BH100 3¼	110-130	100°	34 "	B: BRACING C: CHORD
8	BH100 3¼	110	100°	4 (ONDERZIJDE)	

DE GROOT CONSTRUCTIE B.V. - ZWIJNDRECHT

0/24509	T.N.O. I.B.B.C.	TUBEPROGRAM EEG-SMOZ	T.H. STEVINLAB	TEST 11_12 (A)

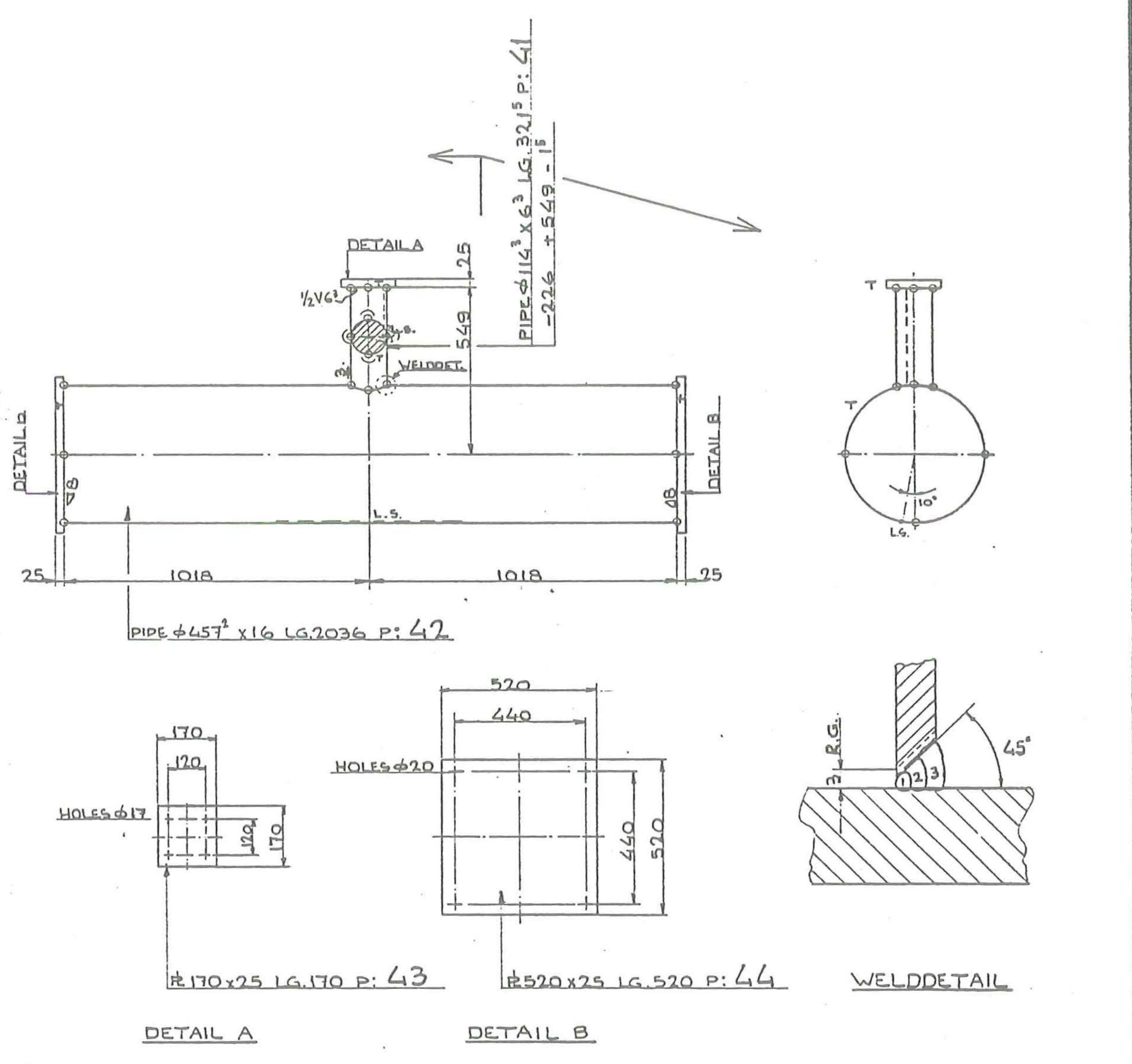

				STAMP HEAT NR. NEAR L.S. AT THE END OF THE PIPE	
				MATERIAL QUALITY: B.	/ C. 9055
				CONNECTION: PIPE ϕ114^3 x 6^3 TO PIPE ϕ457^2 x 16	
				METHOD OF WELDING: MANUAL	PREHEAT: 65°C
U.S. RESEARCH ACCORDING TO ASME VIII				POSITION: 5G	WELDER NAME: UOO
PASSNUMBER	ELECTRODE	AMP.	TEMP.	REMARKS	SYMBOLS
1	BH 100 2½	85	65°	8 ELECTRODES	o : LOCATION ℄ ON PIPE-CIRCUMFERENCE
2	BH 100 3¼	110	65°	6 "	∩ : LOCATION TACK WELD
3	BH 100 3¼	110 - 130	65°	8 "	— : LOCATION REPAIR WELD
					... : LOCATION ARCSTRIKE OUTSIDE W. SEAM
					L.S. : LONGITUDINAL SEAM (10° BESIDE ℄)
					T. : TOP
					B. BRACING C. CHORD

DE GROOT CONSTRUCTIE B.V. - ZWIJNDRECHT

0/24509	T.N.O. I.B.B.C.	TUBEPROGRAM EEG-SMOZ	T.H. STEVINLAB.	TEST 4-10 (A)

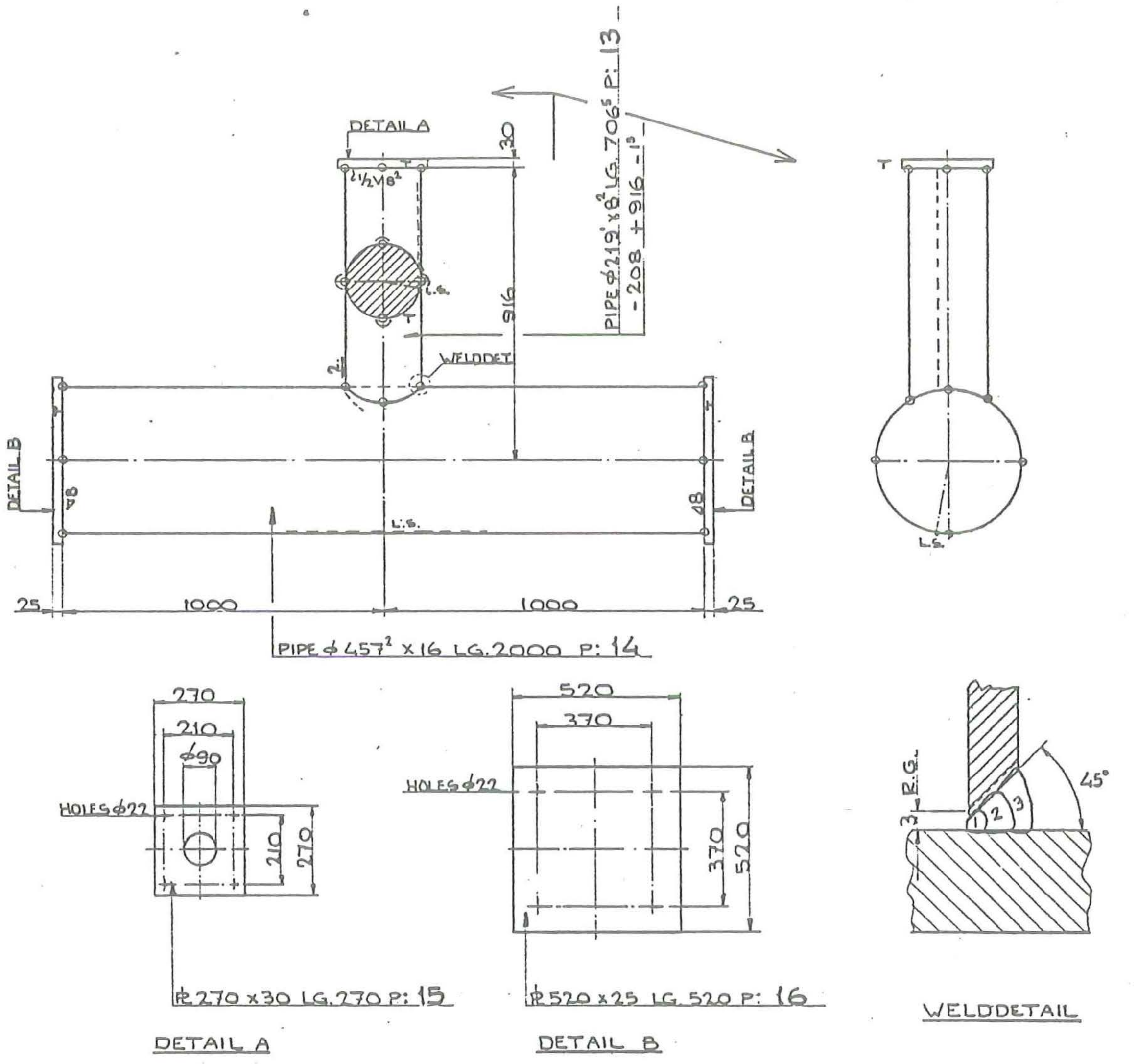

STAMP HEATNR. NEAR L.S. AT THE END OF THE PIPE	
MATERIAL QUALITY: B = 1664 /C = 9055	
CONNECTION: PIPE ⌀219¹ x 8² TO PIPE ⌀457² x 16	
METHOD OF WELDING: MANUAL	PREHEAT: 65°C
POSITION: 5G	WELDERNAME: FRANKEN

U.S. RESEARCH ACCORDING TO ASME VIII

PASSNUMBER	ELEKTRODE	AMP.	TEMP.	REMARKS	SYMBOLS
1	BH 100 2½	80-95	65	16 ELECTRODES	o : LOCATION ℄ ON PIPE - CIRCUMFERENCE
2	BH 100 3¼	110-130	65	16 "	⌒ : LOCATION TACK WELD
3	BH 100 3¼	100-130	65	19 "	— : LOCATION REPAIRWELD
					__ : LOCATION ARC STRIKE OUTSIDE W. SEAM
					L.S. : LONGITUDINAL SEAM (10° BESIDE ℄)
					T. : TOP
					B = BRACING C = CHORD

DE GROOT CONSTRUCTIE B.V. - ZWIJNDRECHT

0/24509	T.N.O. I.B.B.C.	TUBEPROGRAM EEG-SMOZ	T.H. STEVINLAB	TEST 1_3 (A)

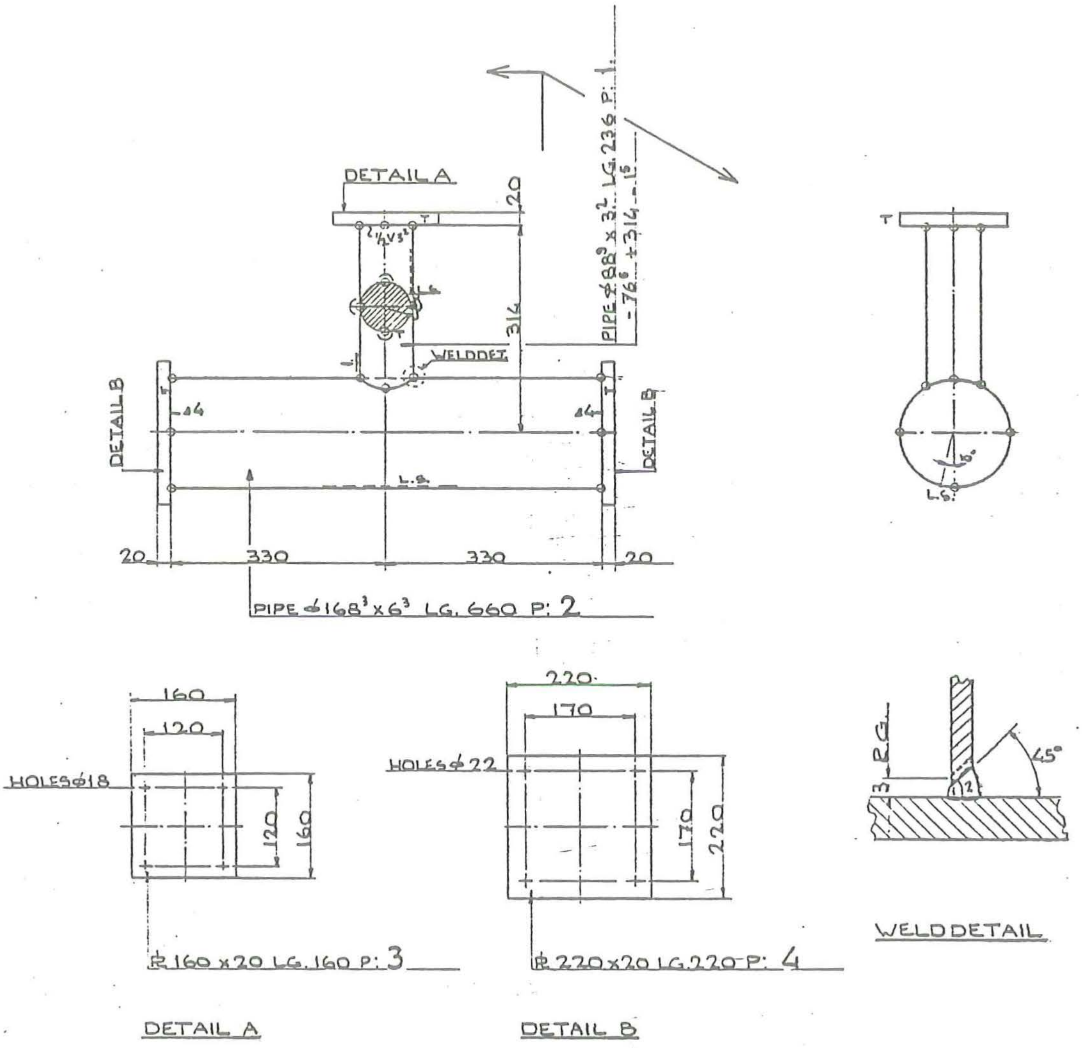

STAMP HEATNR. NEAR L.S. AT THE END OF THE PIPE
MATERIAL QUALITY : B = ST. 52-3 /C = V.K.0204
CONNECTION : PIPE ⌀88³ x 3² TO PIPE ⌀168³ x 6³
METHOD OF WELDING: MANUAL | PREHEAT : 65° C
U.S. RESEARCH ACCORDING TO ASME VIII | POSITION : 5G | WELDER NAME : FRANKEN

PASSNUMBER	ELECTRODE	AMP.	TEMP.	REMARKS	SYMBOLS
1.	BH 100 2½	80	65°	6 ELECTRODES	o : LOCATION ℄ ON PIPE-CIRCUMFERENCE
2	BH 100 2½	85	65°	(8) "	∩ : LOCATION TACK WELD
					— : LOCATION REPAIRWELD
					--- : LOCATION ARCSTRIKE OUTSIDE W. SEAM
					LS. : LONGITUDINAL SEAM (10° BESIDE ℄)
					T : TOP
					B . BRACING C . CHORD

DE GROOT CONSTRUCTIE B.V. - ZWIJNDRECHT

Appendix 3-I

Fabrication data sheets

5. APPENDICES TO CHAPTER 3

5. APPENDICES TO CHAPTER 3

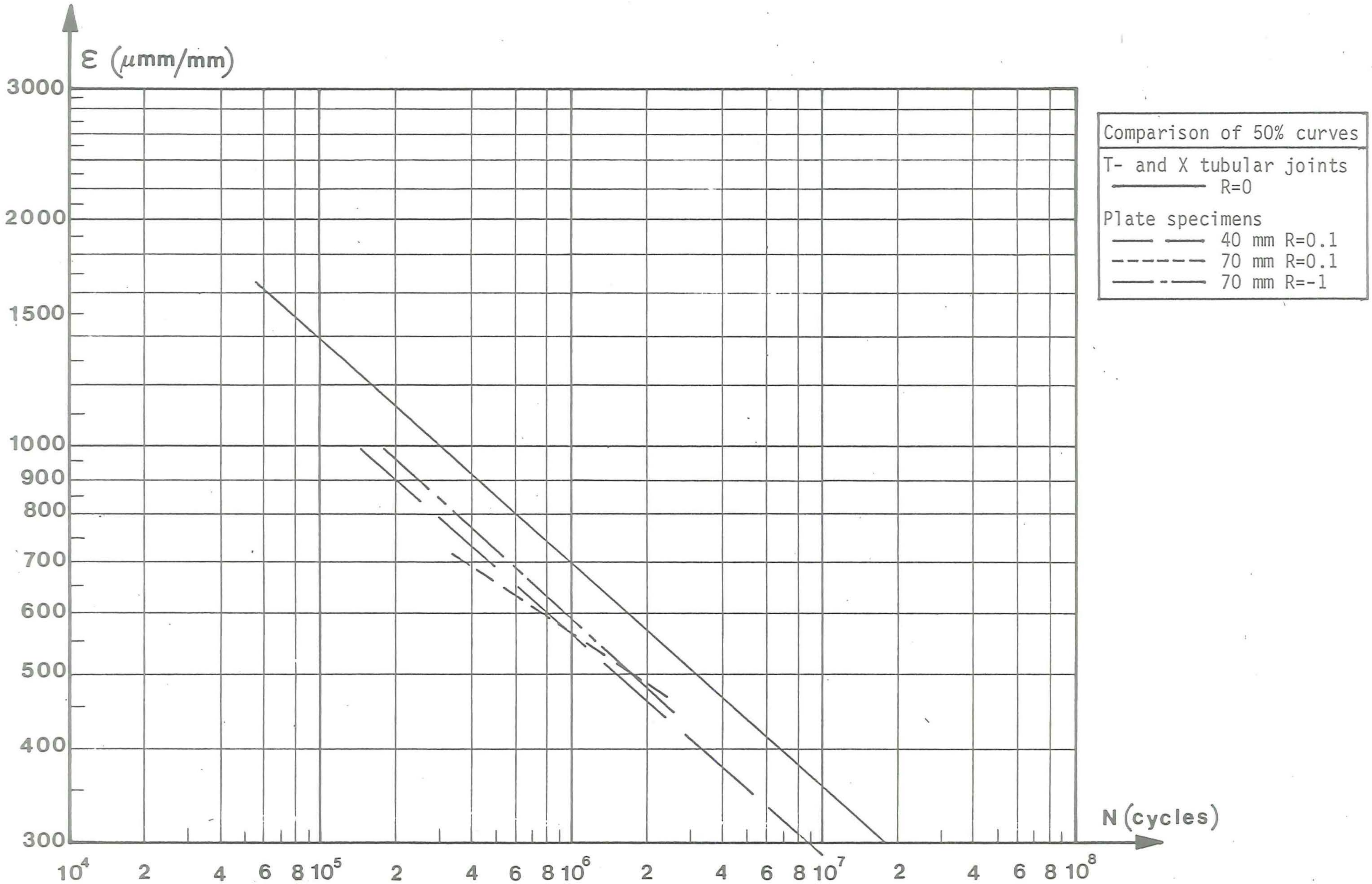

Fig. 4.1 Comparison between the results of the 4-point bending plate tests and the results of the tubular joints (T- and X joints with D=914.4 mm)

4.6. Summary of the main conclusions

For more detailed conclusions see pages 2-9 and 2-10, 2-52 and 2-53, 2-62 and 2-63, 2-132, 2-164 and 2-165, 3-24.

1. The tubular joint testing shows a significant size effect. The larger the joint, the lower the fatigue strength (for sizes from Ø 168 - 6 mm to Ø 914 mm - 32 mm). The tested plate specimens of 40 and 70 mm thickness do not show an influence of the thickness.
2. Some fatigue results of the large tubular joints at long lives fall below the AWS-X line, it is advisable to rotate this design-line.
3. Artificial seawater of $20^{\circ}C$ decreases the endurance of tubular joints and plate specimens (constant amplitude and random loading) by a factor of 2-3.
4. A less steep weld angle (45° versus 70°) has only a slight beneficial effect. When the weld angle is smaller than 45° this effect seems to increase.
5. Finishing of the weld toe by means of TIG- and Plasma dressing and Grinding increases the fatigue life in air as well in seawater. Seawater, however, reduces the favourable effect of the finishing techniques although a beneficial effect still remains.
6. The stress ratio has a small influence on the fatigue strength in air and seawater of welded joints loaded in bending. The effect was found not to depend on the environment and to be more pronounced for the stress relieved specimen, than for the as welded specimen.
7. Cathodic protection seems to be most effective at lower stress ranges however, the test on a tubular joint with cathodic protection showed no beneficial effect compared to the joints tested in seawater.
8. The endurance of the flat specimens tested under two different spectrum loadings is a factor 1.0 - 1.3 larger than the expected life as calculated through Miner's Rule.
9. The orientation of the crack plane proves to have no significant influence on the fatigue crack propagation rate which at R = 0.1 can be described by the relation $da/dN = 6.1 \times 10^{-9} \Delta k^{3.0}$ in the region $6 < \Delta k < 80$ MPa $\sqrt{m}$
10. In seawater the fatigue crack growth rate is about a factor 3 higher than that in air.

by these techniques.
A significant improvement can not be reached by changing the weld angle from 70^0 to 45^0, (fig. 2.2.26).
If other weld shapes, (e.g. a convex weld) can improve the fatigue life, it has to be determined on test specimen with realistic dimensions and welded under circumstances as can be used for large platforms.

4.5. Crack growth

Besides hot spot strain and number of cycles to failure, crack propagation was observed in all tests on tubular joints. Furthermore complimentary to the endurance tests crack propagation studies on plate specimens have been carried out in order to generate diagrams in which the crack growth rate is plotted as a function of the range of the stress intensity factor. This outlines that the alternative method of fatigue analysis using linear fracture mechanics is also a method which the investigators have in mind.
However the application of fracture mechanics is complicated by the fact that the cracks grow in two dimensions: along the weld toe (and sometimes away from the weld toe into the chord material) and through the thickness of the parent material. This complication together with the very complex stress distribution in tubular joints cause a lot of uncertainties in calculating endurances by fracture mechanics, up till now, but considerable effort is going on in all countries to solve this problem.
Besides the use of the crack growth data that can be made by investigators trying to predict the life by fracture mechanics, these data can also be used in predicting the remaining life of joints already cracked.
At this moment for design purposes S-N lines and the Miner summation formula will be used, but it is quite clear that in future improved fracture mechanics calculations will provide a better prediction of the life of a tubular joint.

carried out (outside of this programme) in the Netherlands, seems to indicate that PWHT will not have an advantage at short and moderate lives, but only at long lives (low stresses).

Concluding: for large as-welded joints it seems advisable to rotate the AWS-X design curve in such a way that the slope will be steeper, with shorter design lives at low stress levels and longer lives at high stress-levels.

4.3. Size effect

It has been already stated that there is a significant effect of size. There is no complete understanding which factors cause this effect and to what extent they contribute to this effect. By using crack growth laws based on linear fracture mechanics it can be shown that the endurance of thicker plates is shorter than that of thinner plates, but this can not explain the very large difference found in these tests.

Other factors may be:

1. Initial stresses due to welding
2. Larger probability of defects in the hot spot area
3. Shallower stress gradients in thickness and circumferential direction, which causes larger plastic zones, and higher strain rates.

Future research is needed to clarify this effect.

4.4 Improvement of the fatigue strength

Fig. 2.2.30 page 2-94 shows a benificial effect of Post Weld Heat Treatment on plate specimen This effect is more pronounced at R = -1 than at R = 0.1. It has been stated already that there are indications that the advantage of PWHT is less for large tubular joints, especially for those with high strain concentrations. It may be that at low stress levels (important for offshore structures) there is a significant benificial effect, however then the question arises, how this joint will behave under a complex service loading. More research to clarify this problem will be needed.

Weld finishing technique such as grinding, TIG- and Plasma-dressing increase the fatigue life in air as well as in seawater (fig. 2.2.27 page 2-92). Although seawater reduces the favourable effect of all these finishing techniques still a benificial effect remains. It has to be checked how far the fatigue life of real tubular joints can be improved

be seen that strain concentration factors do not change very much. Far more important is the shape of the weld toe. However it is very hard to influence with efficient accuracy the shape of the toe of the weld in practice without using weld finishing techniques. Fig. 2.2.26 page 2.92 shows that changing the weld angle from 70 to 45^{o} improves the fatigue strength only very slightly.
Furthermore all the tubular joints (fabricated by a firm which has experience in constructing offshore structures) were welded in horizontal position with both chord and brace horizontal, however, no significant difference in the fatigue behaviour of the top- or bottom side was found thus no influence of the welding position could be discovered. A number of times the cracks started at both saddle points (top- and bottom sides) of the intersection in the chord wall at the weld toe; in other cases the cracks started at random at the "top" saddle point or at the "bottom" saddle point. Fig. 4.1. gives a comparison between the regression lines of the results of the tubular joints ø 918-32 mm, R = 0 and the plate specimens 40 mm, R = 0.1; 70 mm, R = 0.1; and 70 mm, R = -1 plotted against the strain. It can be seen that the results of the plate specimen are a little bit lower than those of the tubular joints.

Looking at all the results and the factors which can have influenced these results or which are important for a design life (service loading) there is in our opinion no reason to assume, that the results are too pessimistic for as-welded tubular joints tested at R = 0.
The results of the tests carried out in the U.K. on tubular joints with a chord diameter of 914 mm and a wall thickness of 32 mm lie somewhat higher than the Dutch results, but they are conducted at R = -1.
Fig. 2.2.28, page 2-93, shows that the fatigue strength of flat 70 mm specimen tested at R = -1 is also somewhat higher than those tested at R = 0.1.
The specimens with a diameter of 1830 mm and a wall thickness of 76 mm tested in the U.K. with R = -1, Post Weld Heat Treated, in air, give nearly the same results as the 914 mm diameter joints R = -1 tested in the U.K., Comparing this with the Dutch tests on flat specimens the following can be said. The flat specimens with a thickness of 70 mm show (especially at R = -1) a significant beneficial effect of Post Weld Heat Treatment (fig. 2.2.30). No influence of the thicknesses between 40 and 70 mm (AW) could be found (fig. 2.2.32), so the results of the tests on 70 mm plate thickness-PWHT are higher than those on 40 mm plate thickness-AW. This seems to be in contradiction with the above metioned results of the tubular joints ø 1830 - 76 mm PWHT and ø 914-32 mm AW.
However recent tests on PWHT-specimens with a chord diameter of 918 mm

There are three more factors which can influence the life of an as-welded tubular joint: the environment (seawater), the loading (service loading instead of constant amplitude loading) and the shape of the weld.

- A seawater environment of 20^{0}C decreases life by a factor of 2½ to 3, as can be seen in the graphs. This is in good agreement with tests done on plate specimens. It may be that this factor will be smaller in seawater of 5^{0}C. Tests on plate specimens in the U.K. show, at this temperature, nearly no influence of the seawater.
  Future tests in the U.K. will perhaps provide information whether this is also true for tubular joints.
  In general cathodic protection will avoid the influence of the corrosion on the fatigue behaviour. Some tests in the U.K. and in Germany even show better results than in air.
  The Dutch tests with cathodic protection on plate specimens confirm this at long lives, but at shorter lives (high stresses) the cathodic protection seems to be less effective and the only corrosion fatigue test on a tubular joint with cathodic protection done during the Dutch investigation shows an increase in the number of cycles to crack initiation but a higher crack growth rate, so the total life is nearly the same as in seawater. How far this test is representative for the behaviour of tubular joints has to be determined in future tests.
- The two tubular joint tests, that were carried out with a random loading give good agreement with the constant amplitude tests if the random tests were plotted on the base of the rms-value. Also Miner's rule seems to be valid for these tests. The same conclusion can be drawn from the random tests on plate specimens (see page 2-132).
  However, after analysing the results of tests in several countries, Dr. Schütz states in his rapporteur's report for the ECSC Offshore Colloquium in Paris, October 1981, that it is better to use a Miner's summation factor of ½ for design purposes. That means that by accepting his proposal the design life will be a factor of 2 shortened.
- A lot of discussion is going on about the influence of the shape of the weld. Clear distinction has to be made between the angle of the weld and the shape of the toe of the weld. It is our opinion that weld angles between 70^{0} and 45^{0} do not influence the fatigue strength very much. From finite element calculations (3.5 page 3.25), it can

4. GENERAL DISCUSSION OF THE RESULTS

4.1. Introduction

This investigation is aimed to provide the designer and certification authorities relevant data about the (corrosion) fatigue behaviour of tubular joints. To be sure that the results will be of direct use, it was decided that the steels, welding procedures, specimen design and manufacturing (especially of the large tubular joints), should be chosen within the ranges which are used in the North Sea.

In discussing the results of the project it therefore seems appropriate to start with the results of the tubular joint tests and to see what kind of additional information can be got from tested plate specimens.

The results of the fatigue tests on tubular joints are given in Figs. 3.4.41 to 3.4.44 on pages 3.92 to 3.95.

Looking at these figures two important observations can be made.

There is a significant influence of the size; and the fatigue results of the large tubular joints at long lives are lower than was expected.

4.2. Fatigue strength of tubular joints

Starting with the latter observation it has to be remarked that the place where a fatigue result of a tubular joint will be plotted in an S-N graph completely depends on the definitions of S and N.

The definition of the strain, however, as adopted by the Working Group III of the ECSC Offshore Programme and explained on page 3.11 seems reasonable. For the extrapolation, perhaps it will be better to take 0.4 times the wall thickness as the smallest distance of the strain-gauges instead of $0.2\sqrt{rt}$, but this will have nearly no influence on the results plotted in this case. Comparison of the values determined in this way from the test specimens and finite element calculations and/or parameter formulae show a good correlation, so it may be expected that the results can be used directly for design purposes.

In the figures 3.4.41 to 3.4.44 the definition of N is end of the test ; a not very clear definition. However, the tests are carried out far enough to cover any reasonable failure criterion, such as through crack, a decrease in stiffness or a specified crack length.

Accepting the through crack as a failure criterion means that the life will be reduced by a factor of about 0.8. Specifying a crack of about 30 mm as a failure criterion will reduce the life with a factor of 2-3.

Delft University of Technology
Department of Civil Engineering
Stevin Laboratory

4. GENERAL DISCUSSION OF THE RESULTS

Delft, May 1981
Prof. ir. J. de Back.

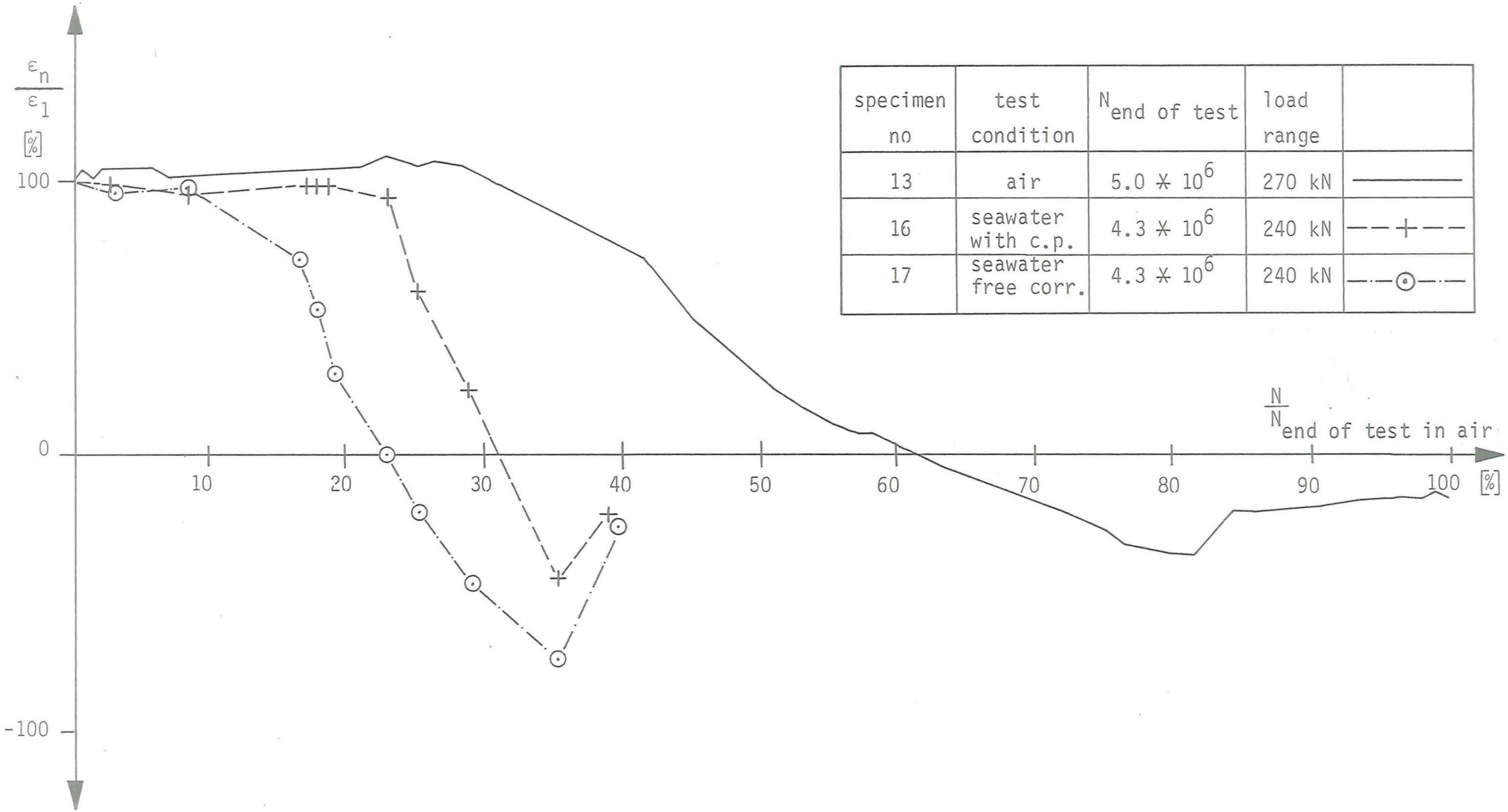

specimen no	test condition	$N_{end\ of\ test}$	load range	
13	air	5.0×10^6	270 kN	———
16	seawater with c.p.	4.3×10^6	240 kN	——+——
17	seawater free corr.	4.3×10^6	240 kN	—·—⊙—·—

Fig.3.4.49 Change in strainrange during fatigue test dependent on the test condition

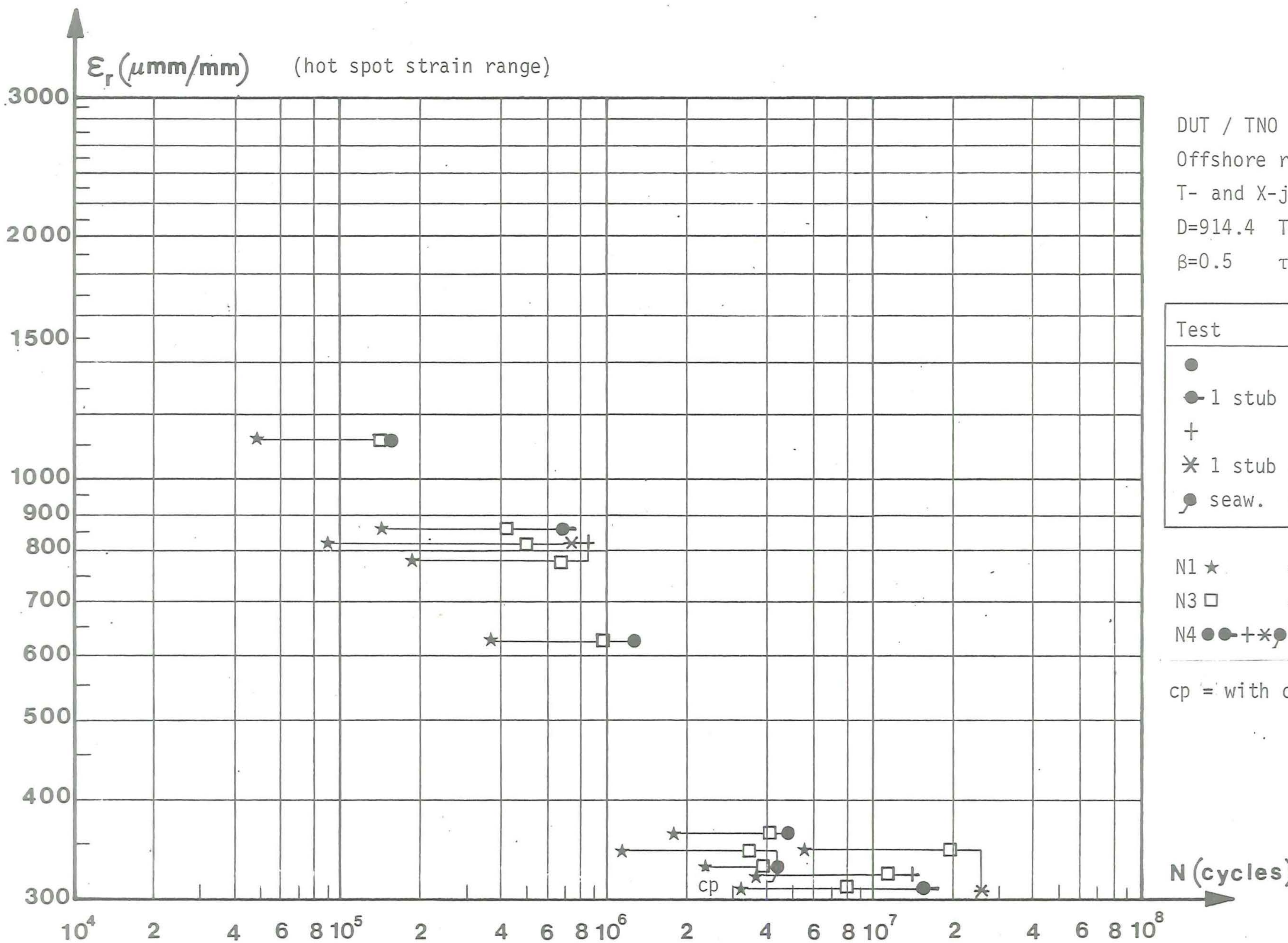

DUT / TNO

Offshore research programme

T- and X-joints

D=914.4 T=32

β=0.5 τ=0.5

Test		Loading	R
●	(T)	Ax	0
●- 1 stub	(T)	Ax	0
+	(X)	Ax	0
✳ 1 stub	(X)	Ax	0
seaw.	(T)	Ax	0

N1 ★ = ε_r - 15%

N3 □ = crack through

N4 ● ●- + ✳ = end of test

cp = with cathodic protection

Fig.3.4.48 Test results to various failure criteria (914.4 mm T- and X-joints)

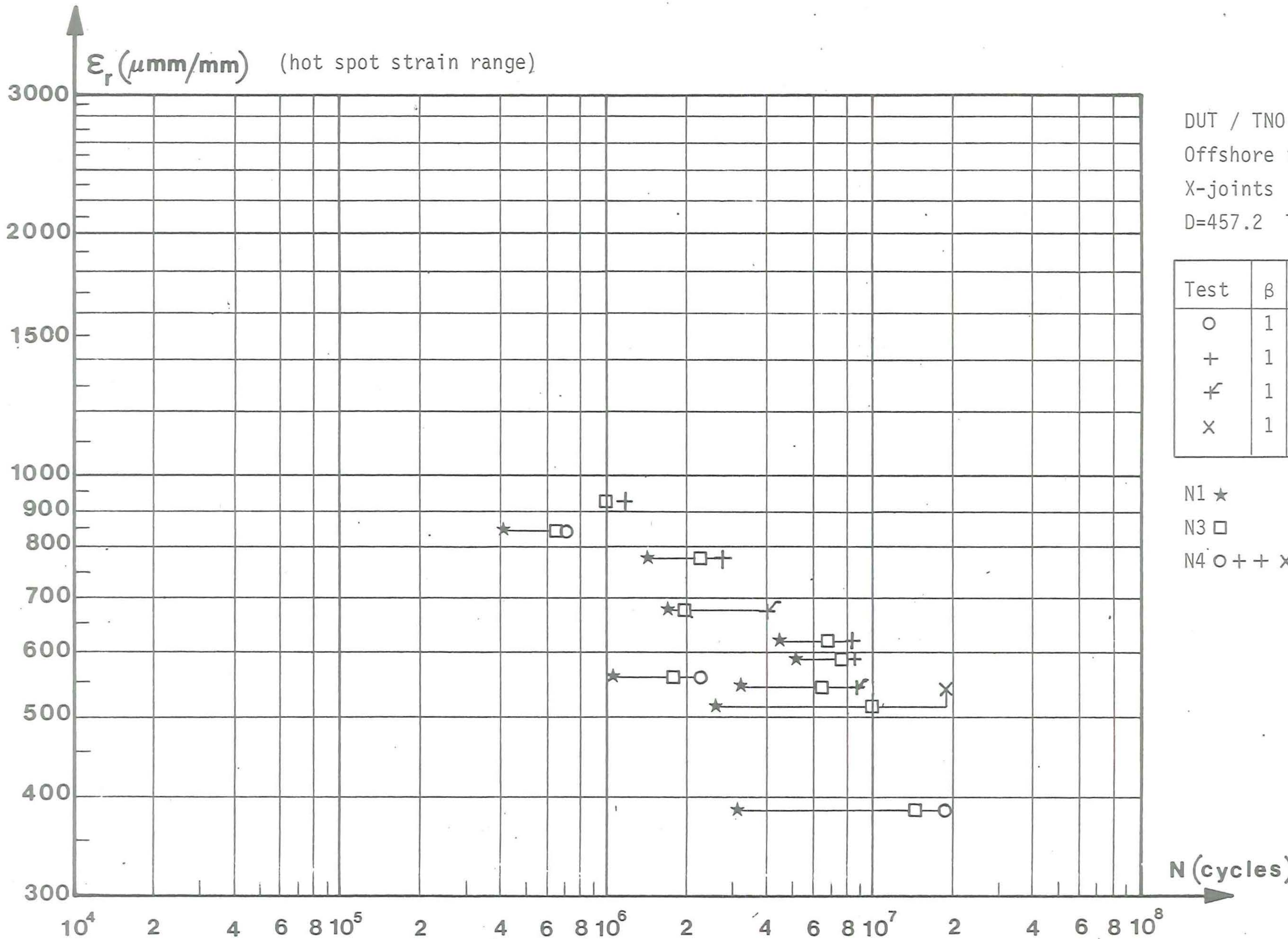

DUT / TNO
Offshore research programme
X-joints
D=457.2 T=16

Test	β	τ	Loading	R
○	1	1	Ax	0
+	1	0.55	Ax	0
+̸	1	0.55	Ax + Random	0
×	1	0.55	Ax + Compr.	0

N1 ★ = ε_r - 15%
N3 □ = crack through
N4 ○ + + × = end of test

Fig.3.4.47 Test results to various failure criteria (Ø457.2 mm X-joints)

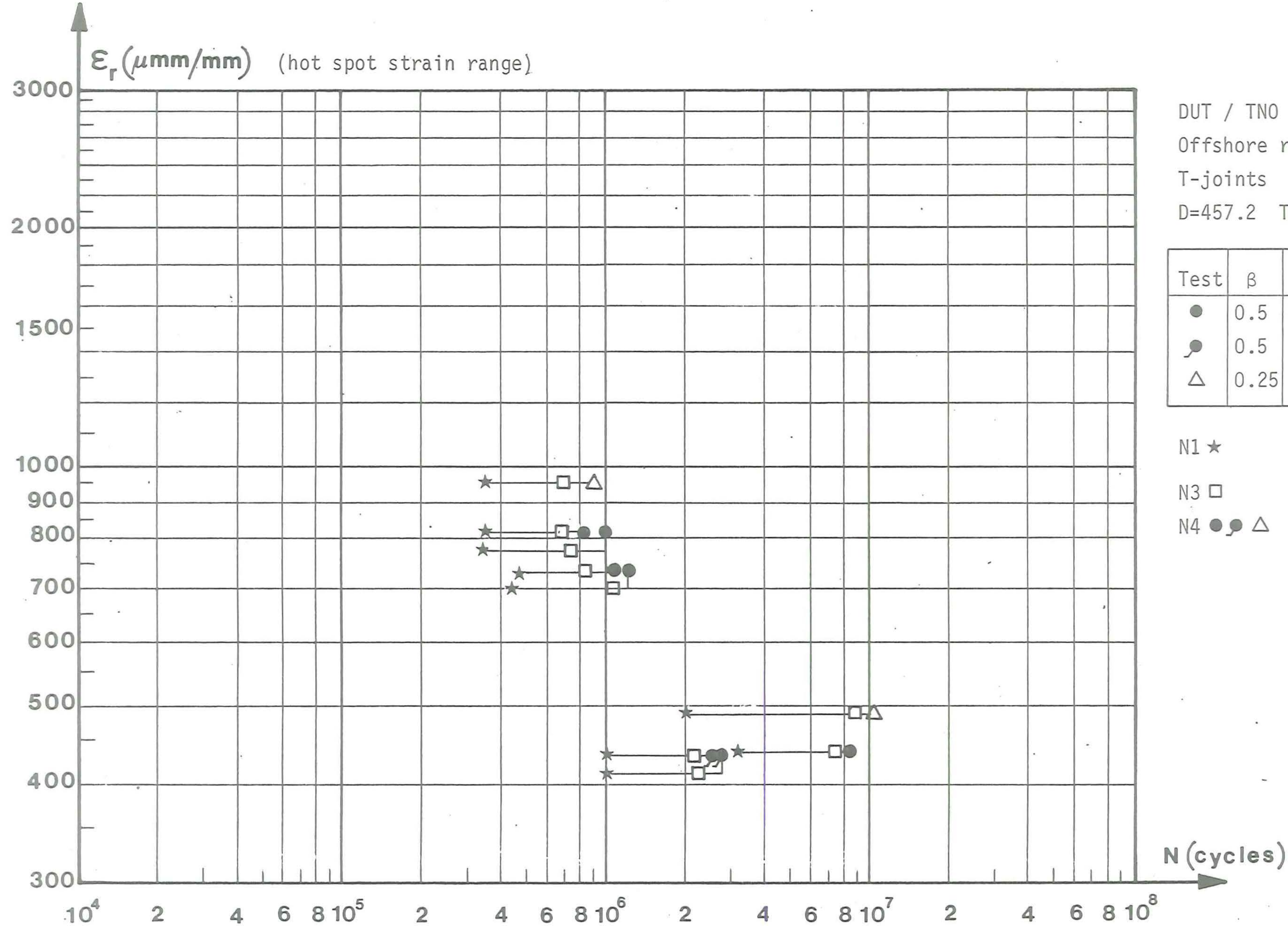

DUT / TNO
Offshore research programme
T-joints
D=457.2 T=16

Test	β	τ	Loading	R
●	0.5	0.5	Ax	0
⚲	0.5	0.5	Ax	-1/0
△	0.25	0.39	Ax	-1

N1 ★ = ε_r - 15%

N3 □ = crack through

N4 ● ⚲ △ = end of test

Fig.3.4.46 Test results to various failure criteria (Ø457.2 mm T-joints)

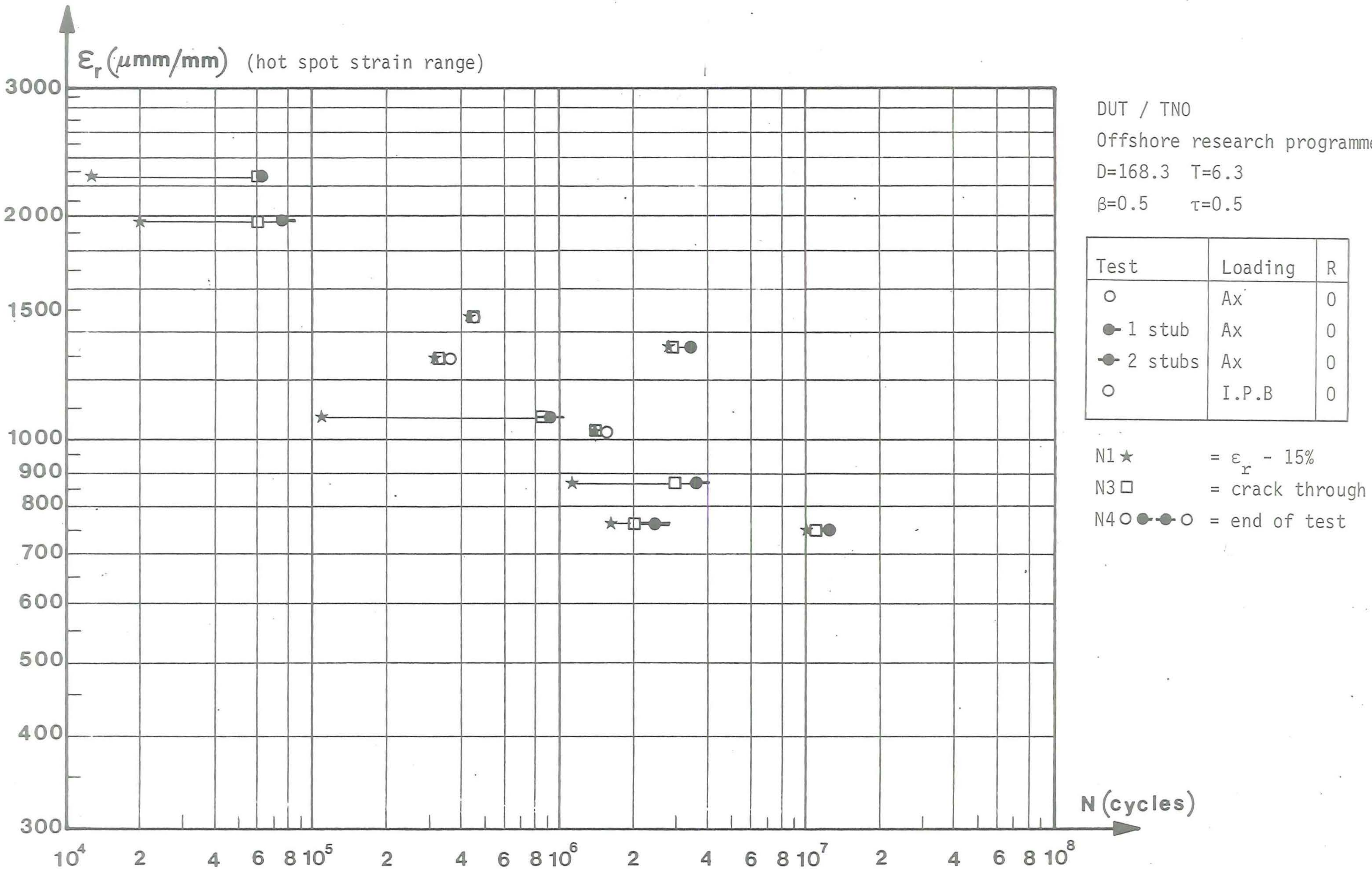

Fig.3.4.45 Test results to various failure criteria (Ø168.3 mm T-joints)

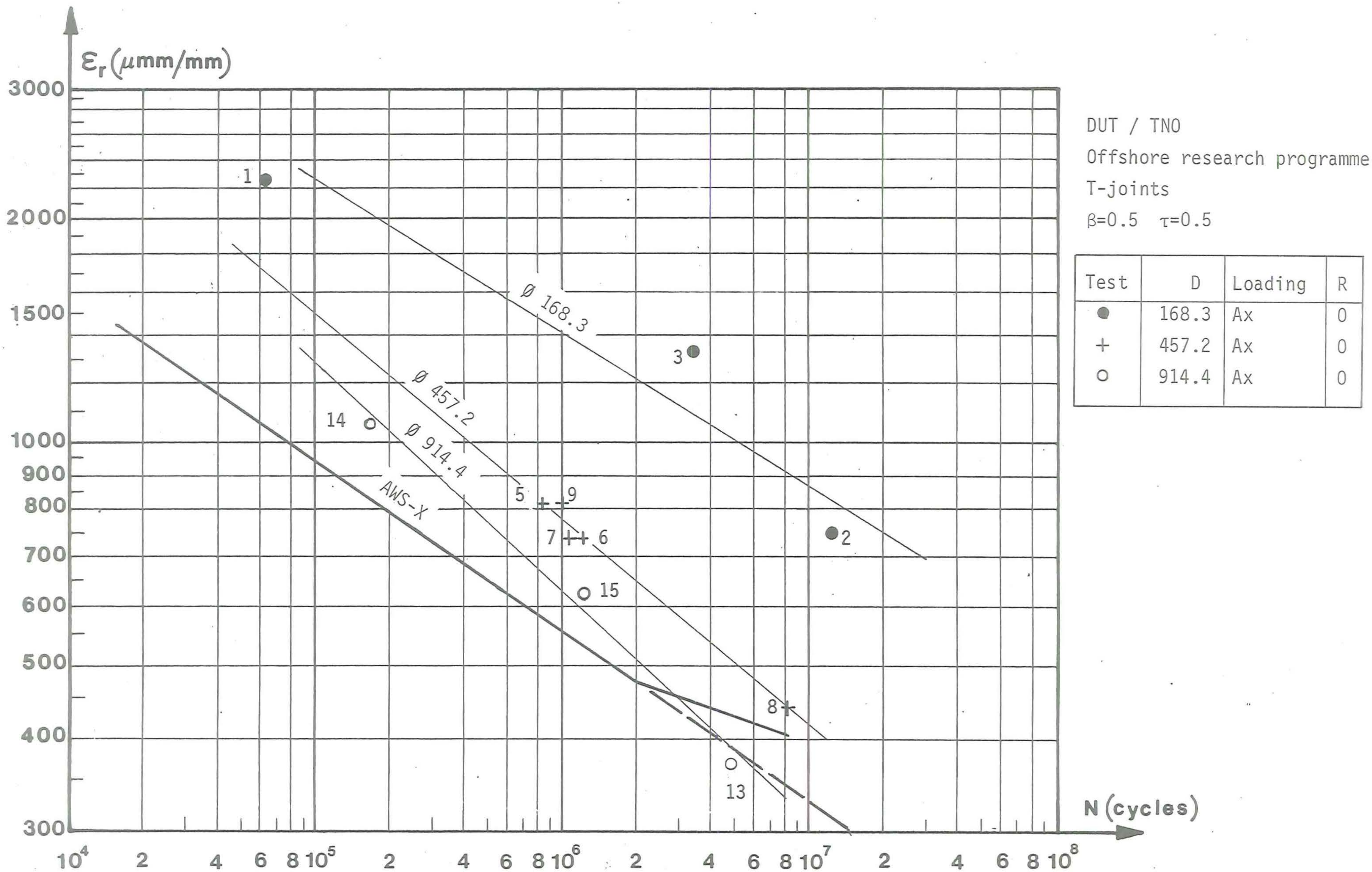

Fig.3.4.44 Comparison of fatigue results of different joint sizes based on hot spot strain range

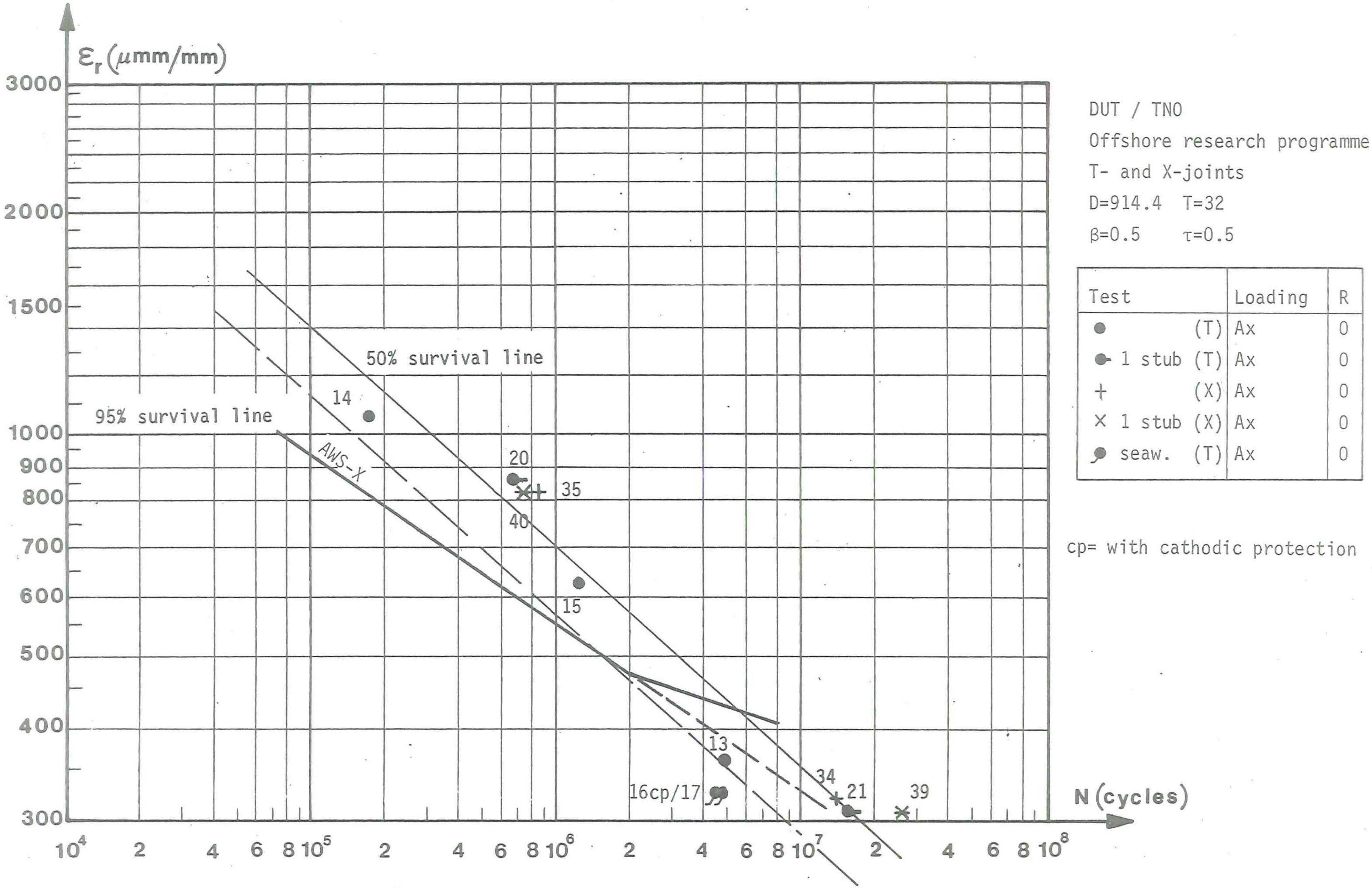

Fig.3.4.43 Fatigue results based on hot spot strain range (Ø914.4 mm)

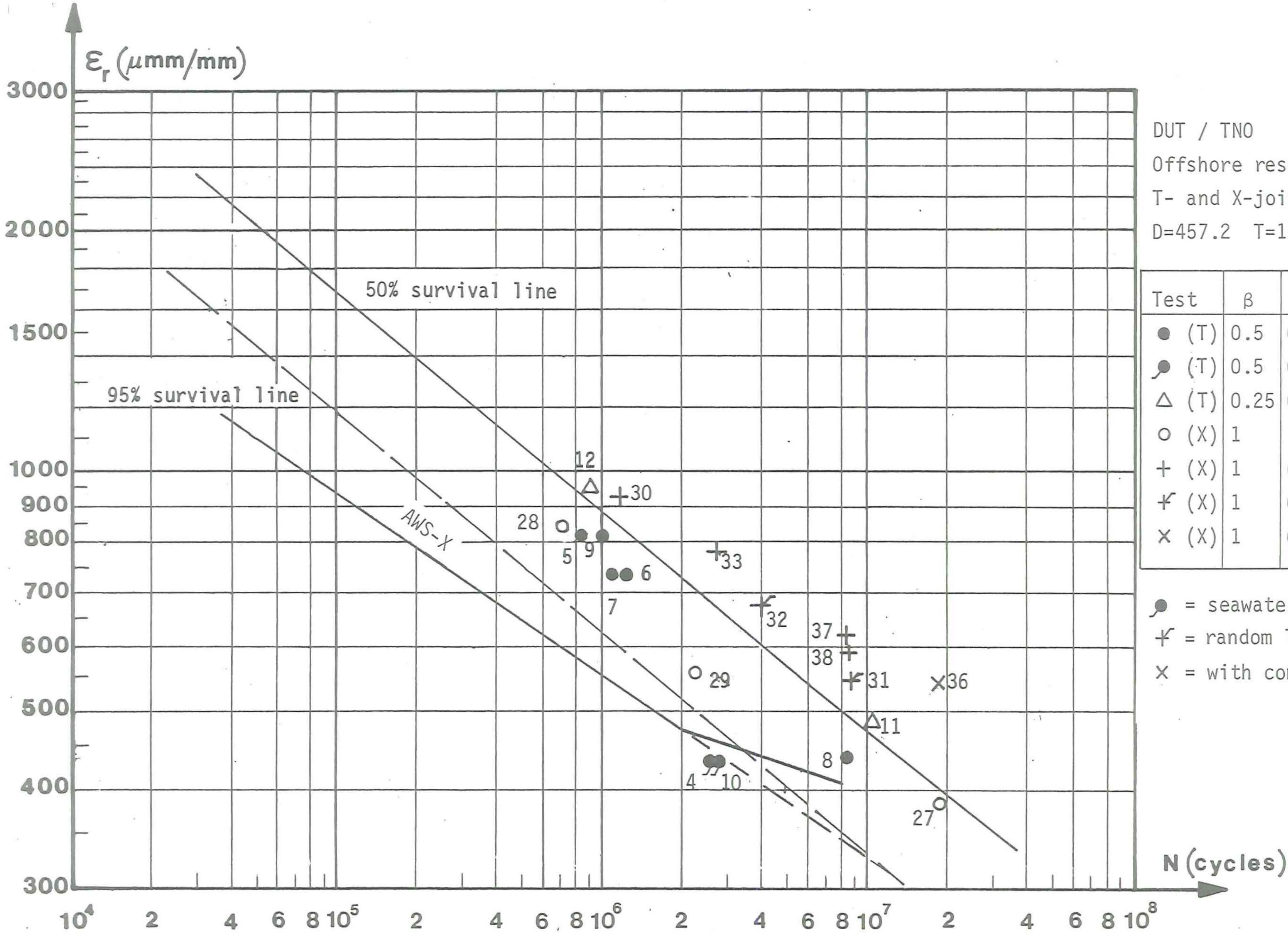

DUT / TNO
Offshore research programme
T- and X-joints
D=457.2 T=16

Test	β	τ	Loading	R
● (T)	0.5	0.5	Ax	0
● (seawater symbol) (T)	0.5	0.5	Ax	10= 0 4=-1
△ (T)	0.25	0.39	Ax	-1
○ (X)	1	1	Ax	-1
+ (X)	1	0.55	Ax	-1
+ (random loading symbol) (X)	1	0.55	Ax	-1
× (X)	1	0.55	Ax	-1

● (seawater symbol) = seawater test
+ (random loading symbol) = random loading
× = with compressive chord load

Fig.3.4.42 fatigue results based on hot spot strain range (Ø457.2 mm)

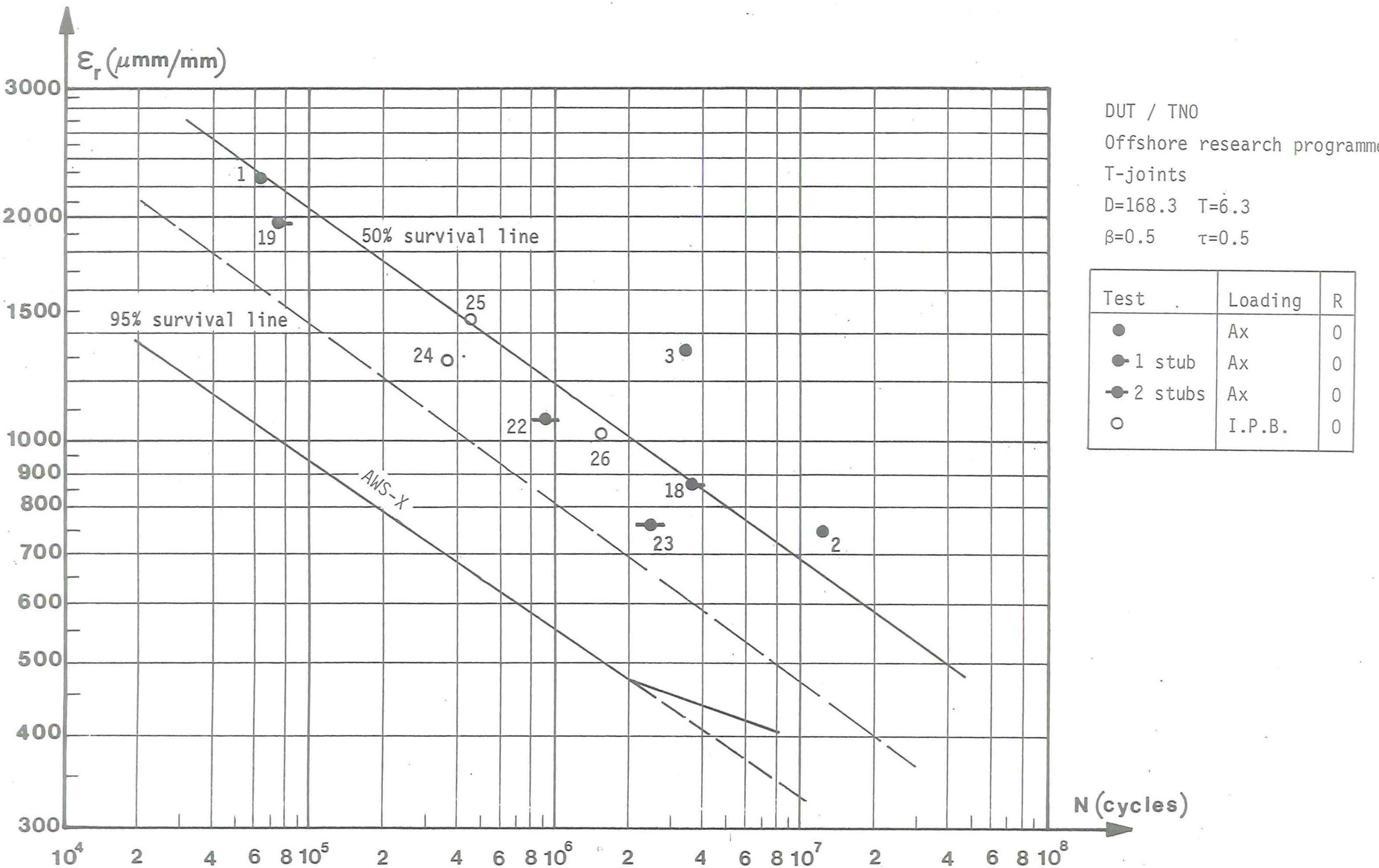

Fig.3.4.41 Fatigue results based on hot spot strain-range (Ø168.3 mm)

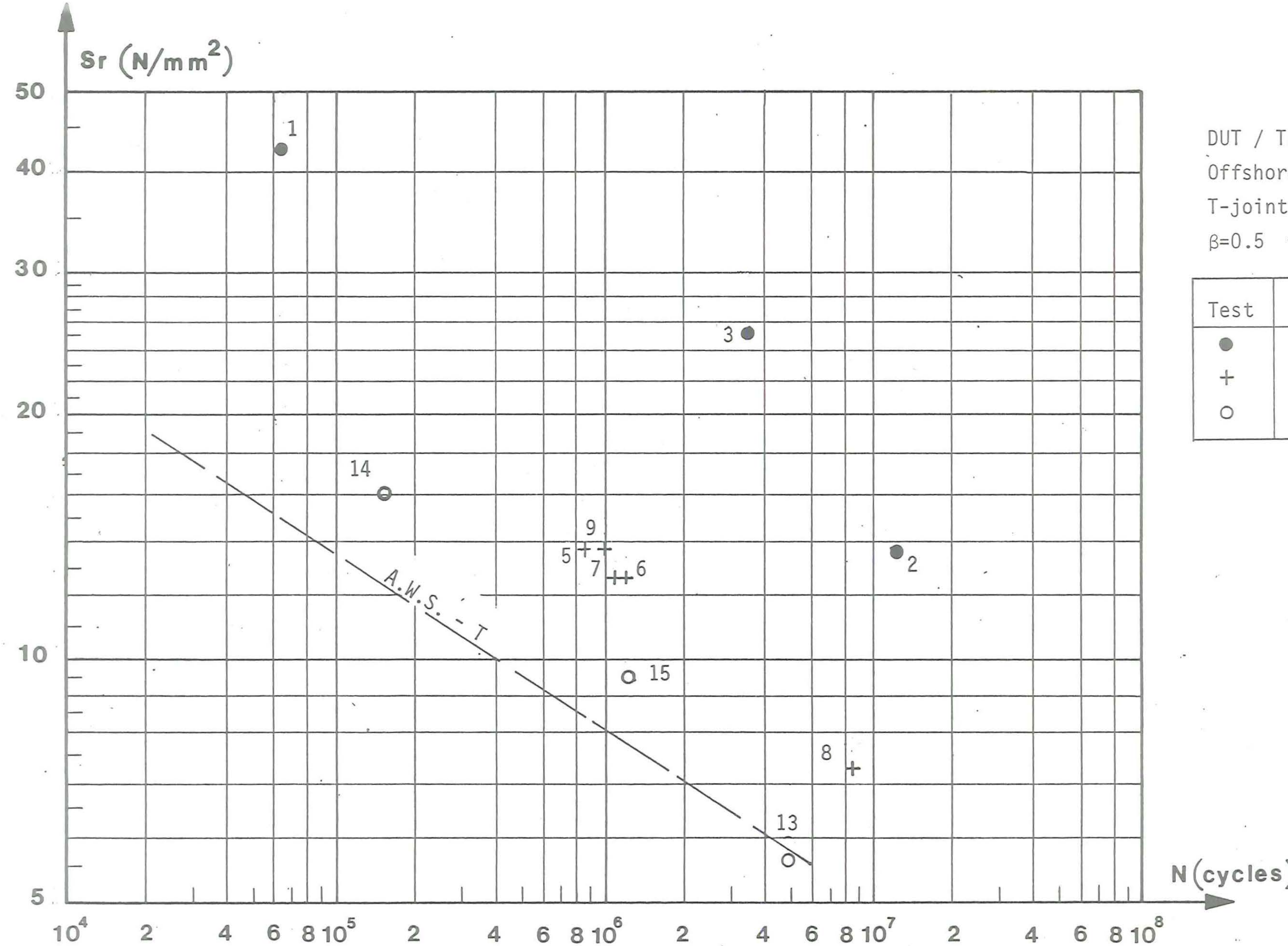

DUT / TNO
Offshore research programme
T-joints
β=0.5 τ=0.5

Test	D	Loading	R
●	168.3	Ax	0
+	457.2	Ax	0
o	914.4	Ax	0

Fig.3.4.40 Comparison of fatigue results of different joint sizes based on punching shear-range

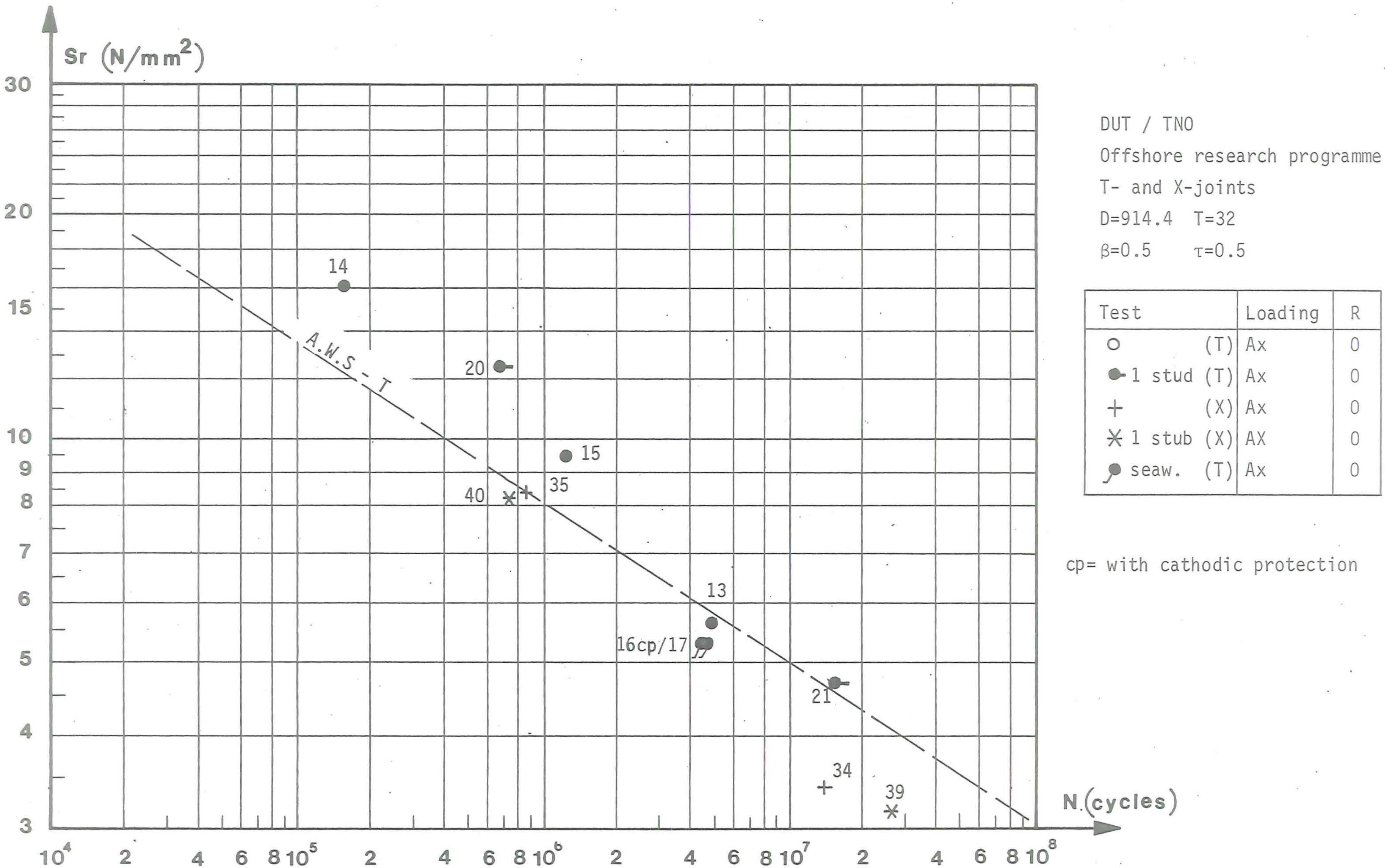

Fig.3.4.39 Fatigue results based on punching shear-range (Ø914.4 mm)

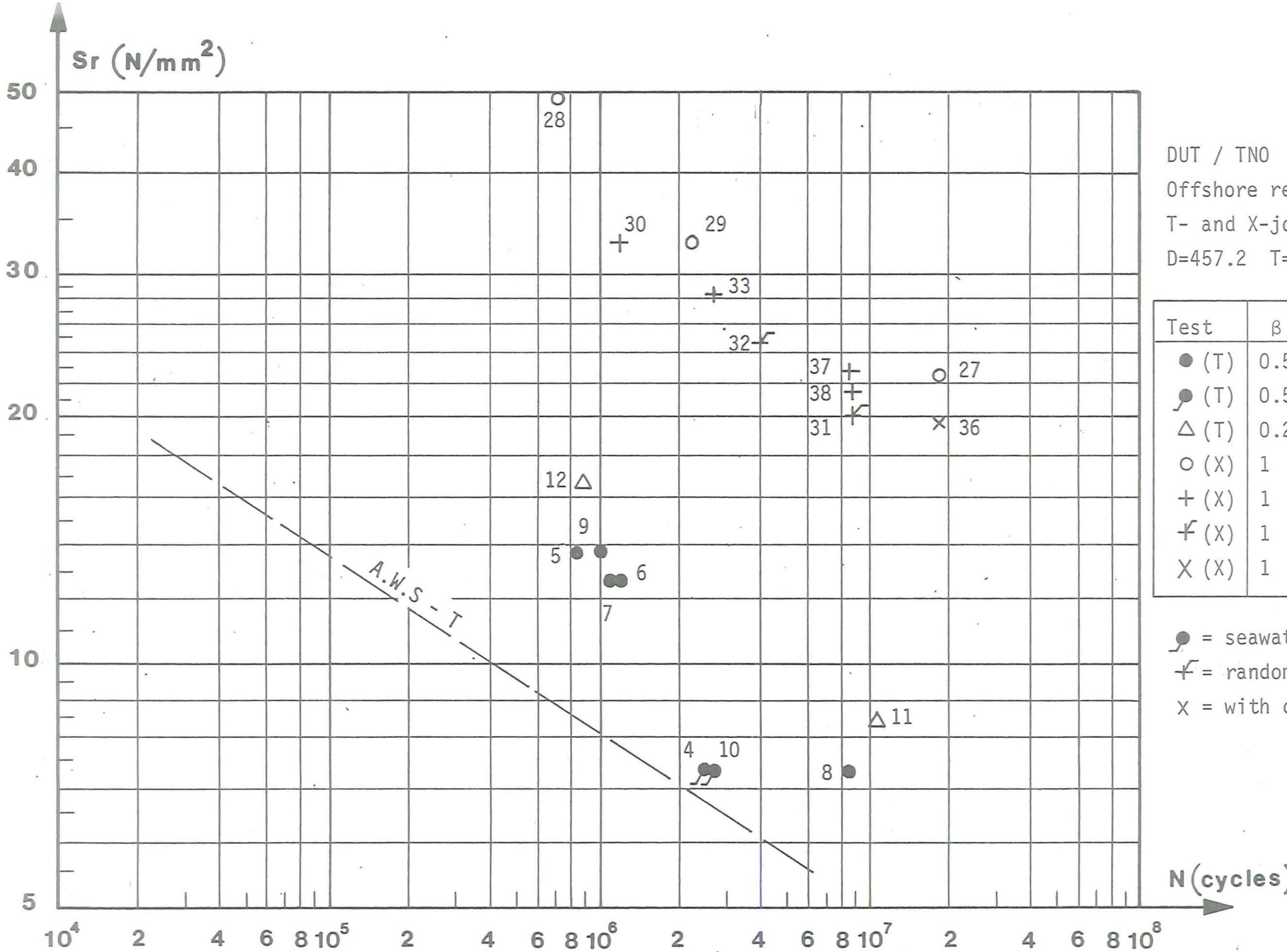

DUT / TNO
Offshore research programme
T- and X-joints
D=457.2 T=16

Test	β	τ	Loading	R
● (T)	0.5	0.5	Ax	0
●̸ (T)	0.5	0.5	Ax------	10= 0 4=-1
△ (T)	0.25	0.39	Ax	-1
○ (X)	1	1	Ax	-1
+ (X)	1	0.55	Ax	-1
+̸ (X)	1	0.55	Ax	-1
X (X)	1	0.55	Ax	-1

●̸ = seawater
+̸ = random loading
X = with compressive chord load

Fig.3.4.38 Fatigue results based on punching shear-range (Ø457.2 mm)

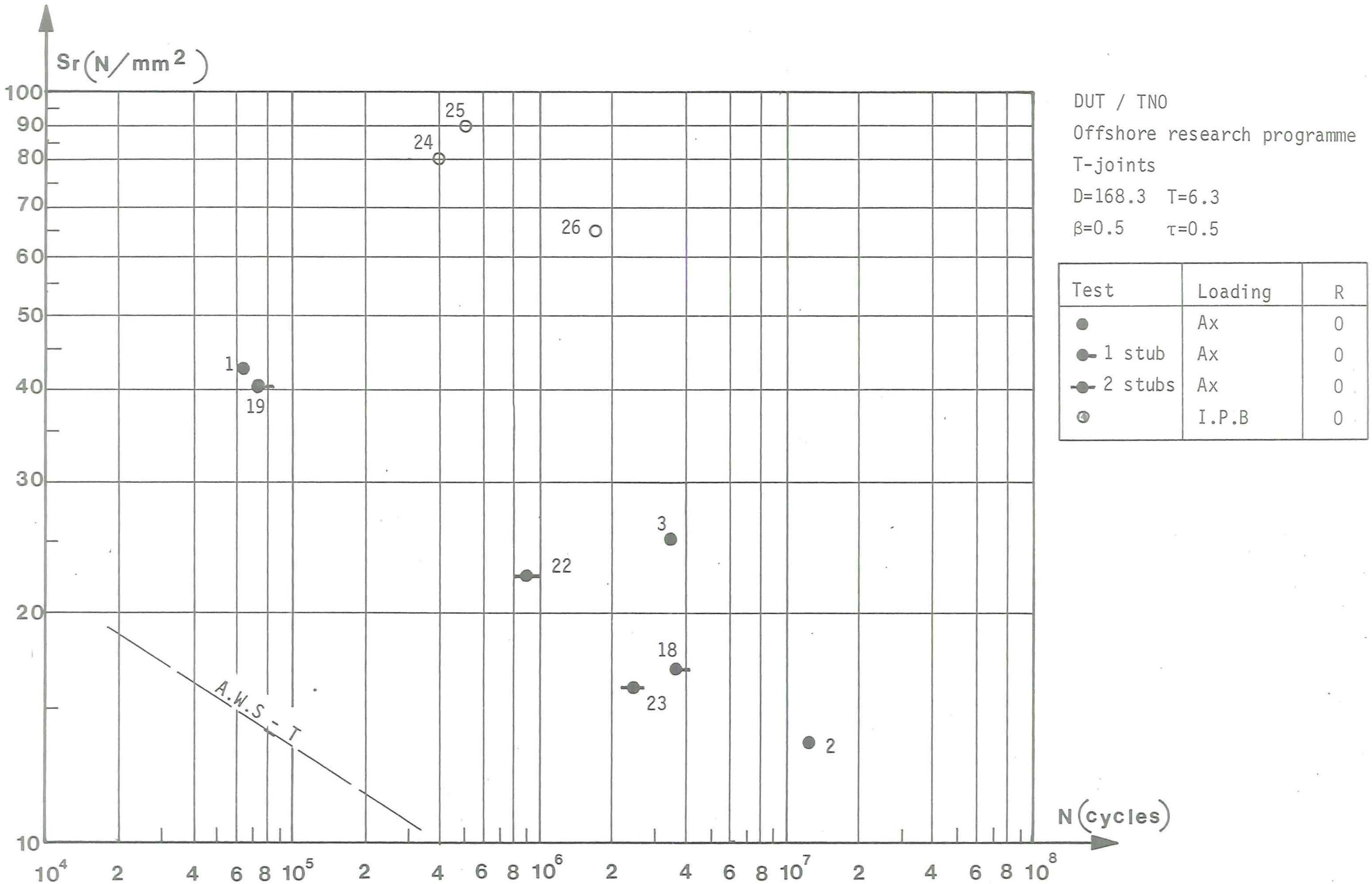

Fig.3.4.37 Fatigue results based on punching shear-range (ø168.3 mm)

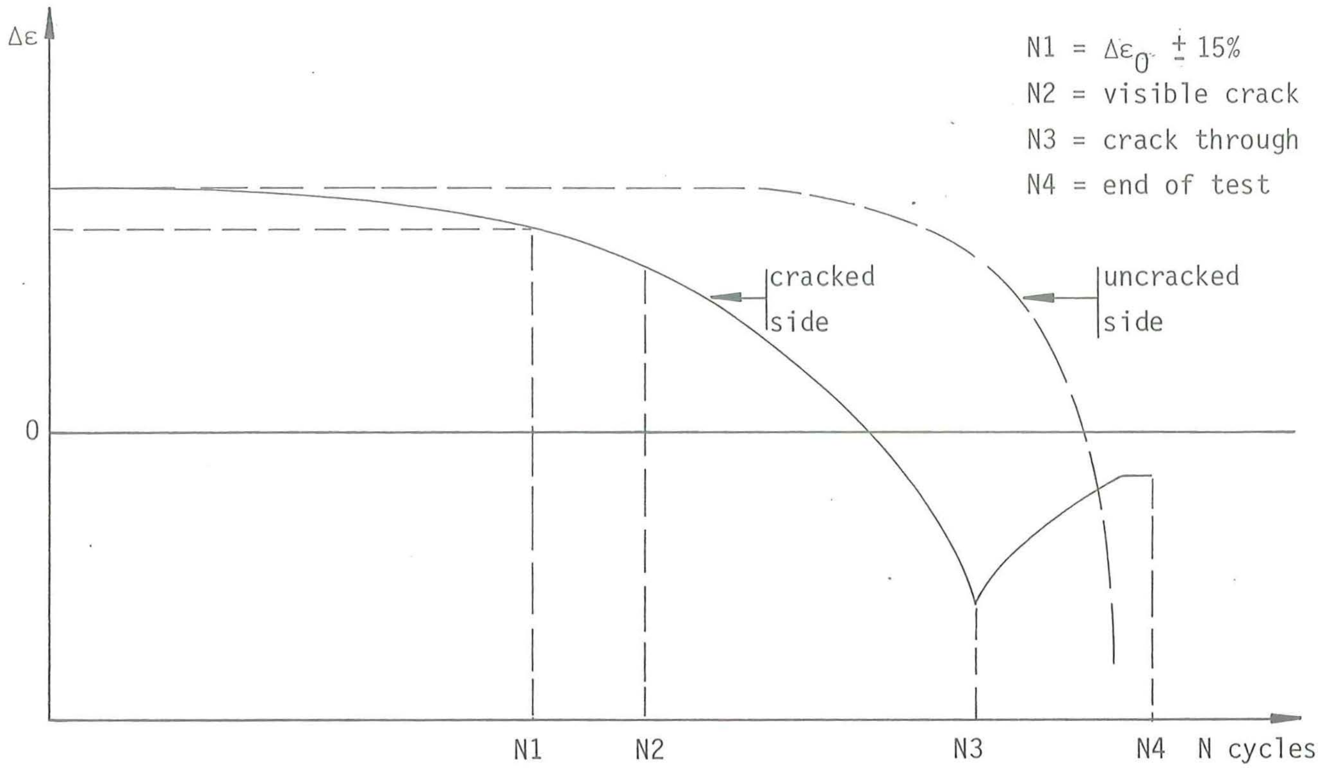

Fig.3.4.36 Typical relation between strainrange and number of cycles for T-joints

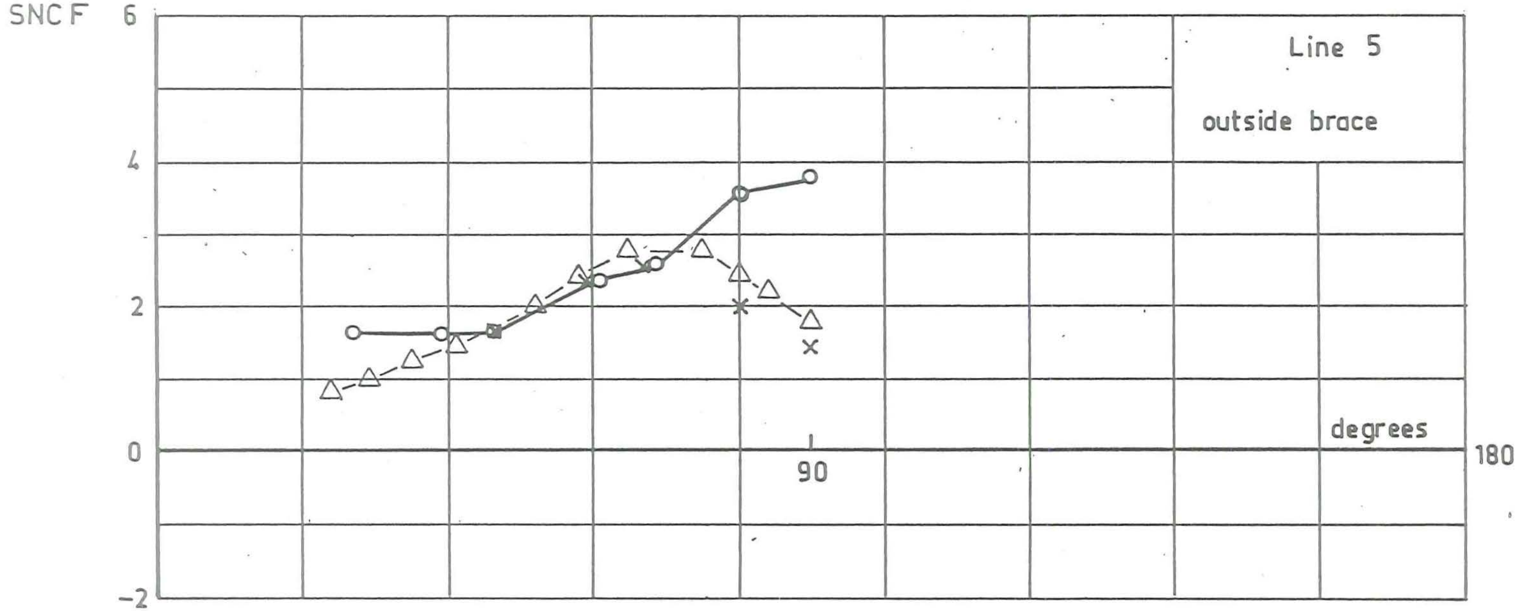

SPECIMEN	36
static load	520 kN
β	1.0
τ	0.55
γ	14.3
chorddim.	ϕ 457.2-16
$\sqrt{r.t}$	44.8
×	test results
—o—	FE program SATE
—Δ—	FE program I.S.

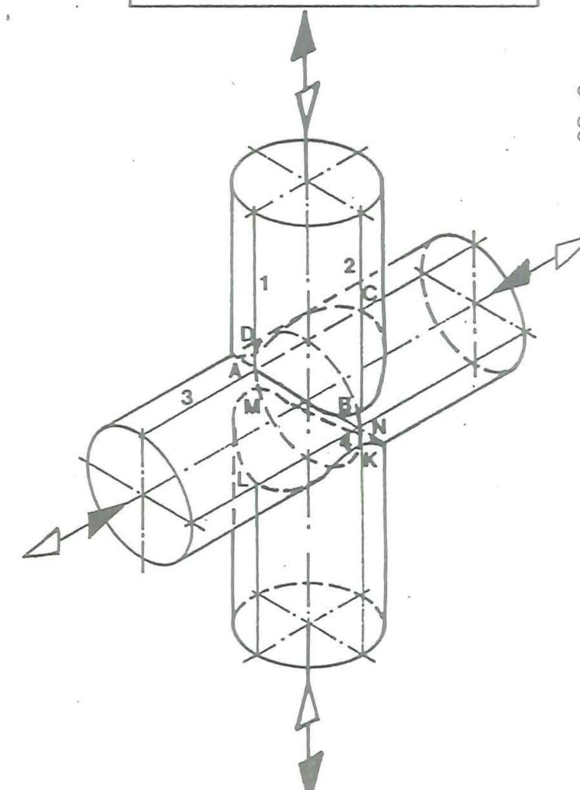

Fig.3.4.35 Specimen 36 : SNCF Comparison (measured/FE) along line 5 (outside brace)

At 90^0 the SNCF values calculated with the F.E program SATE deviates considerable from the measured values. Therefore this area is subjected to a more extensive investigation. The calculation with the SATE program are carried out with thin shell elements in which the mean-diameter plane of the tube is used. This results in a $\beta \neq 1$ if $\tau \neq 1$ ($\beta = \frac{D \text{ outside}}{d \text{ outside}}$) . At the Delft University of Technology the calculations are carried out , therefore , with the ICES STRUDL thin shell F.E program in such a way that the $\beta=1$ and $\beta=0.98$. From these calculations it appears that a small deviation of β causes a large variation in strain at 90^0. The calculation with $\beta=1$ is plotted in the diagram and agrees very well with the measurements on the specimen . (3-15)

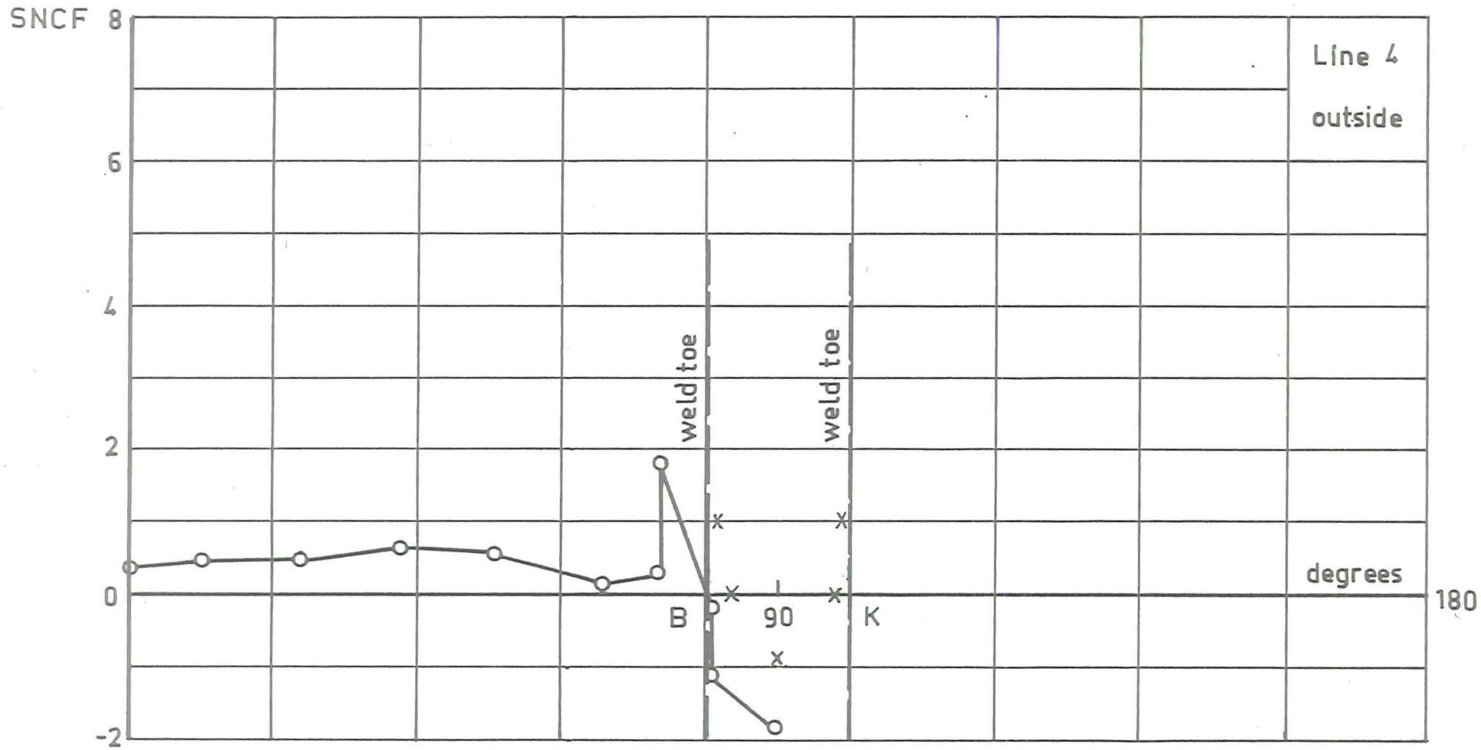

Fig.3.4.33 Specimen 36 : SNCF Comparison (measured/FE) along line 4 (outside)

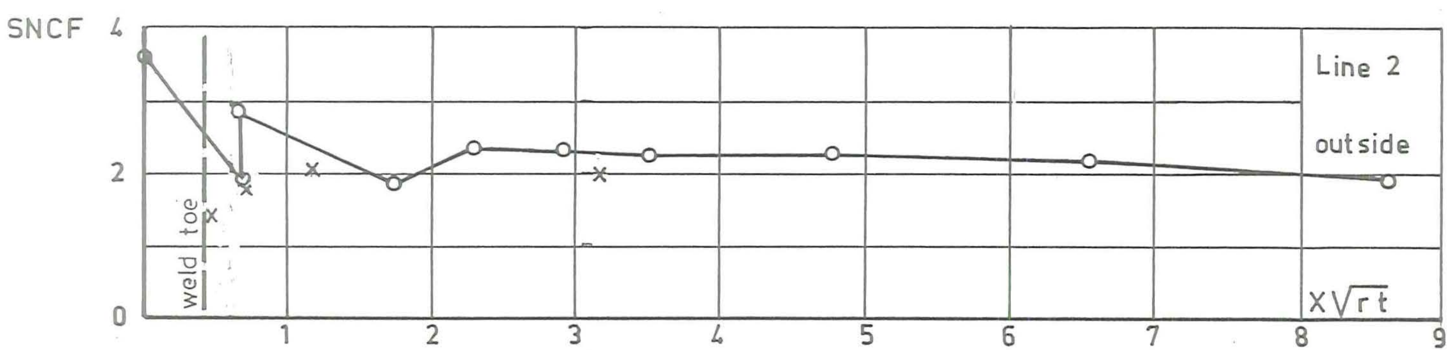

Fig.3.4.34 Specimen 36 : SNCF Comparison (measured/FE) along line 2 (outside)

SPECIMEN	36
static load	520 kN
β	1.0
τ	0.55
γ	14.3
chorddim.	ϕ 457.2-16
$\sqrt{r.t}$	44.85
×	test results
—o—	FE progam SATE

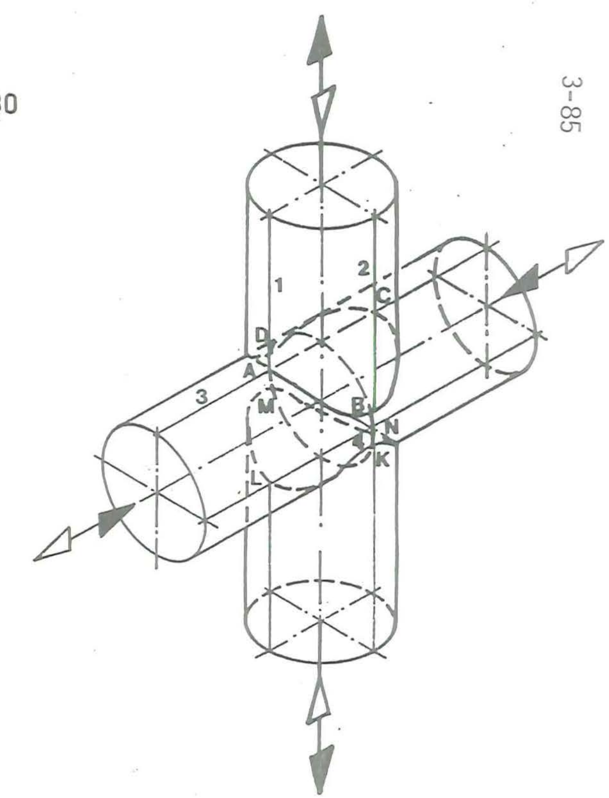

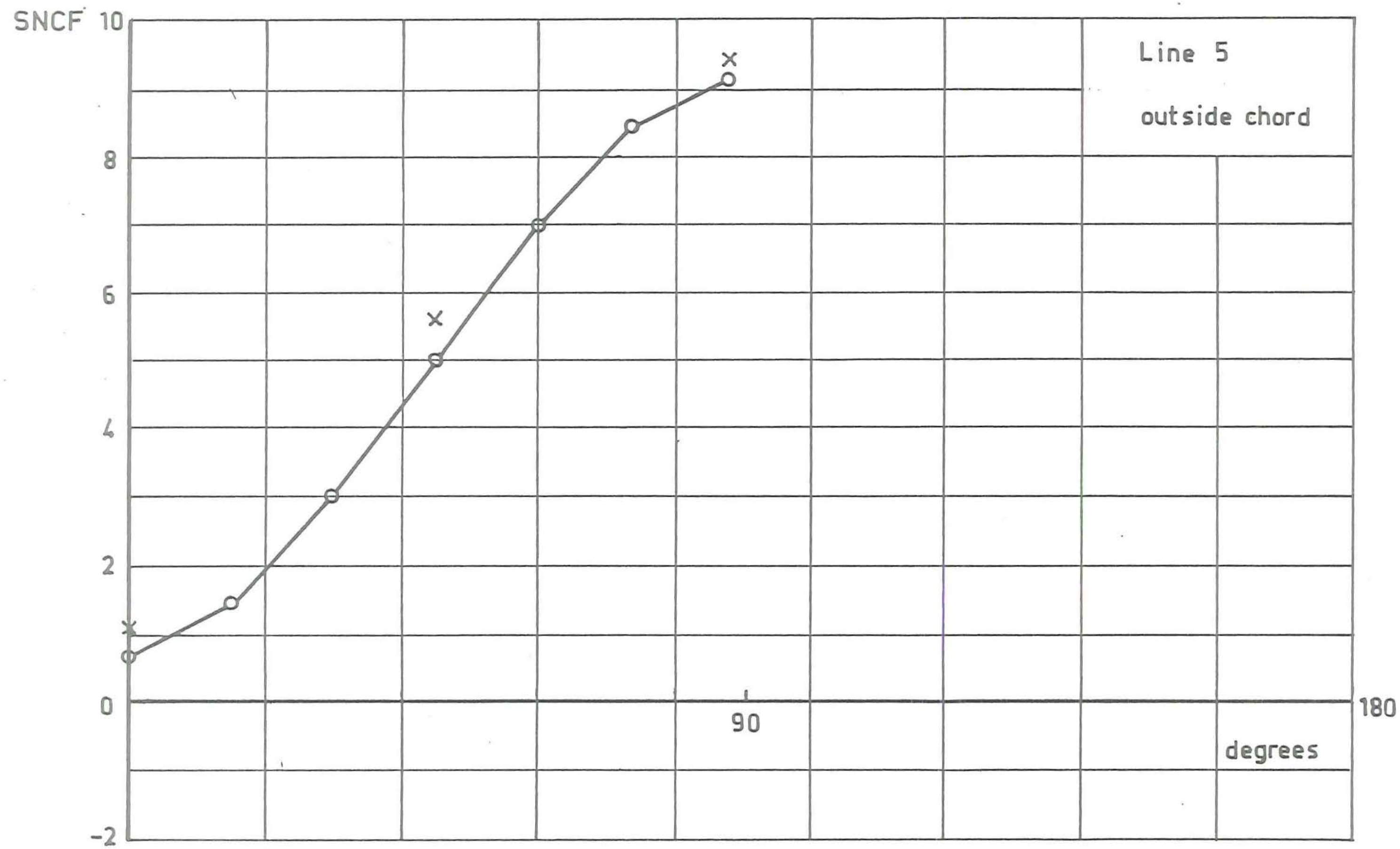

SPECIMEN	35
static load	100 kN
β	0.5
τ	0.5
γ	14.3
chorddim.	ø 914.4 - 32
$\sqrt{r.t}$	60.48 mm
×	test results
—o—	FE program SATE

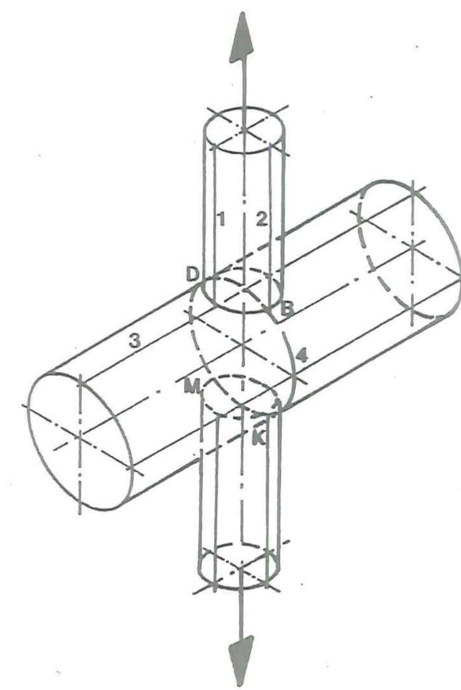

Fig.3.4.32 Specimen 35 : SNCF Comparison (measured/FE) along line 5 (outside chord)

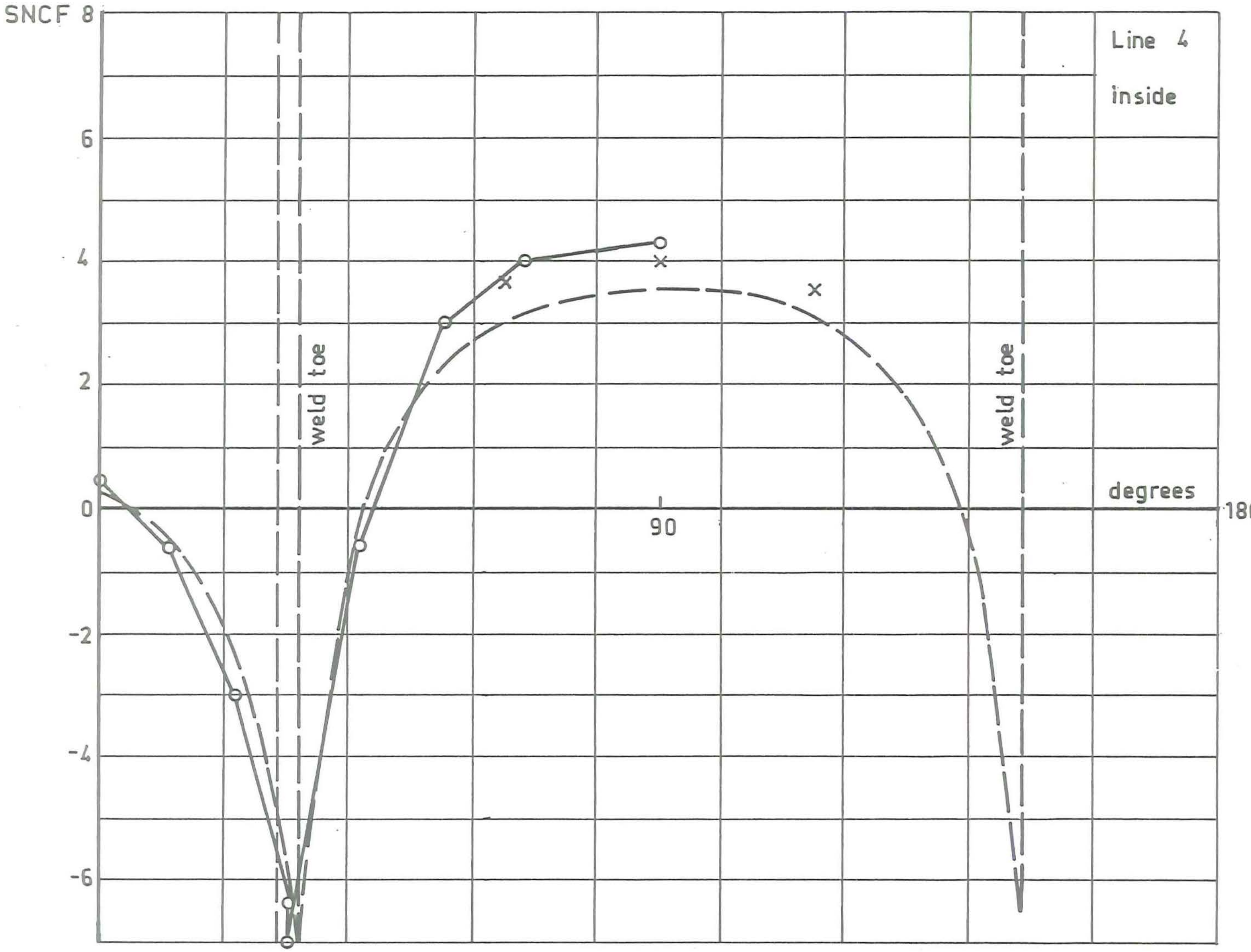

SPECIMEN	35
static load	100 kN
β	0.5
τ	0.5
γ	14.3
chorddim.	ϕ 914.4-32
$\sqrt{r.t}$	60.48 mm
x	test results
—o—	FE program SATE
— — —	FE program ASKA

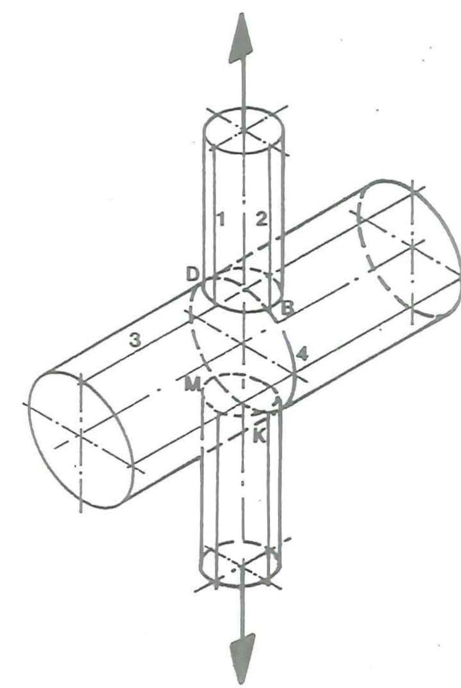

Fig.3.4.31 Specimen 35 : SNCF Comparison (measured/FE) along line 4 (inside)

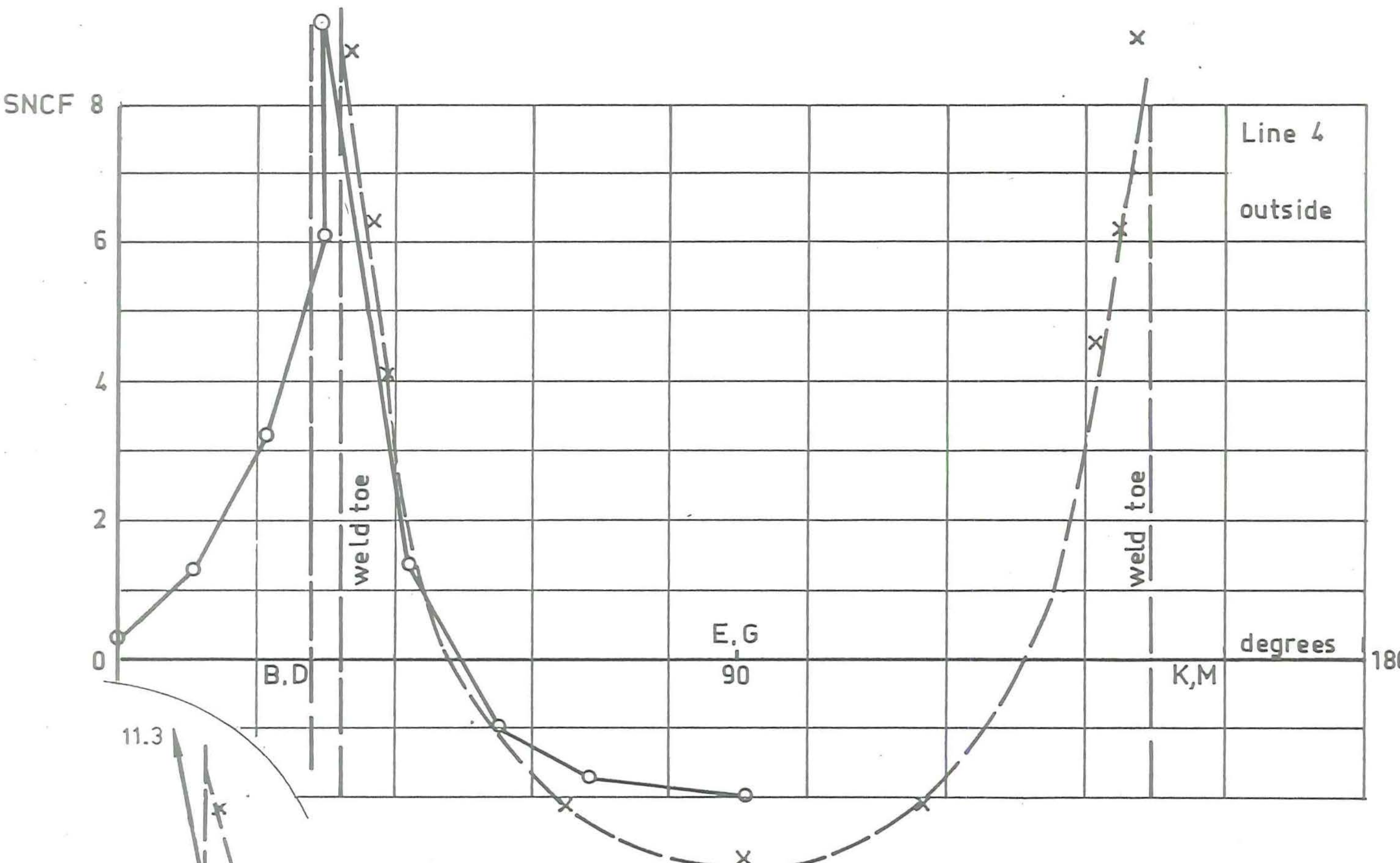

Fig.3.4.29 Specimen 35 : SNCF Comparison (measured/FE) along line 4 (outside)

SPECIMEN	35
static load	100 kN
β	0.5
τ	0.5
γ	14.3
chorddim.	ϕ 914.4 - 32
$\sqrt{r.t}$	60.48 mm
×	test results
—o—	FE program SATE
– – – –	FE program ASKA

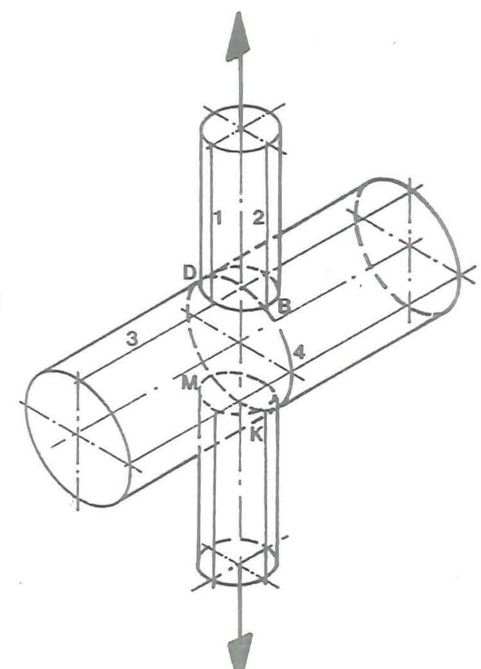

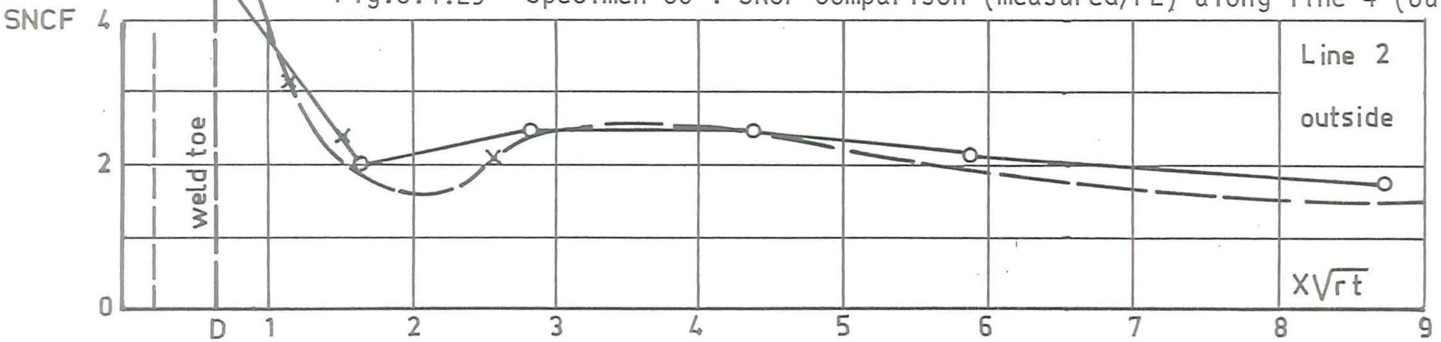

Fig.3.4.30 Specimen 35 : SNCF Comparison (measured/FE) along line 2 (outside)

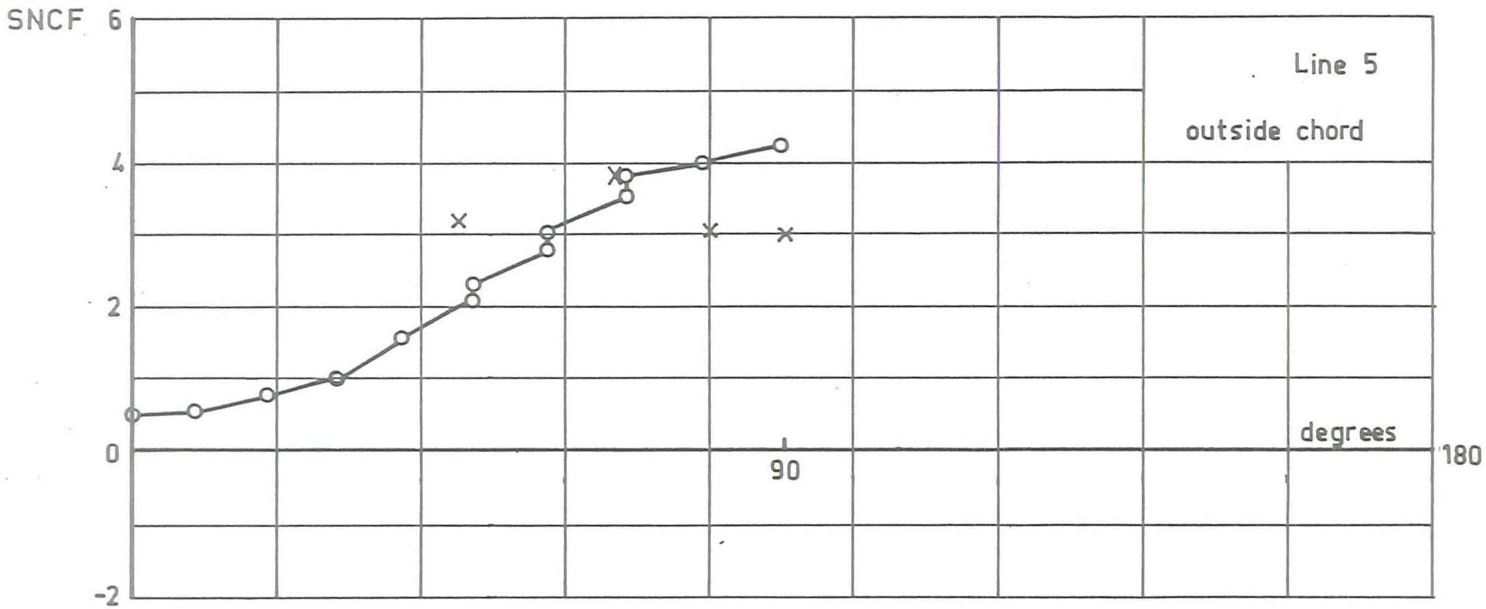

Fig.3.4.28 Specimen 28 : SNCF Comparison (measured/FE) along line 5 (outside chord)

SPECIMEN	28
static load	650 kN
β	1.0
τ	1.0
γ	14.3
chorddim.	457.2−16
$\sqrt{r.t}$	60.48
×	test results
—o—	FE program SATE

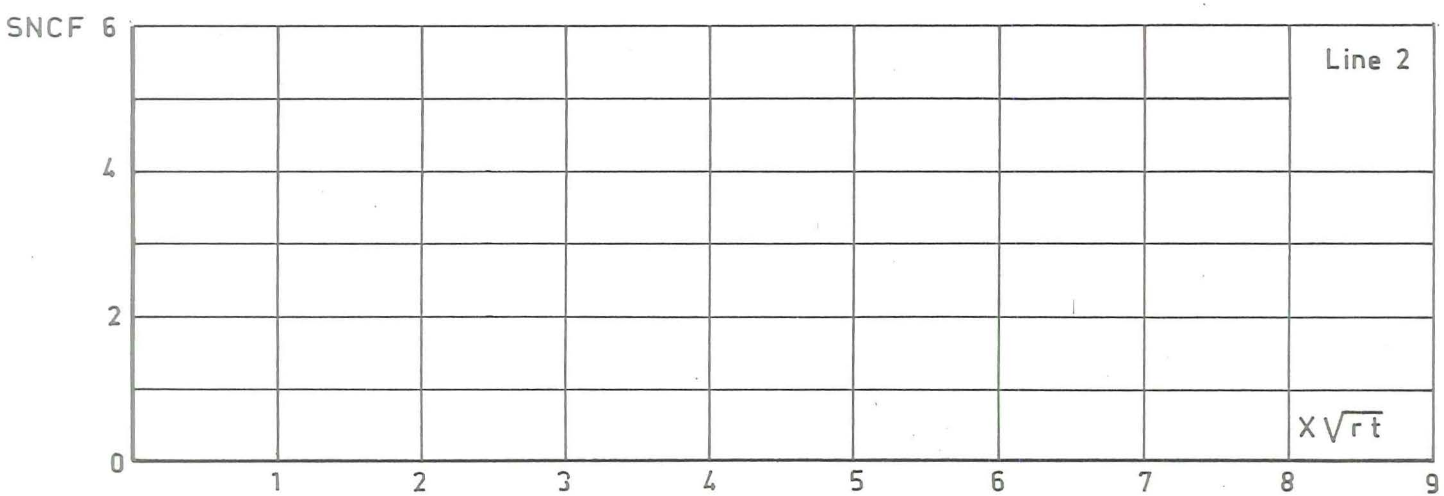

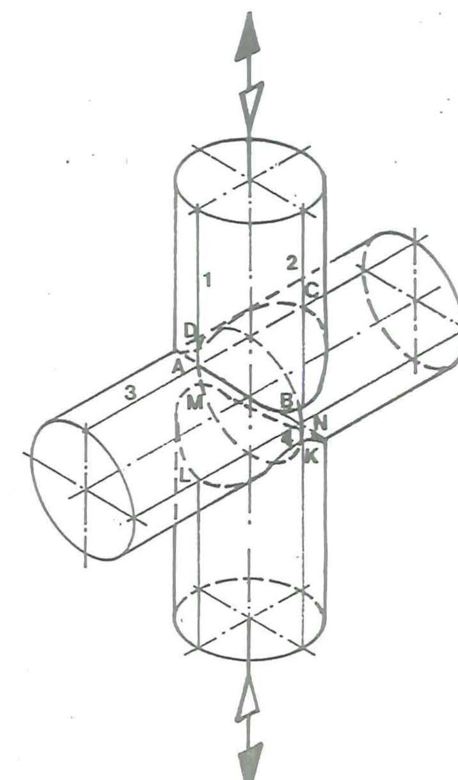

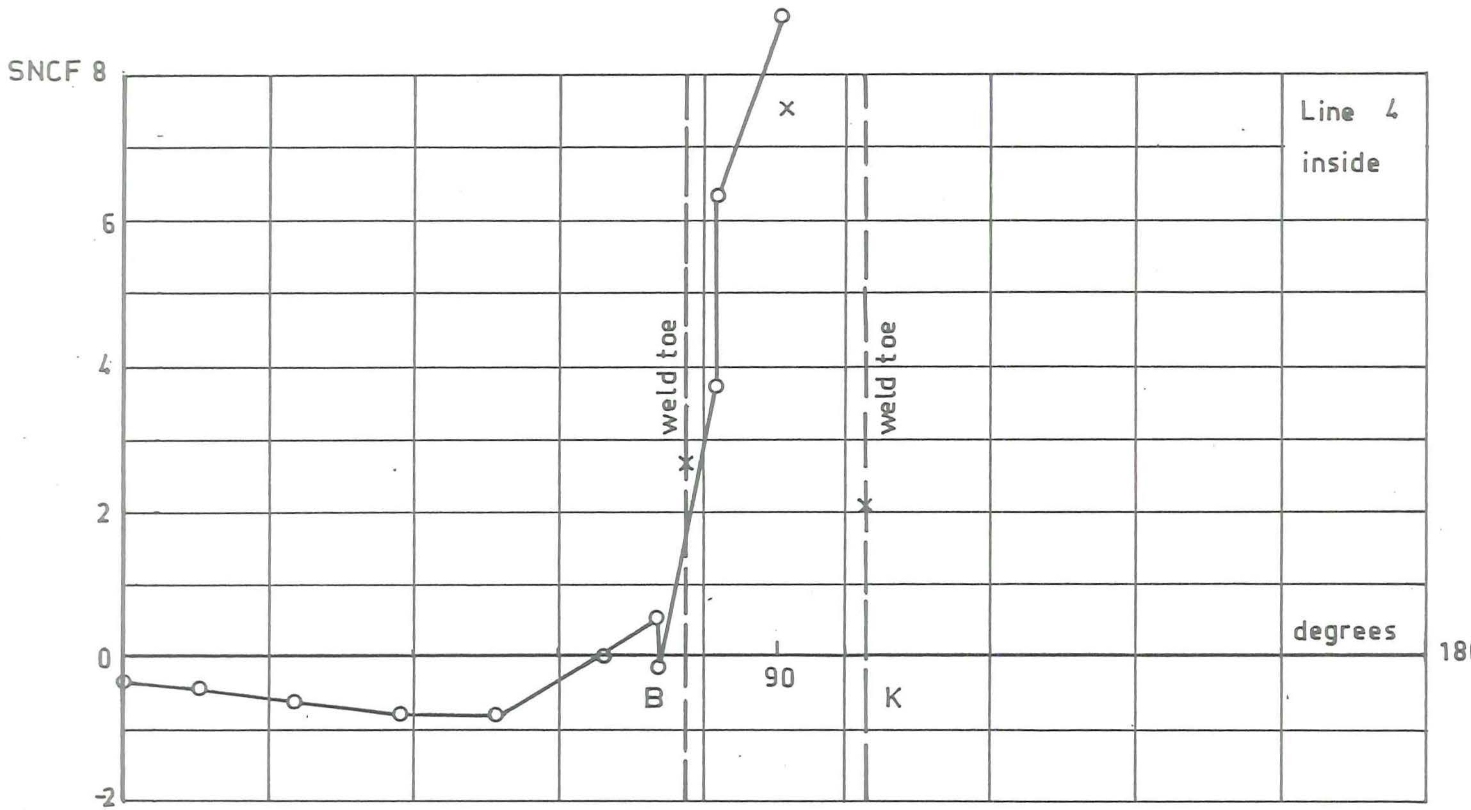

Fig.3.4.27 Specimen 28 : SNCF Comparison (measured/FE) along line 4 (inside)

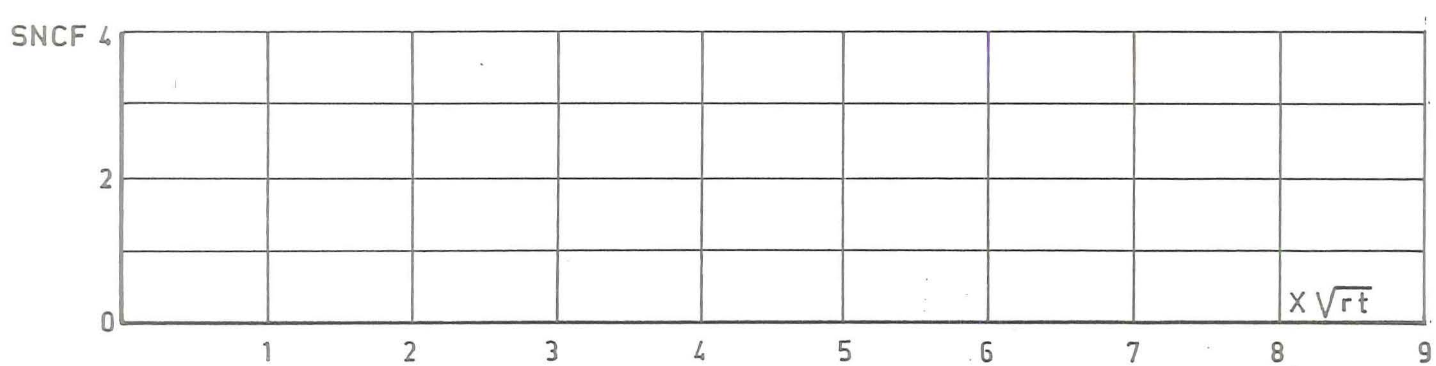

SPECIMEN	28
static load	650 kN
β	1.0
τ	1.0
γ	14.3
chorddim.	ϕ 457.2–16
$\sqrt{r.t}$	60.48 mm
×	test results
—o—	FE program SATE

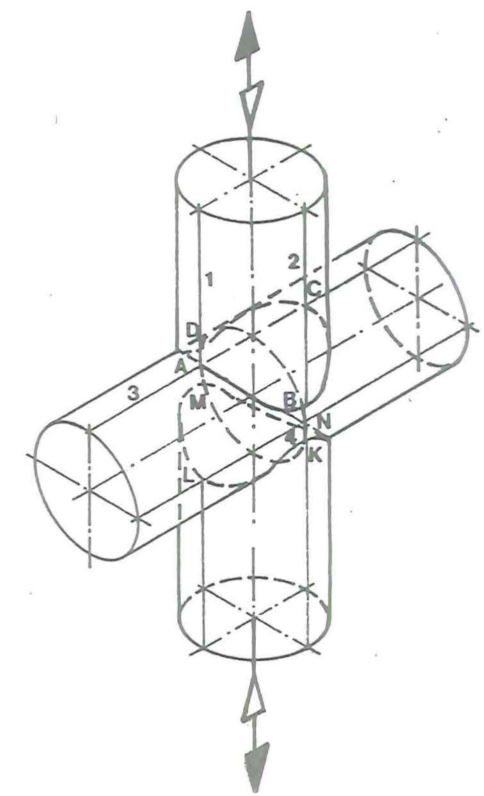

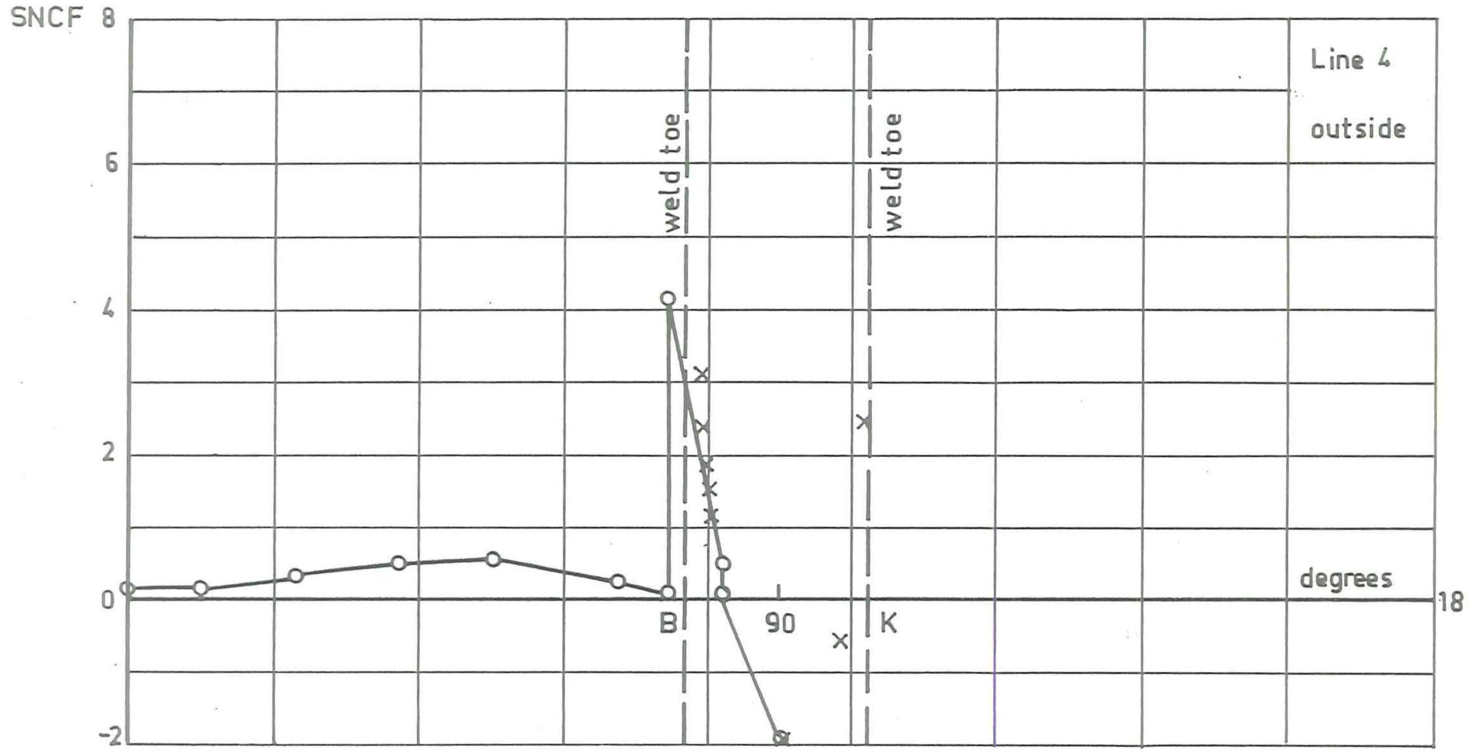

Fig.3.4.25 Specimen 28 : SNCF Comparison (measured/FE) along line 4 (outside)

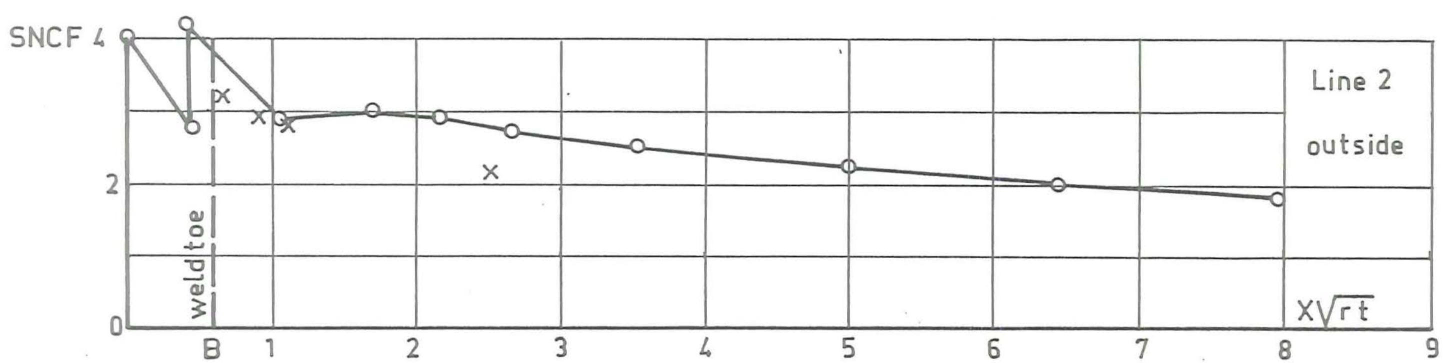

Fig.3.4.26 Specimen 28 : SNCF Comparison (measured/FE) along line 2 (inside)

SPECIMEN	28
static load	650 kN
β	1.0
τ	1.0
γ	14.3
chorddim.	ϕ 457.2-16
$\sqrt{r.t}$	60.48 mm
×	test results
—o—	FE program SATE

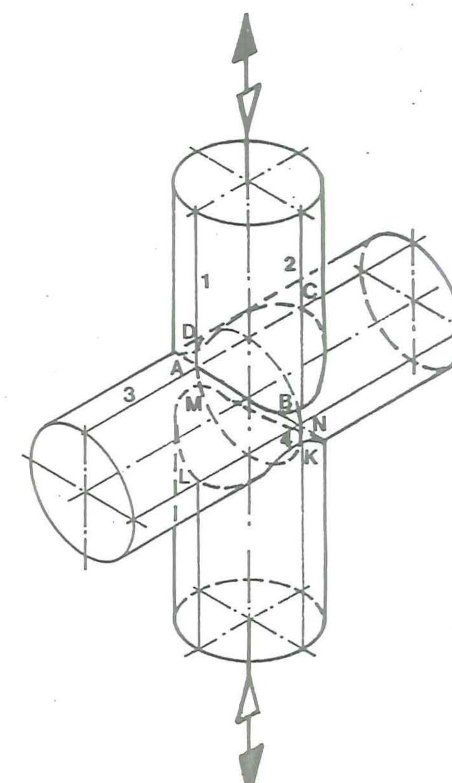

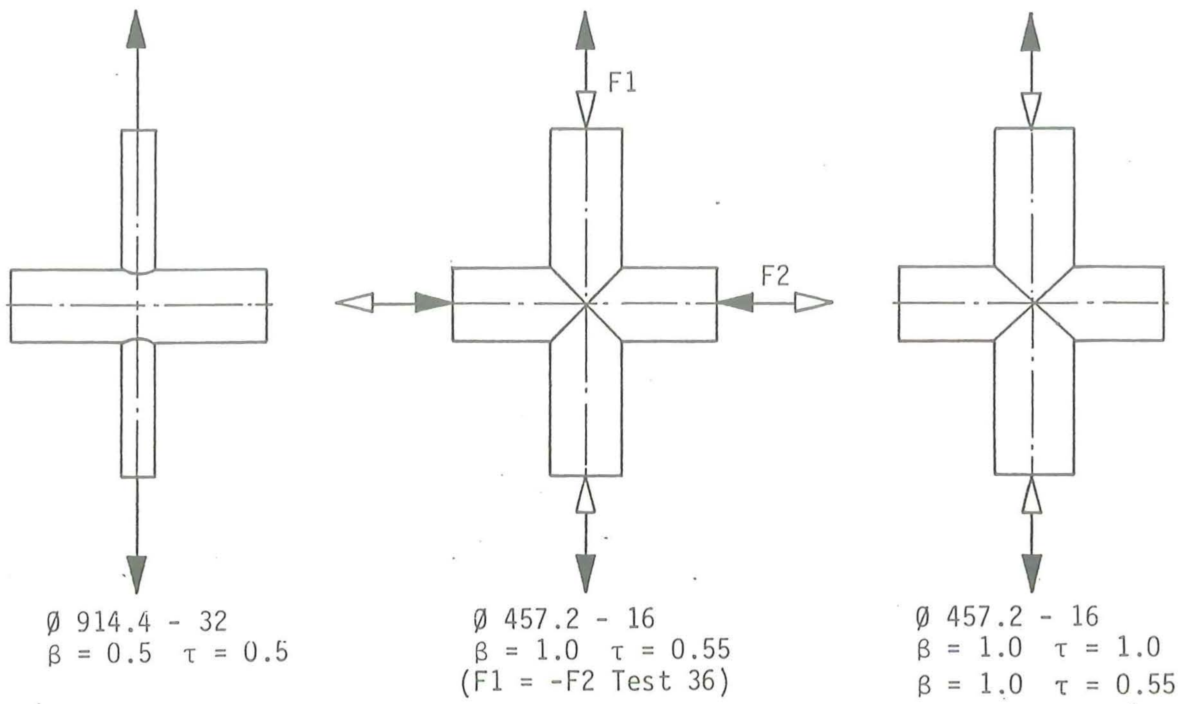

Fig.3.4.24 Loading cases for the joints used in the FE calculation

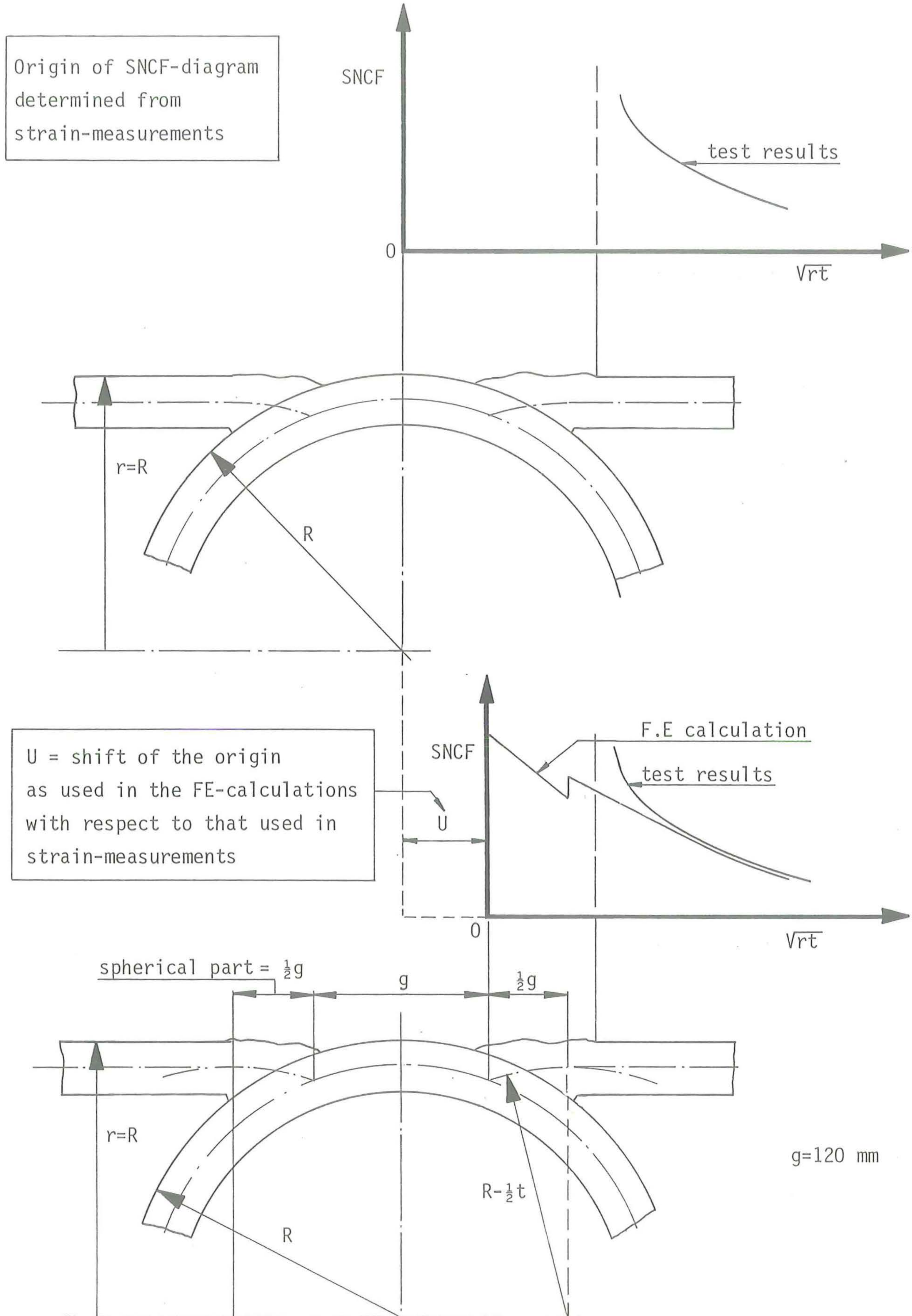

Fig.3.4.23 Location of the origin in the SNCF diagram for joints with β = 1.0

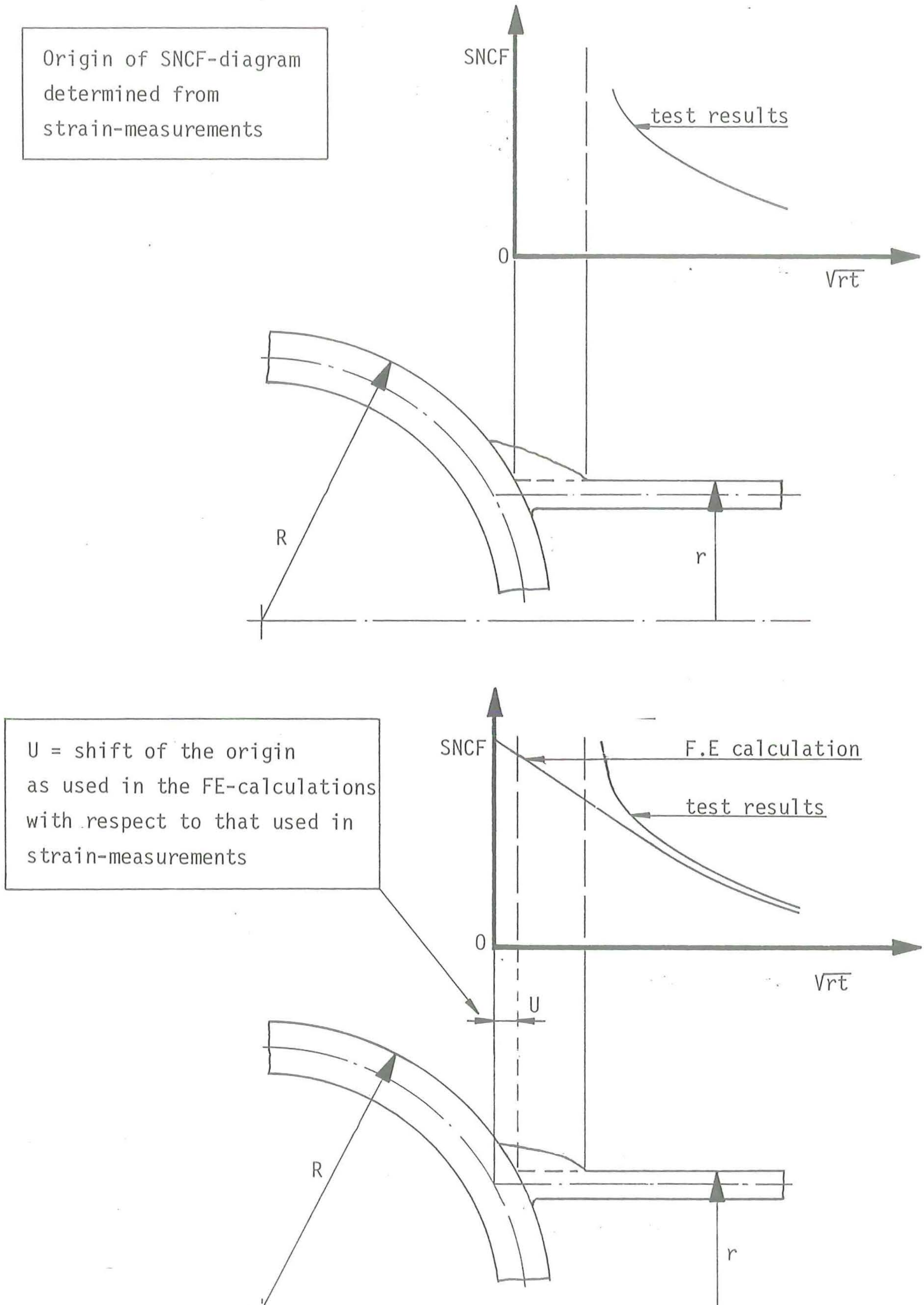

Fig.3.4.22 Location of the origin in the SNCF diagram for joints with $\beta = 0.5$

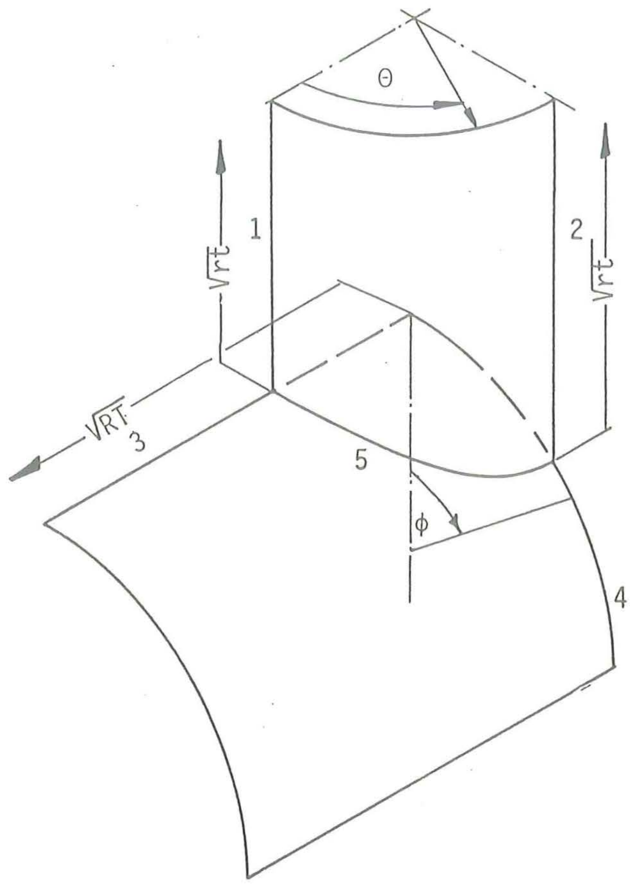

Fig.3.4.21 Indication of the lines (1,2,3,4 and 5) and the angles (φ and θ)

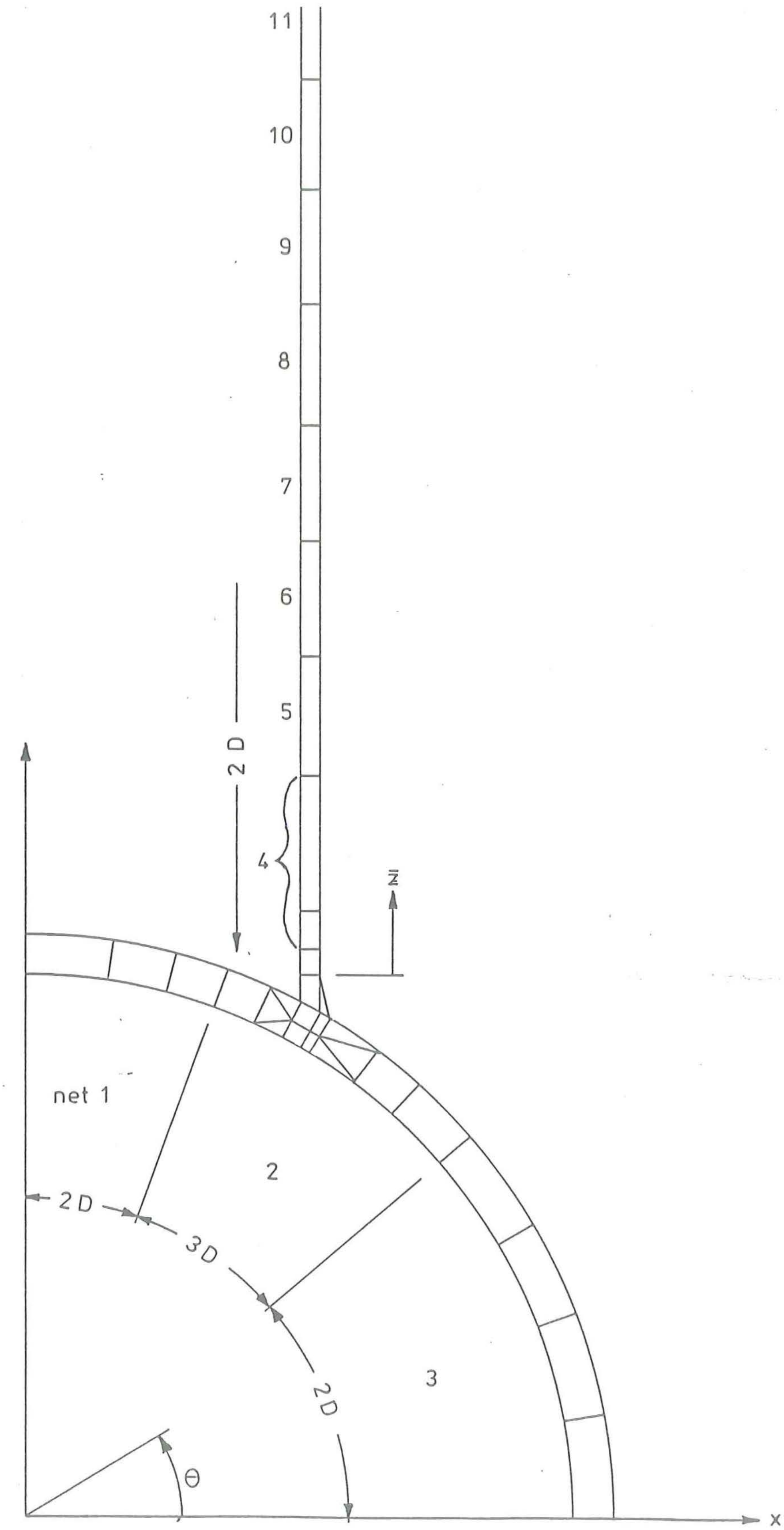

Fig.3.4.20 Element mesh as used in the FE-programme ASKA for X-joints with $\beta = 0.5$

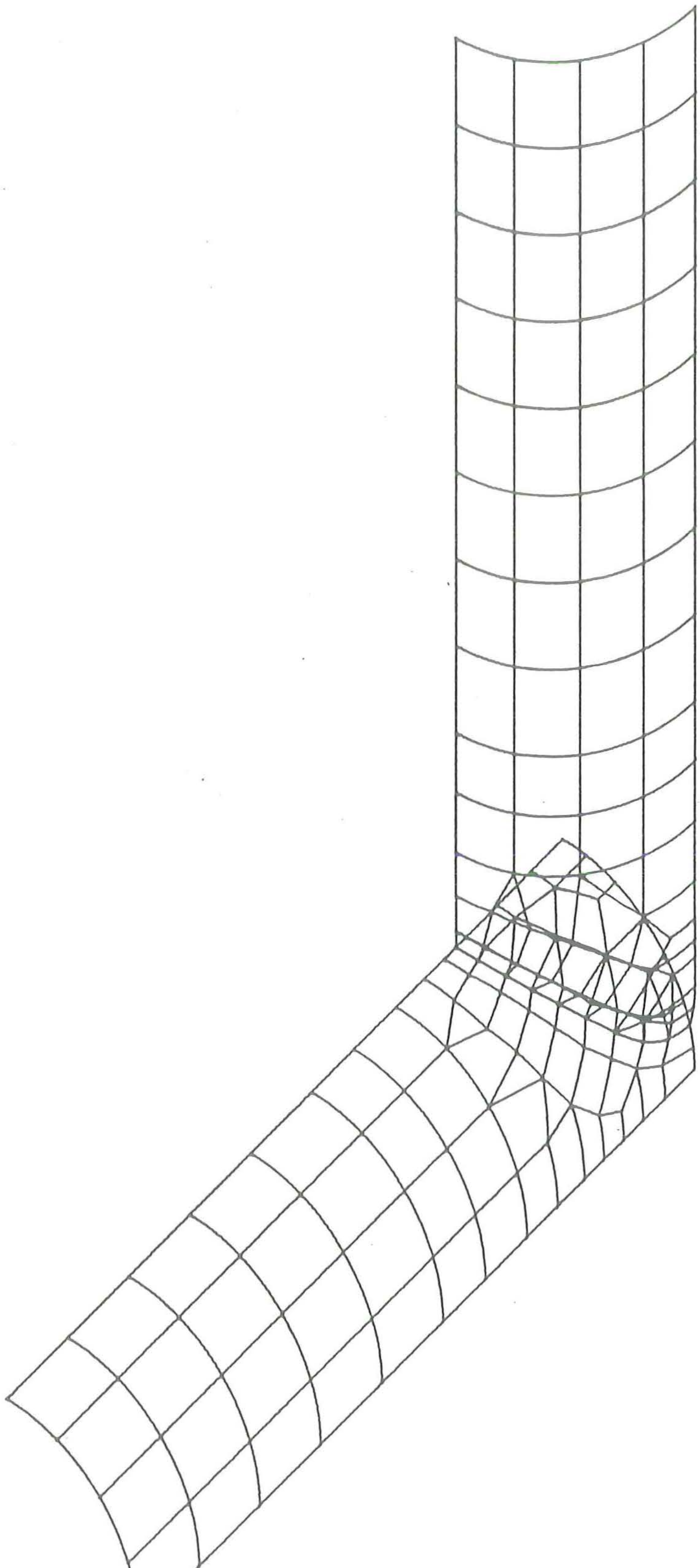

Fig.3.4.19 Element mesh as used in the FE-programme SATE for X-joints with $\beta = 1.0$

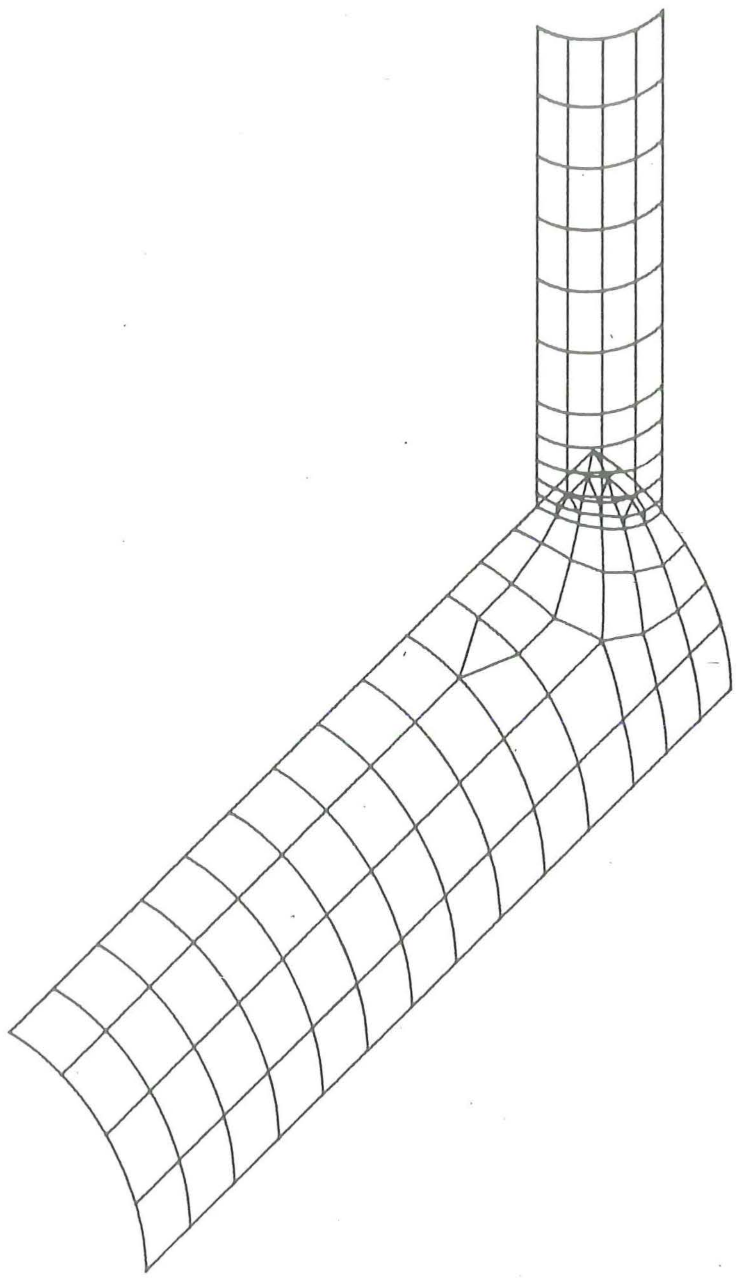

Fig.3.4.18 Element mesh as used in the FE-programme SATE for X-joints with $\beta = 0.5$

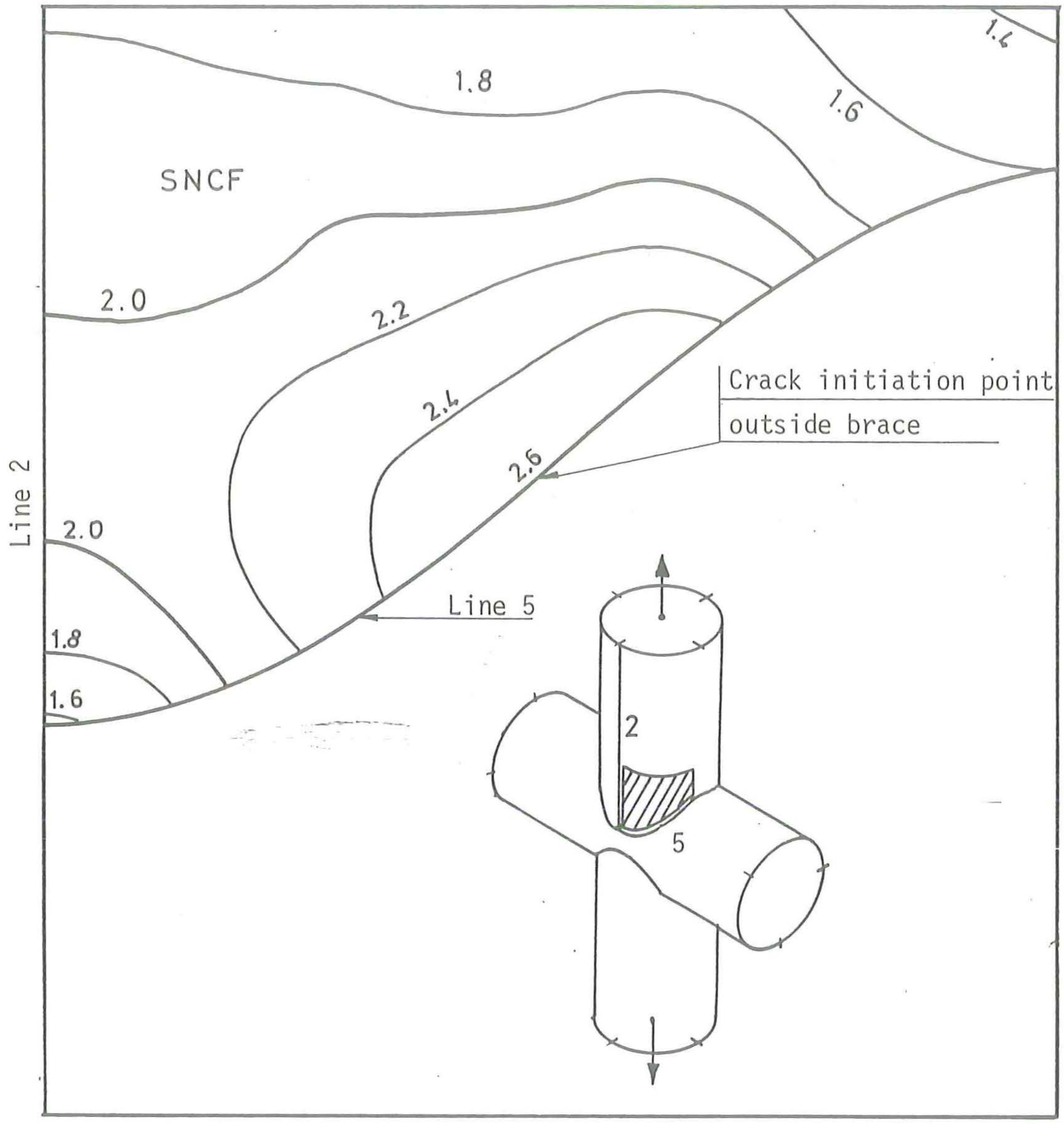

Fig.3.4.17 Strain measurements along line 5 for X-joints β=1.0 τ=0.5

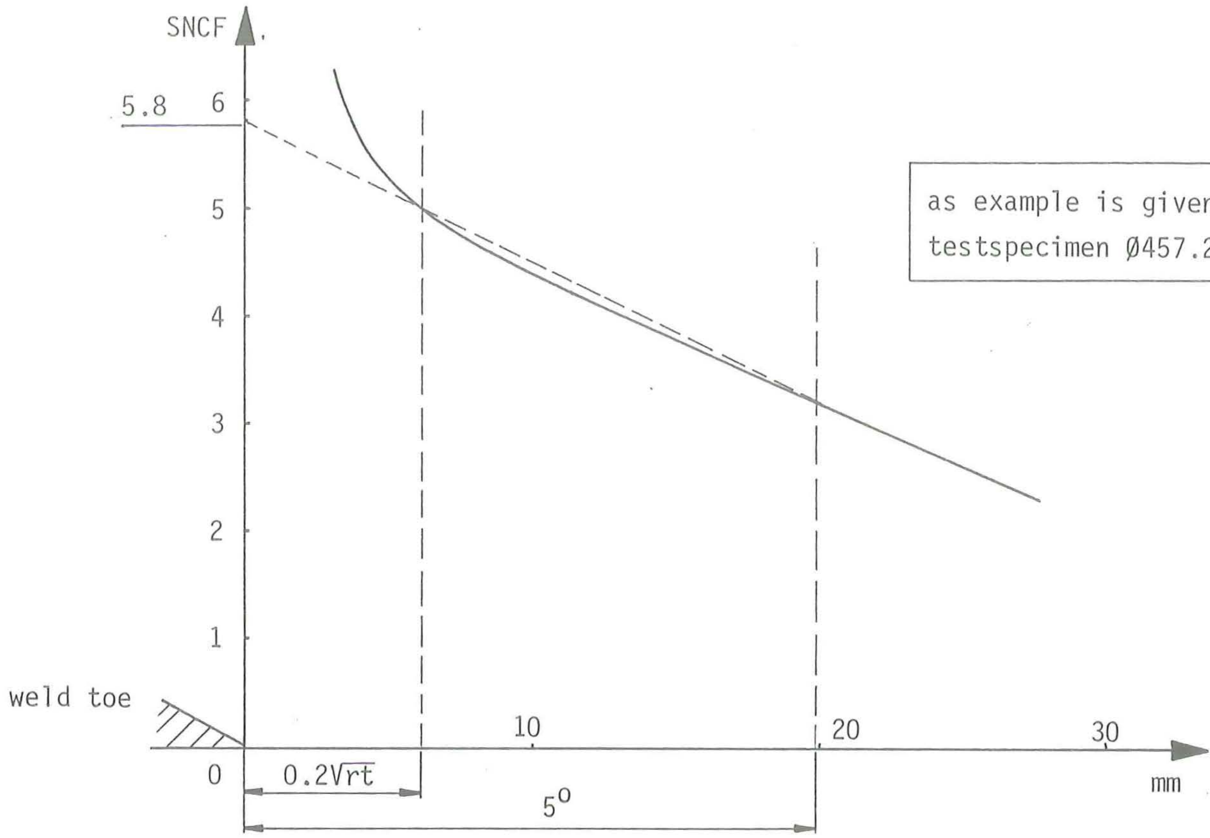

Fig.3.4.15 Strain distribution along line 4 for T-joints with β=0.5 τ=0.5

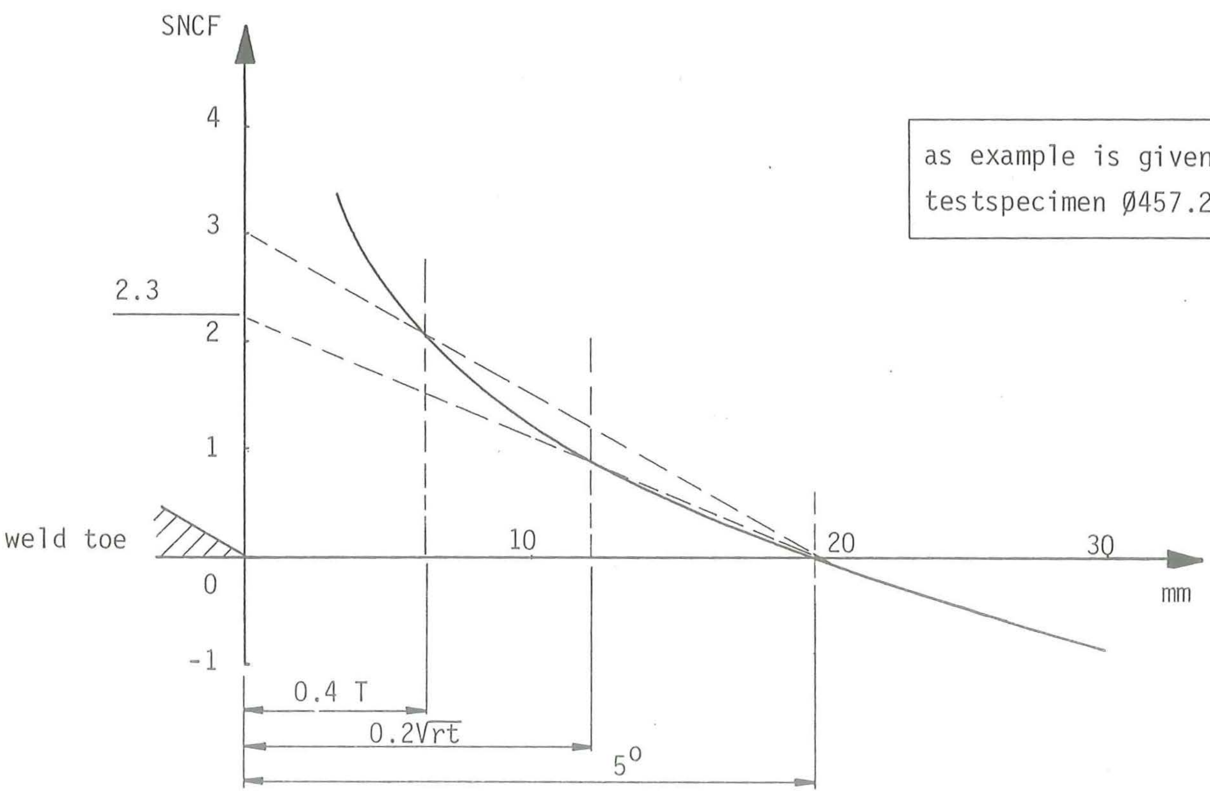

Fig.3.4.16 Strain distribution along line 4 for X-joints with β=1.0 τ=1.0

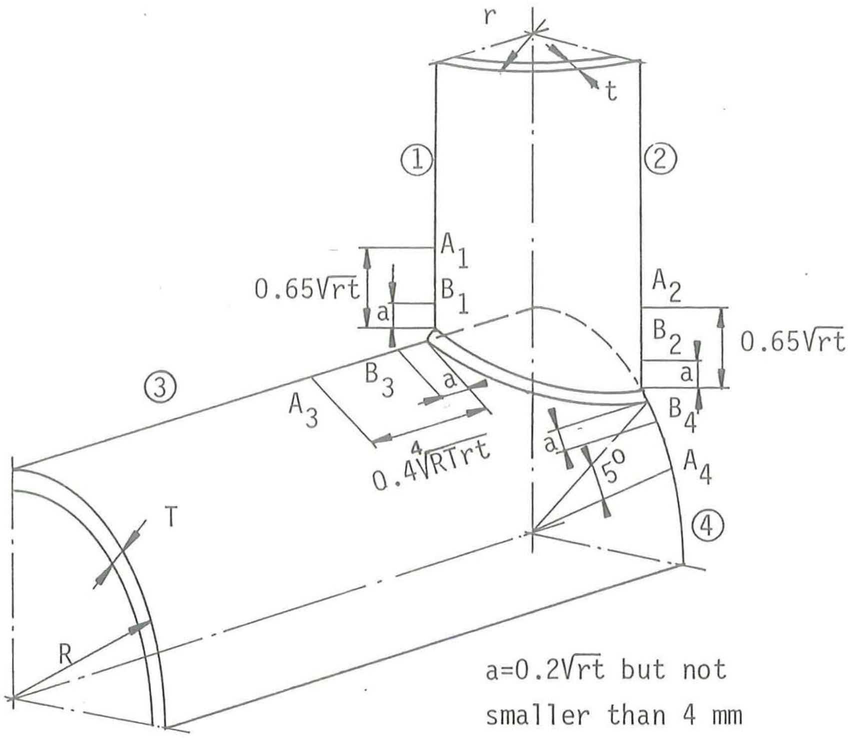

Fig.3.4.14 Location of the points of the SNCF curve which has to be used for the extrapolation to the weld toe

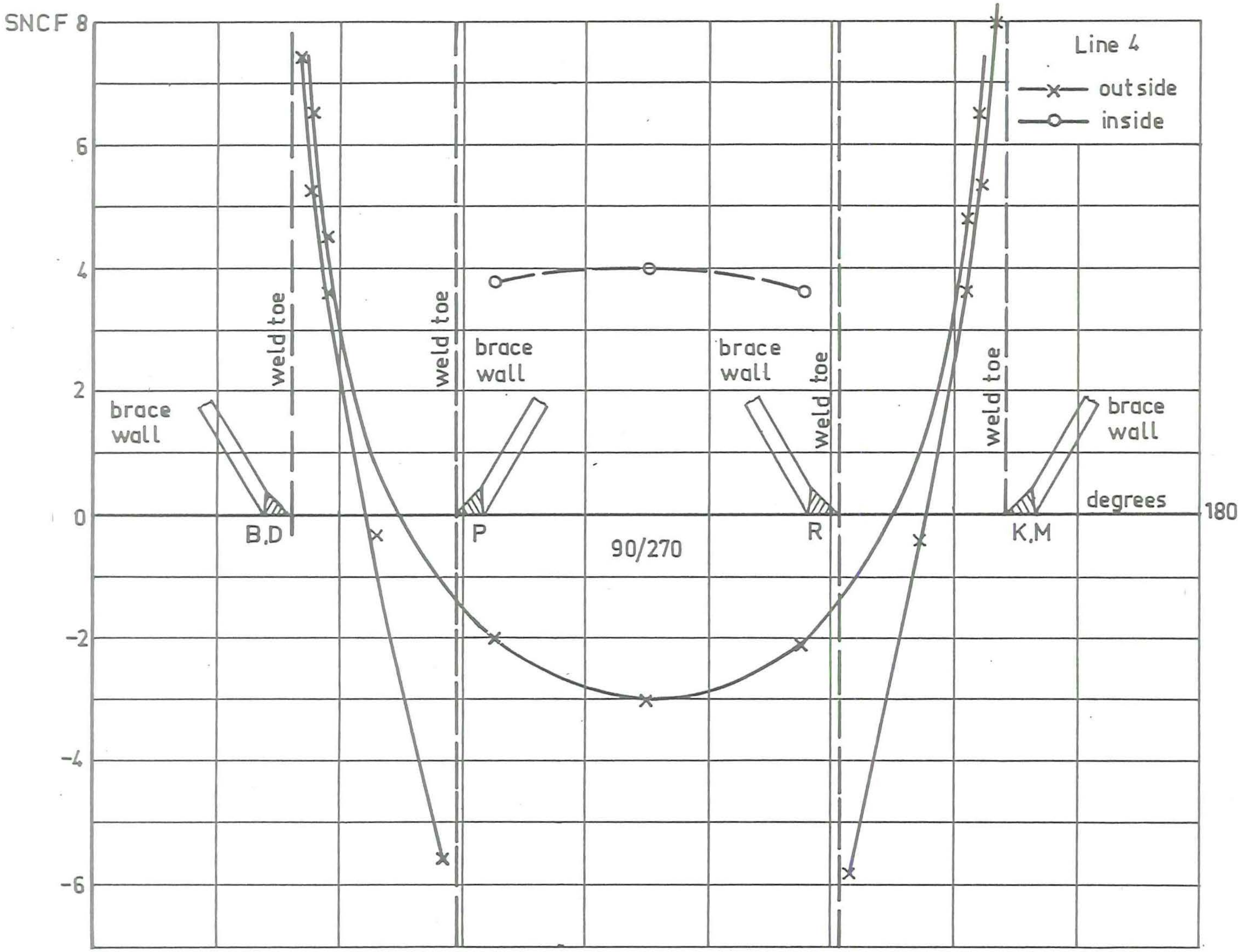

SPECIMEN	40
static load	390 kN
β	0.5
τ	0.5
γ	14.3
chorddim.	ϕ 914.4 - 32
$\sqrt{r.t}$	59.4 mm

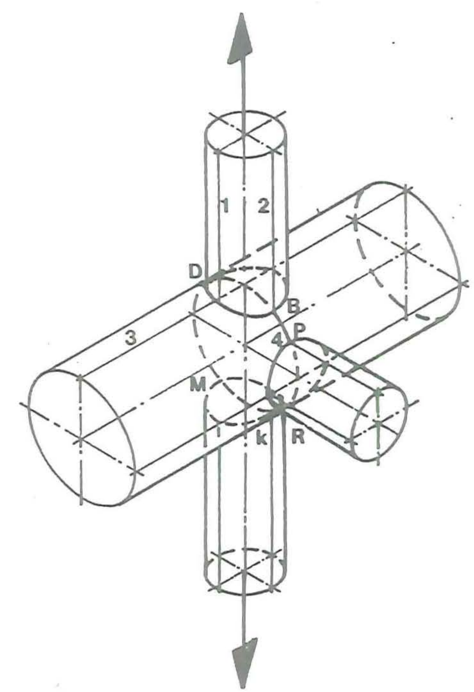

Fig.3.4.13 Specimen 40 : Strain distribution along line 4

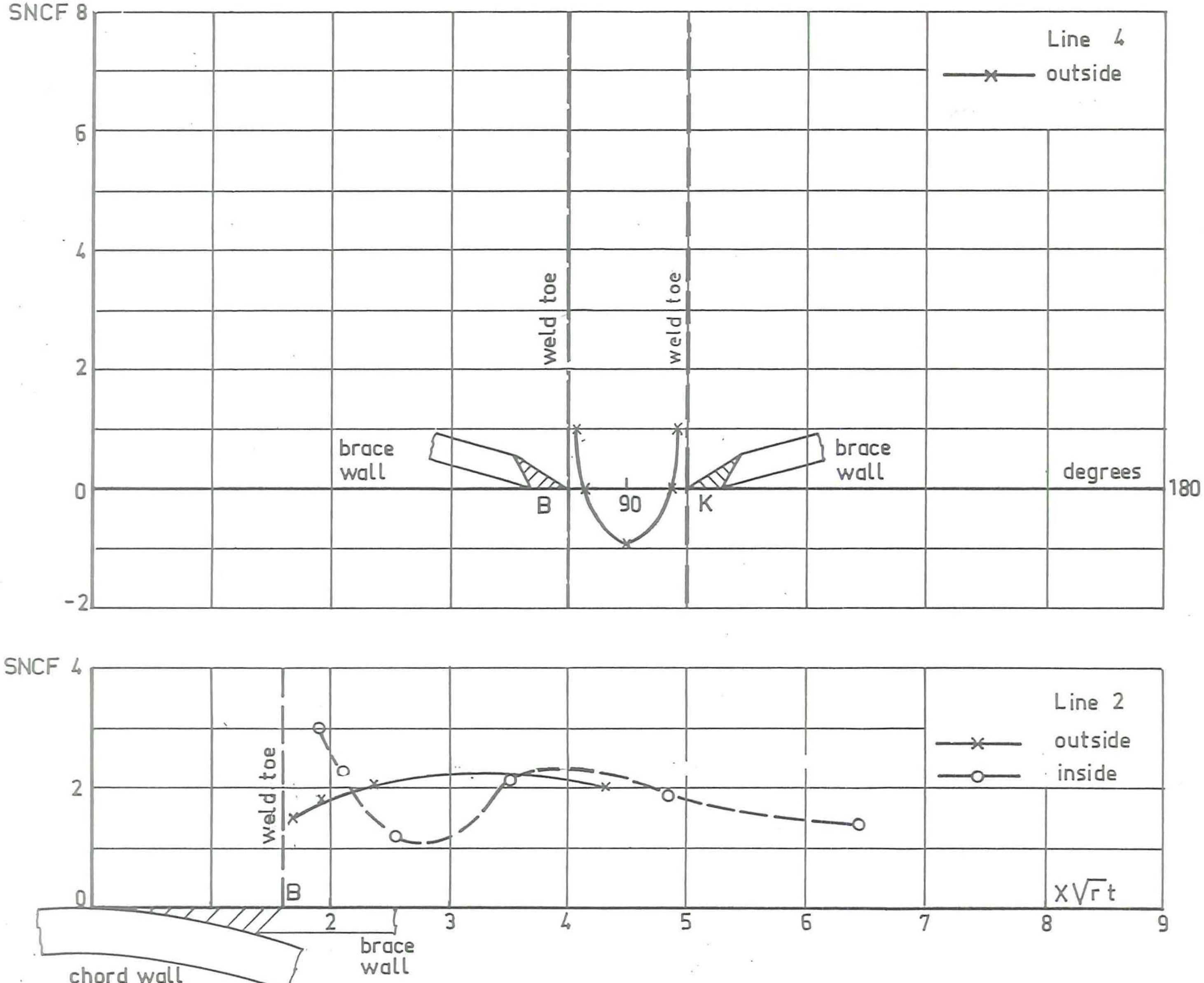

SPECIMEN	36
static load	520 kN
β	1.0
τ	0.55
γ	14.3
chorddim.	φ 457.2–16
√r.t	44.8

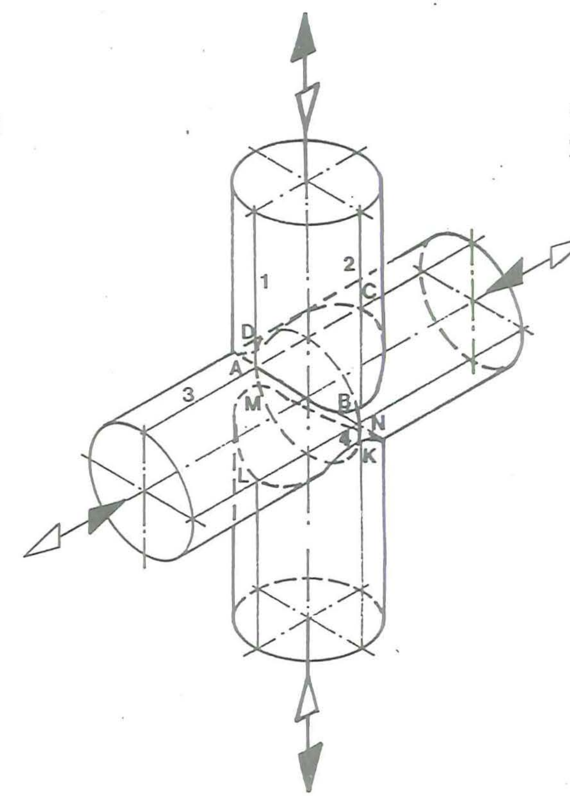

Fig.3.4.12 Specimen 36 : Strain distribution along line 2 and 4

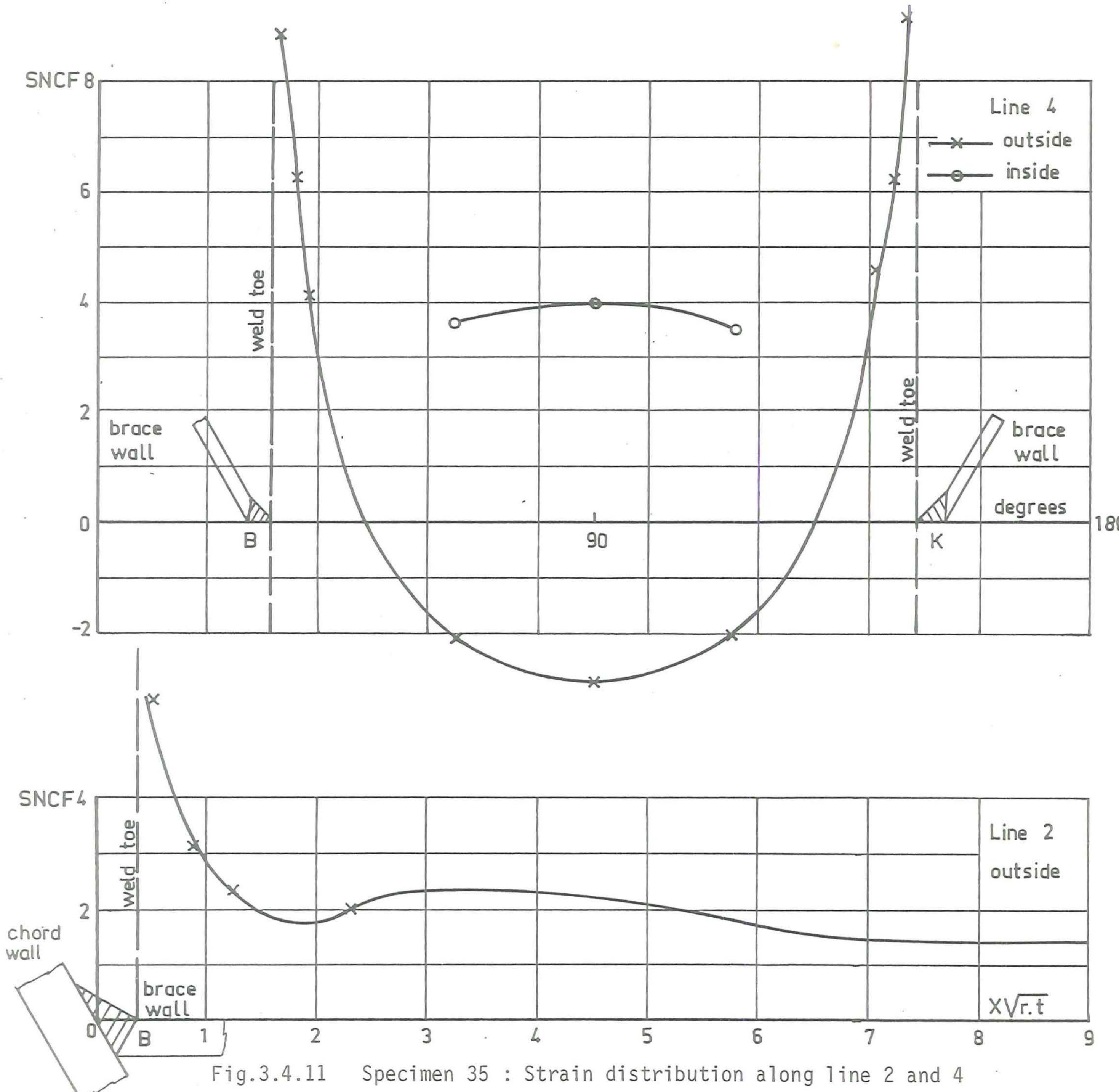

SPECIMEN	35
static load	100 kN
β	0.5
τ	0.5
γ	14.3
chorddim.	ϕ 914.4 − 32
$\sqrt{r.t}$	59.4 mm

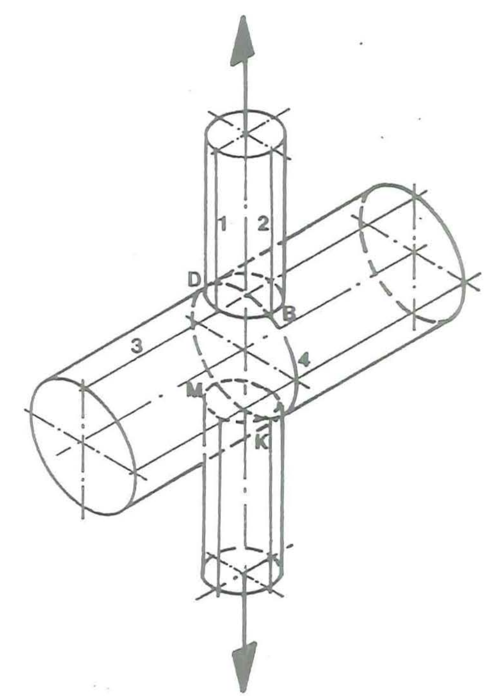

Fig.3.4.11 Specimen 35 : Strain distribution along line 2 and 4

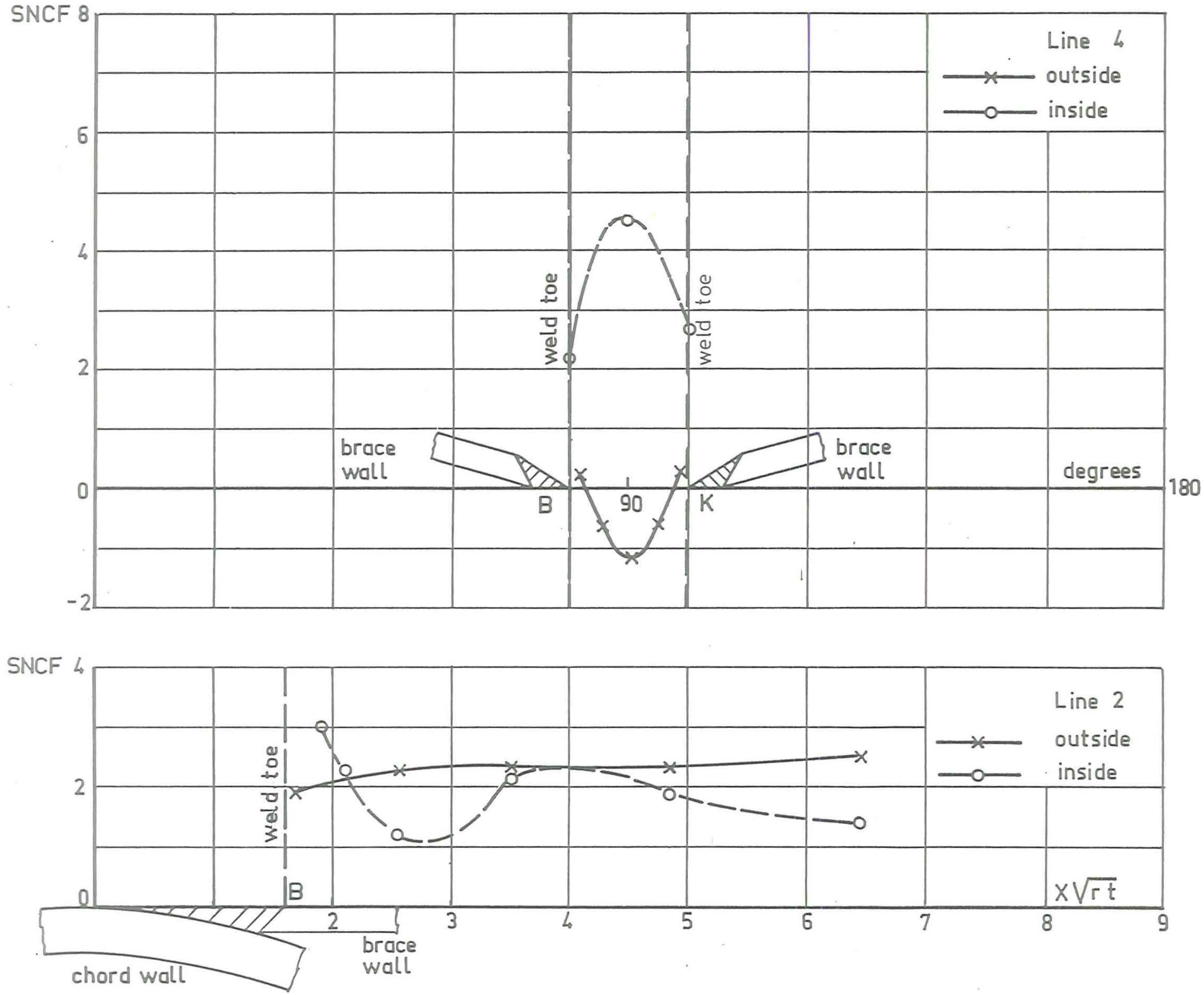

SPECIMEN	30
static load	440 kN
β	1.0
τ	0.55
γ	14.3
chorddim.	ϕ 457.2-16
$\sqrt{r.t}$	44.8

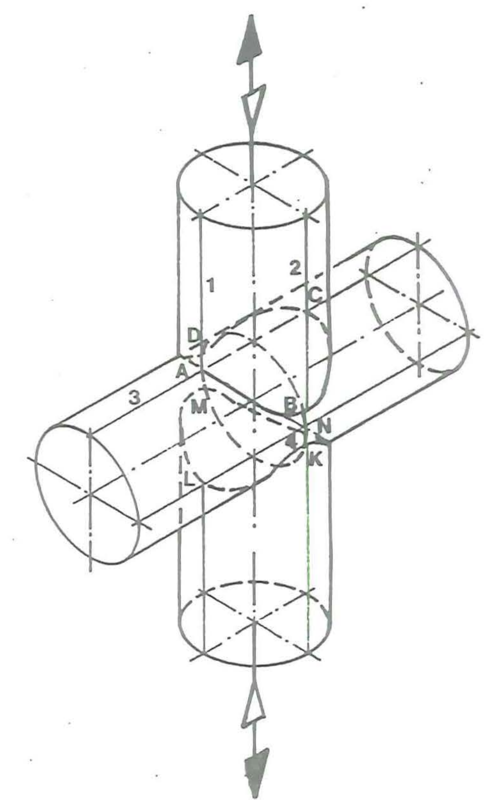

Fig.3.4.10 Specimen 30 : Strain distribution along line 2 and 4

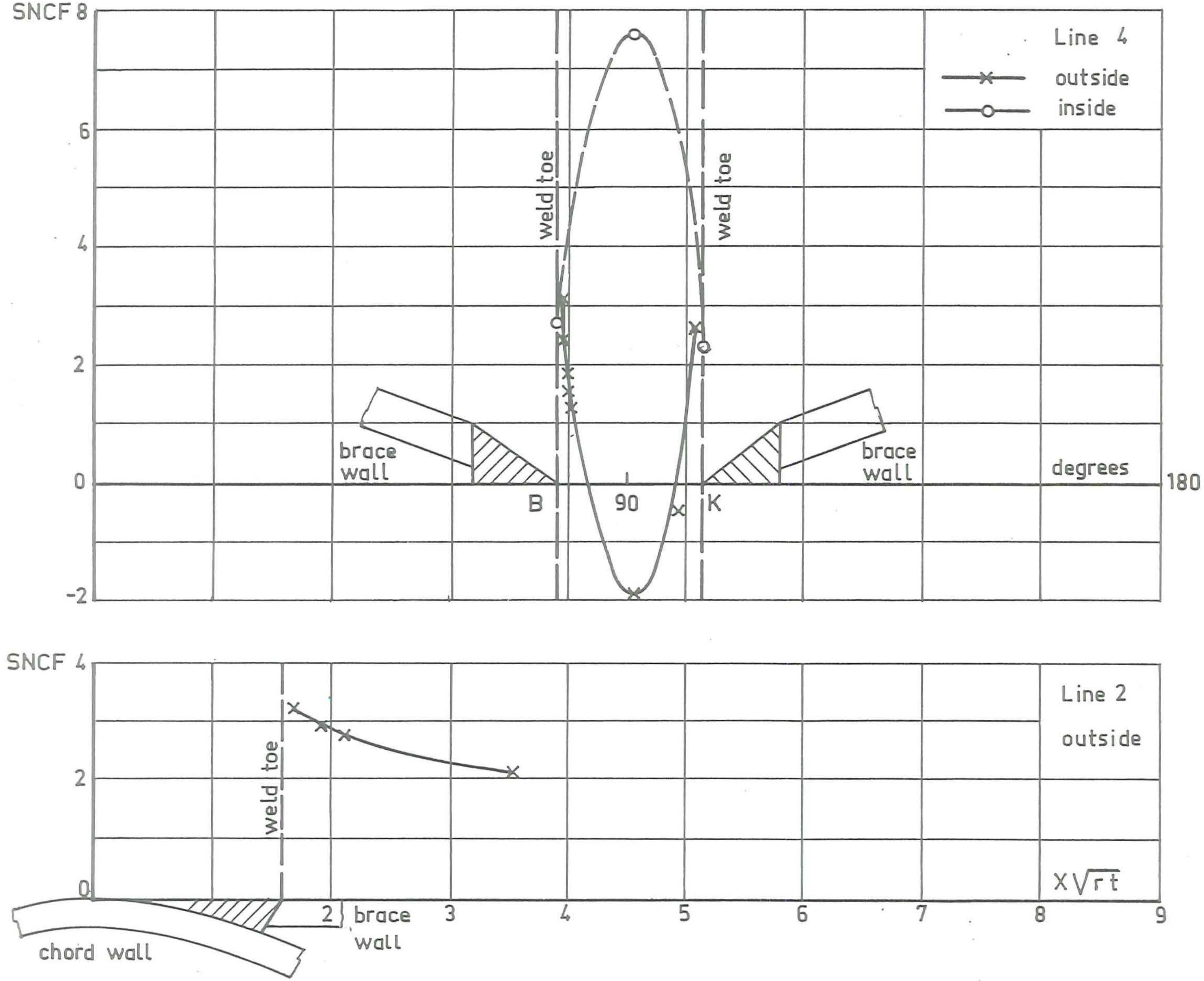

SPECIMEN	28
static load	650 kN
β	1.0
τ	1.0
γ	14.3
chorddim.	ϕ 457. 2 -16
√r.t	60. 48

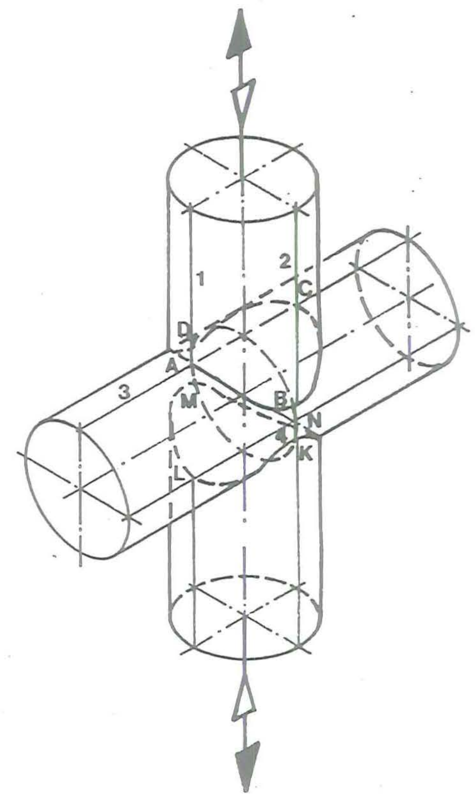

Fig.3.4.9 Specimen 28 : Strain distribution along line 2 and 4

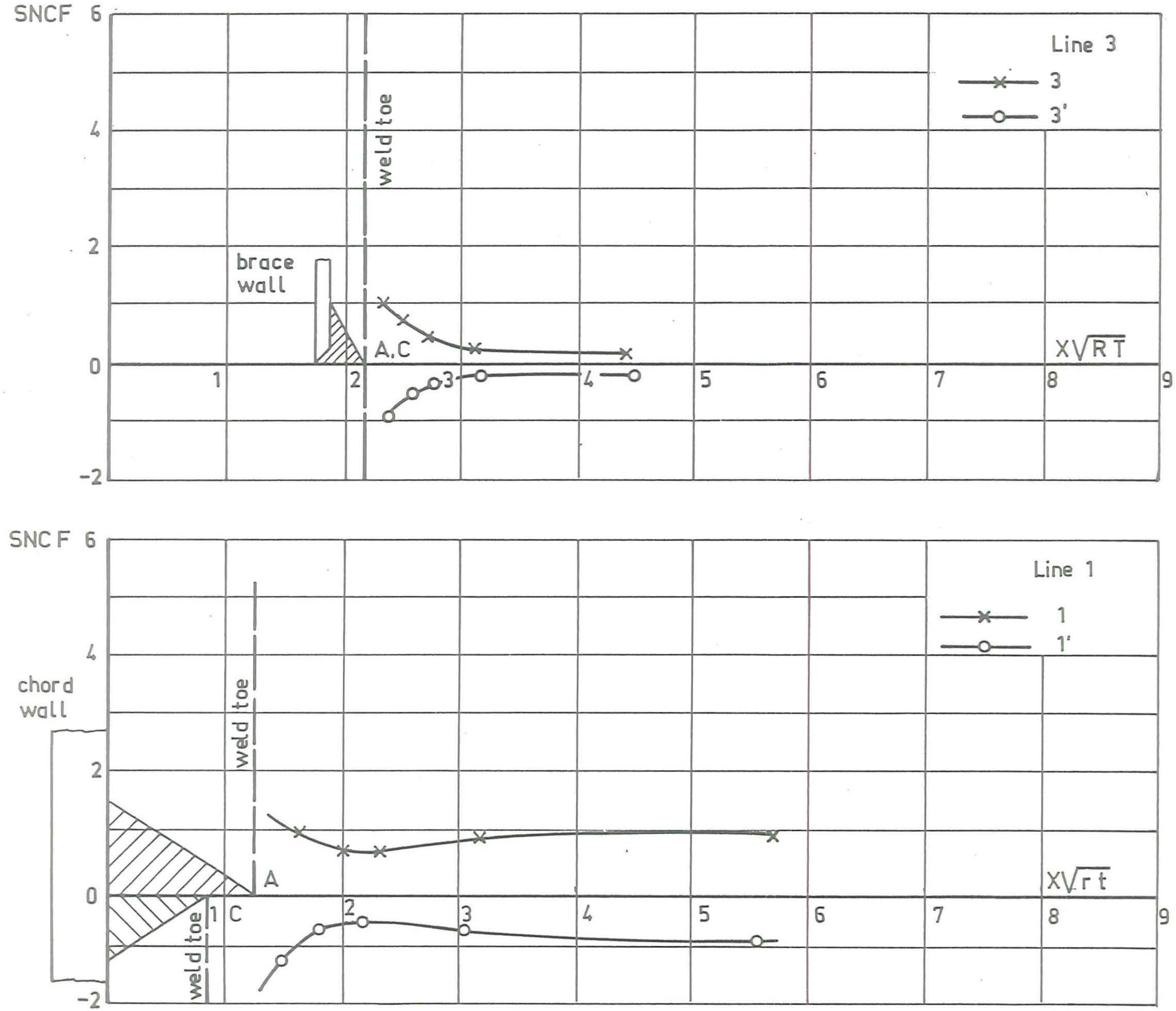

SPECIMEN	26
static load	2 kN
β	0.5
τ	0.5
γ	13.4
chord dim.	ϕ 168.3 – 6.3
$\sqrt{r.t}$	11.9 mm
$\sqrt{RT}$	23 mm

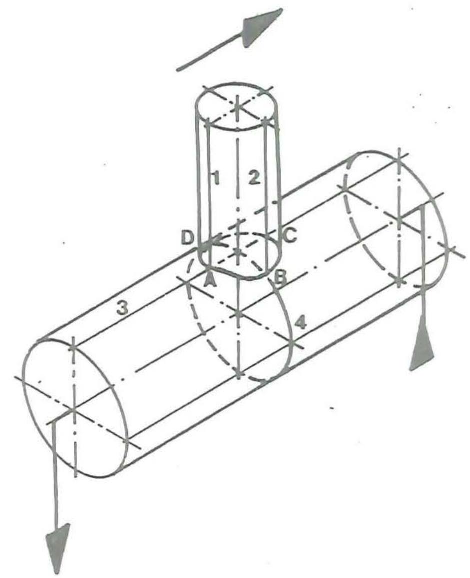

Fig.3.4.8 Specimen 26 : Strain distribution along line 1 and 3

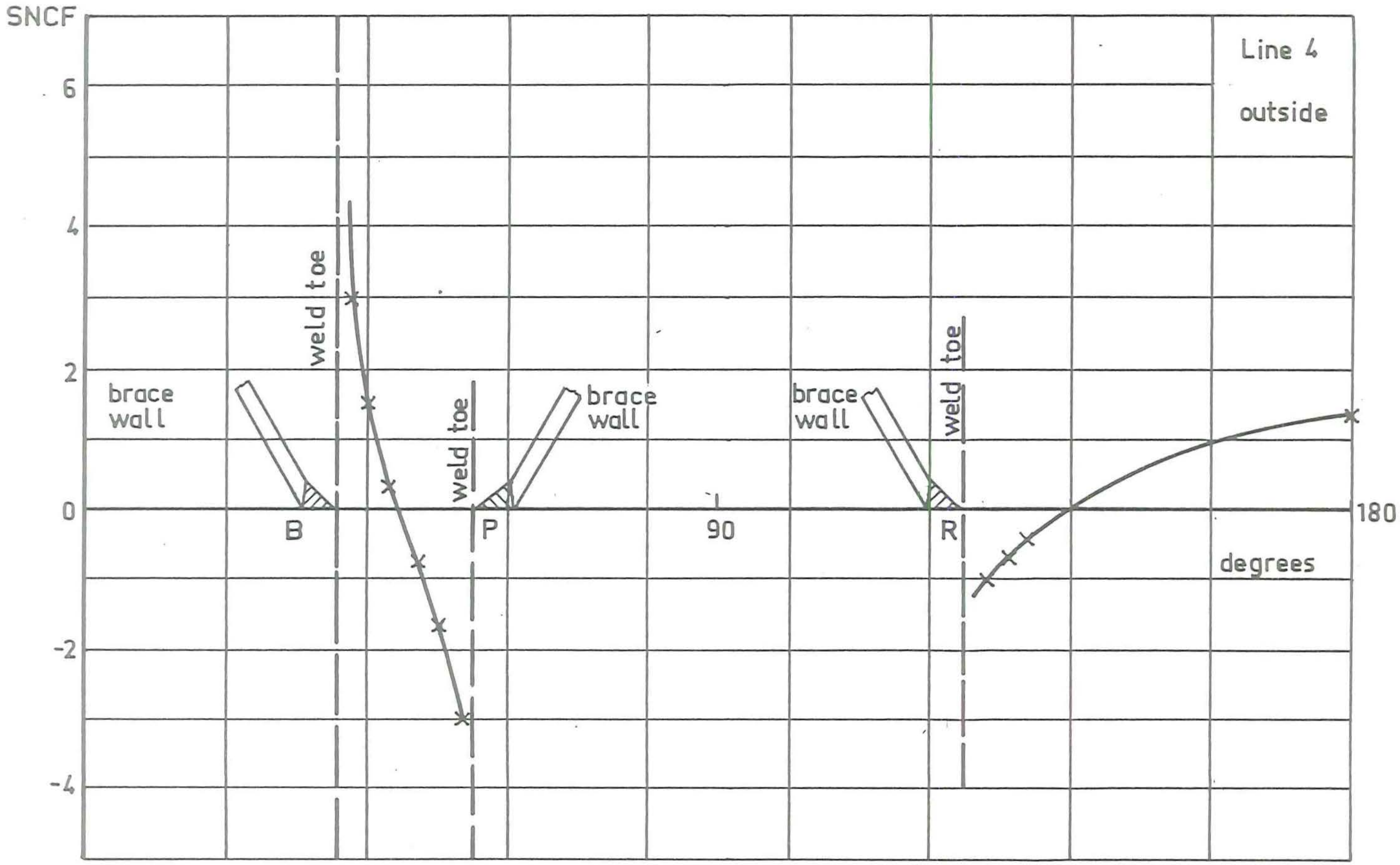

SPECIMEN	23
static load	20 kN
β	0.5
τ	0.5
γ	13.4
chorddim.	ϕ 168.3 - 6.3
$\sqrt{r.t}$	11.9 mm

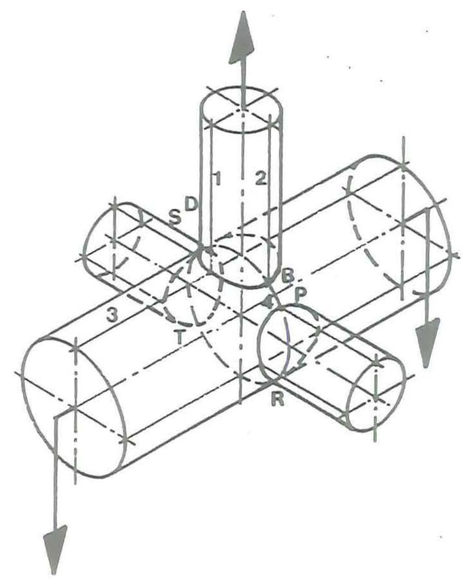

Fig.3.4.7 Specimen 23 : Strain distribution along line 4

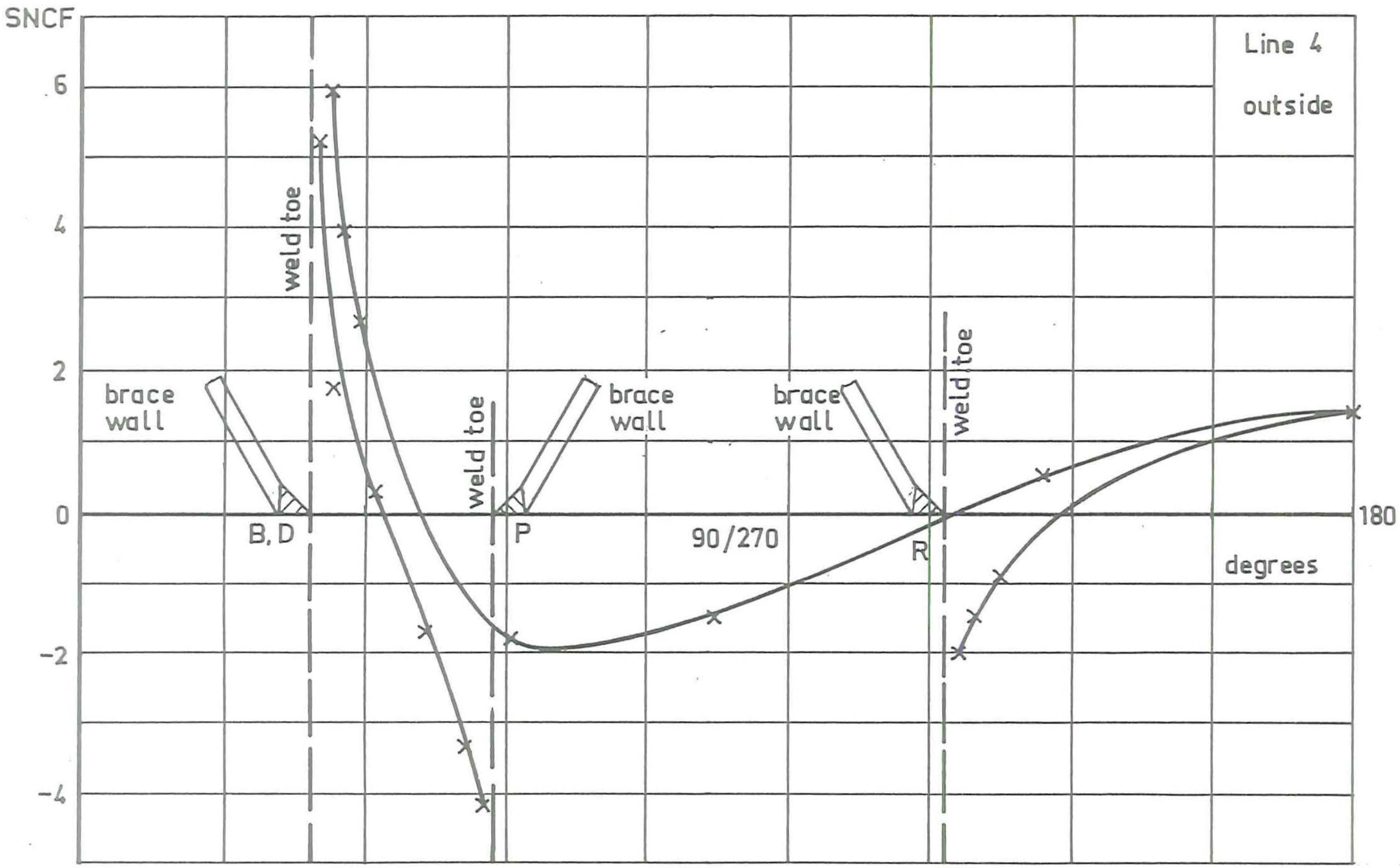

SPECIMEN	21
static load	200 kN
β	0.5
τ	0.5
γ	14.3
chorddim.	ϕ 914.4-32
$\sqrt{r.t}$	59.6 mm

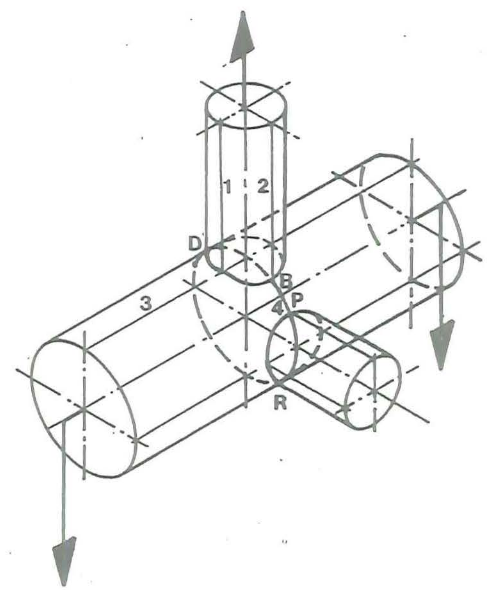

Fig.3.4.6 Specimen 21 : Strain distribution along line 4

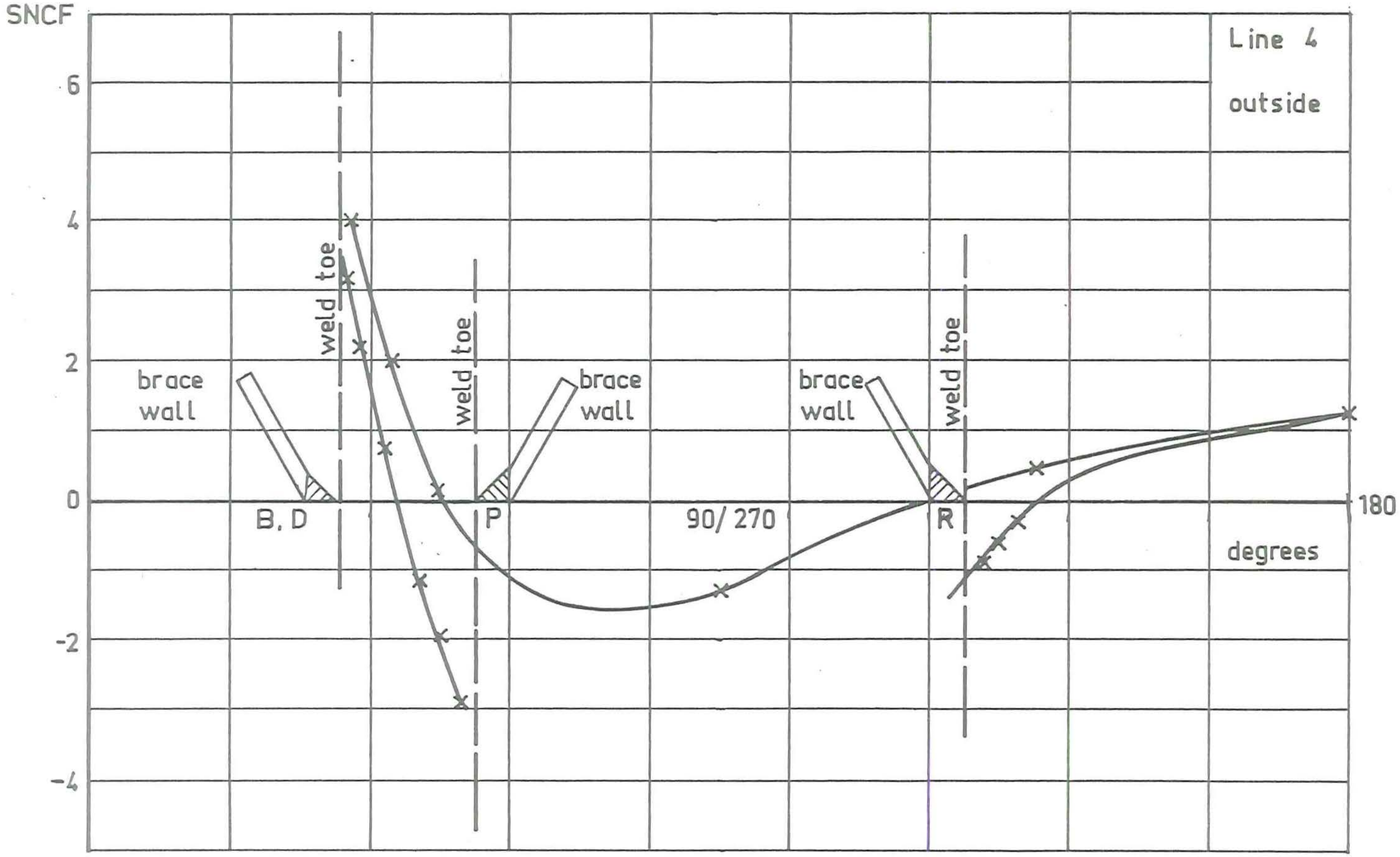

Fig.3.4.5 Specimen 18 : Strain distribution along line 4

SPECIMEN	18
static load	20 kN
β	0.5
τ	0.5
γ	13.4
chorddim.	ϕ 168.3 - 6.3
$\sqrt{r.t}$	11.9 mm

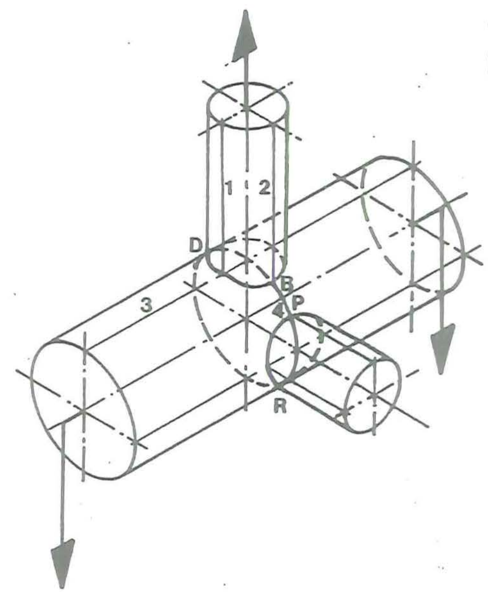

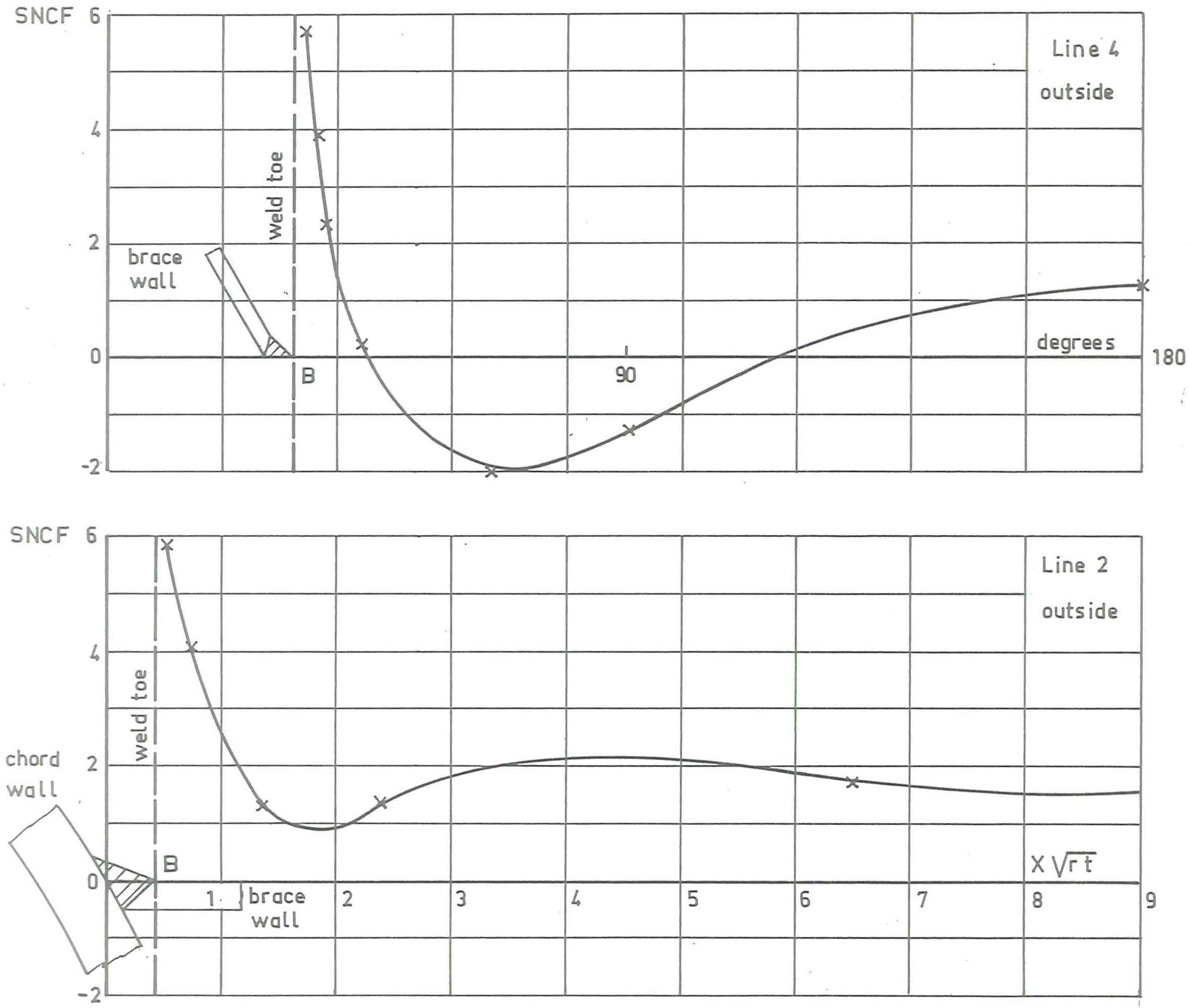

SPECIMEN	13
static load	200 kN
β	0.5
τ	0.5
γ	14.3
chorddim.	ϕ 914.4–32;
$\sqrt{r.t}$	59.4 mm

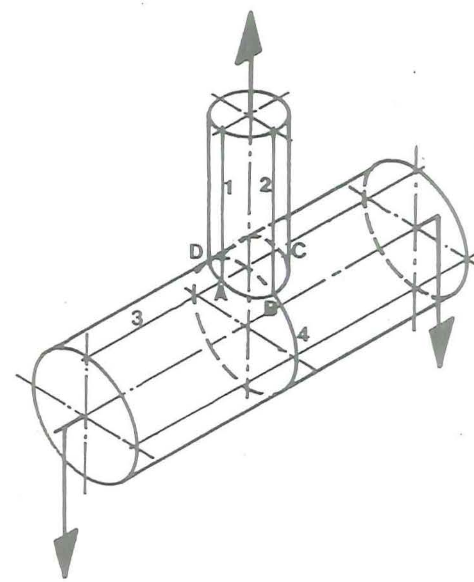

Fig.3.4.4 Specimen 13 : Strain distribution along line 2 and 4

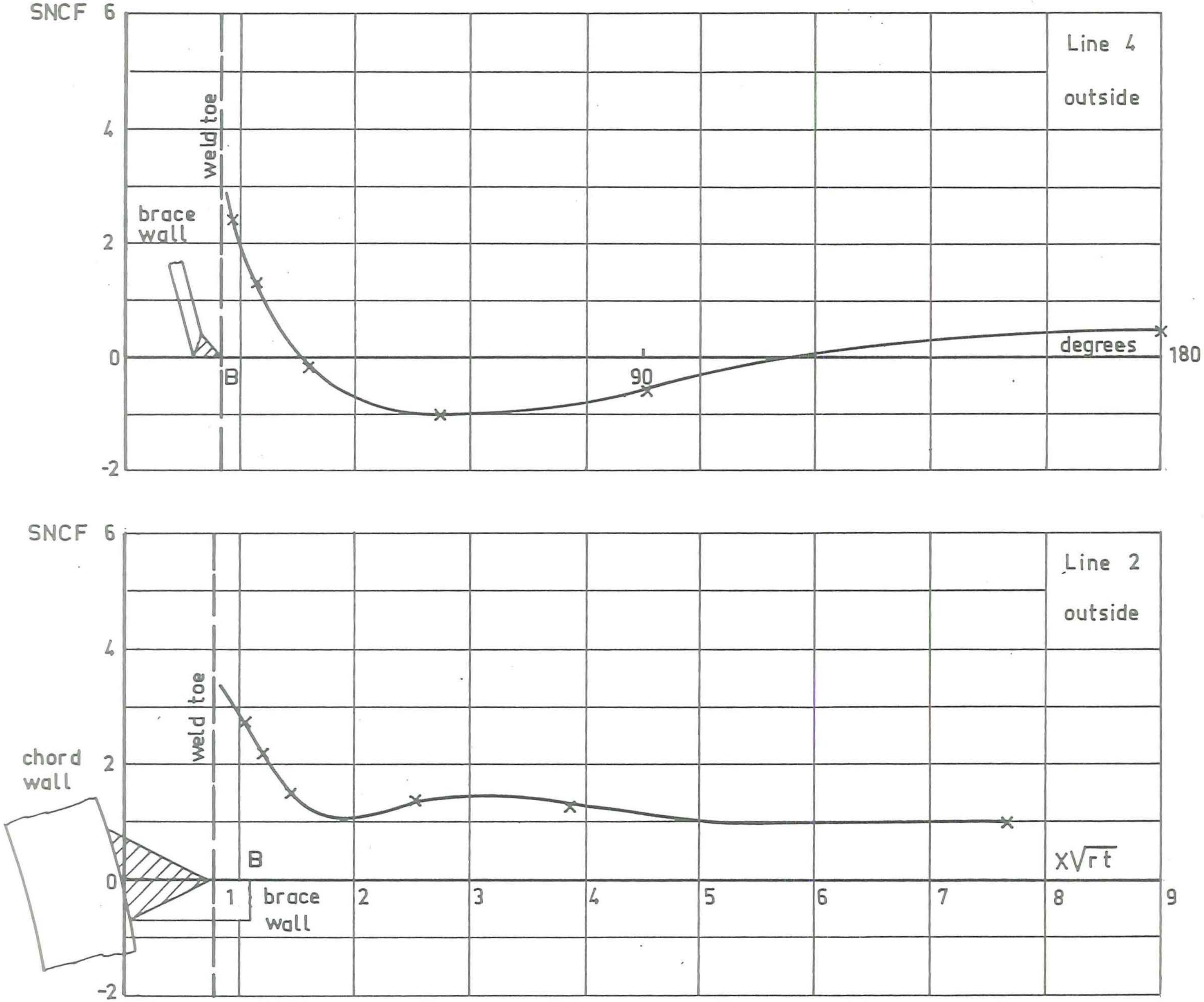

SPECIMEN	11
static load	23 kN
β	0.25
τ	0.39
γ	14.3
chorddim.	ϕ 457.2-16
$\sqrt{r.t}$	19 mm

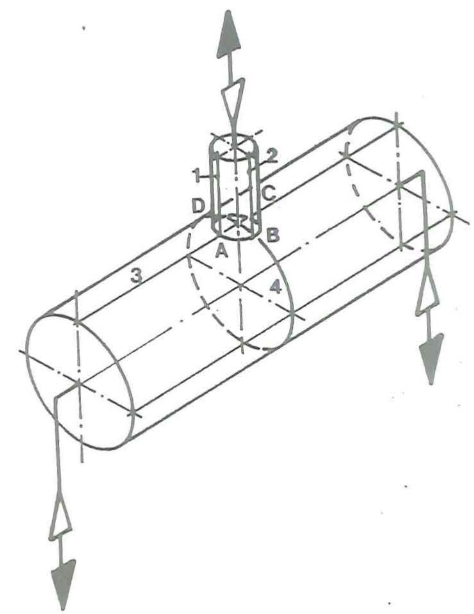

Fig.3.4.3. Specimen 11 : Strain distribution along line 2 and 4

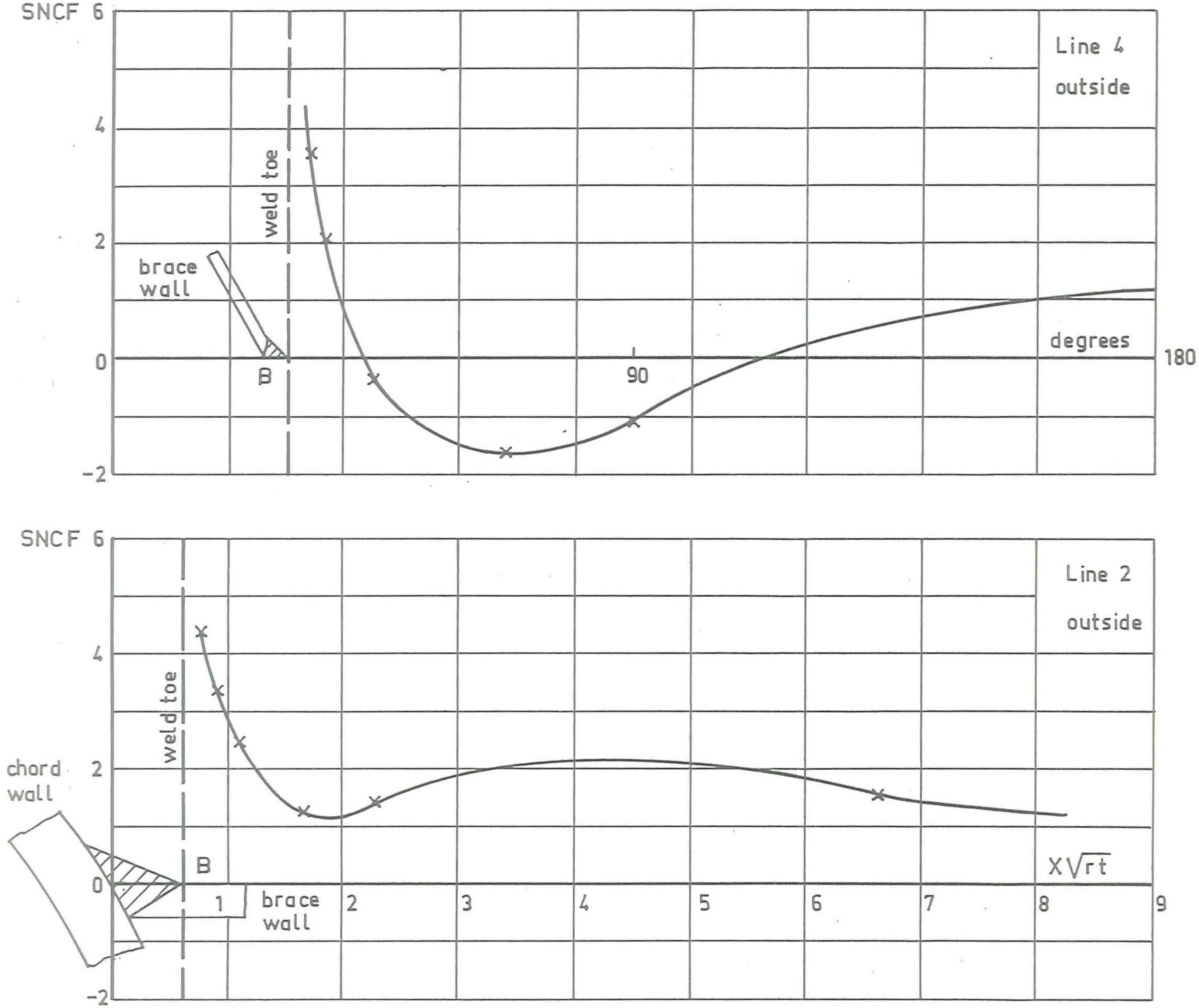

SPECIMEN	5
static load	33 kN
β	0.5
τ	0.5
γ	14.3
chorddim.	ϕ 457.2 − 16
$\sqrt{r.t}$	29.8 mm

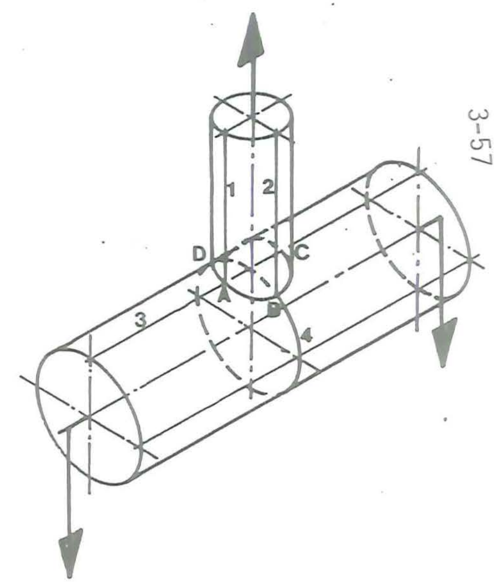

Fig.3.4.2 Specimen 5 : Strain distribution along line 2 and 4

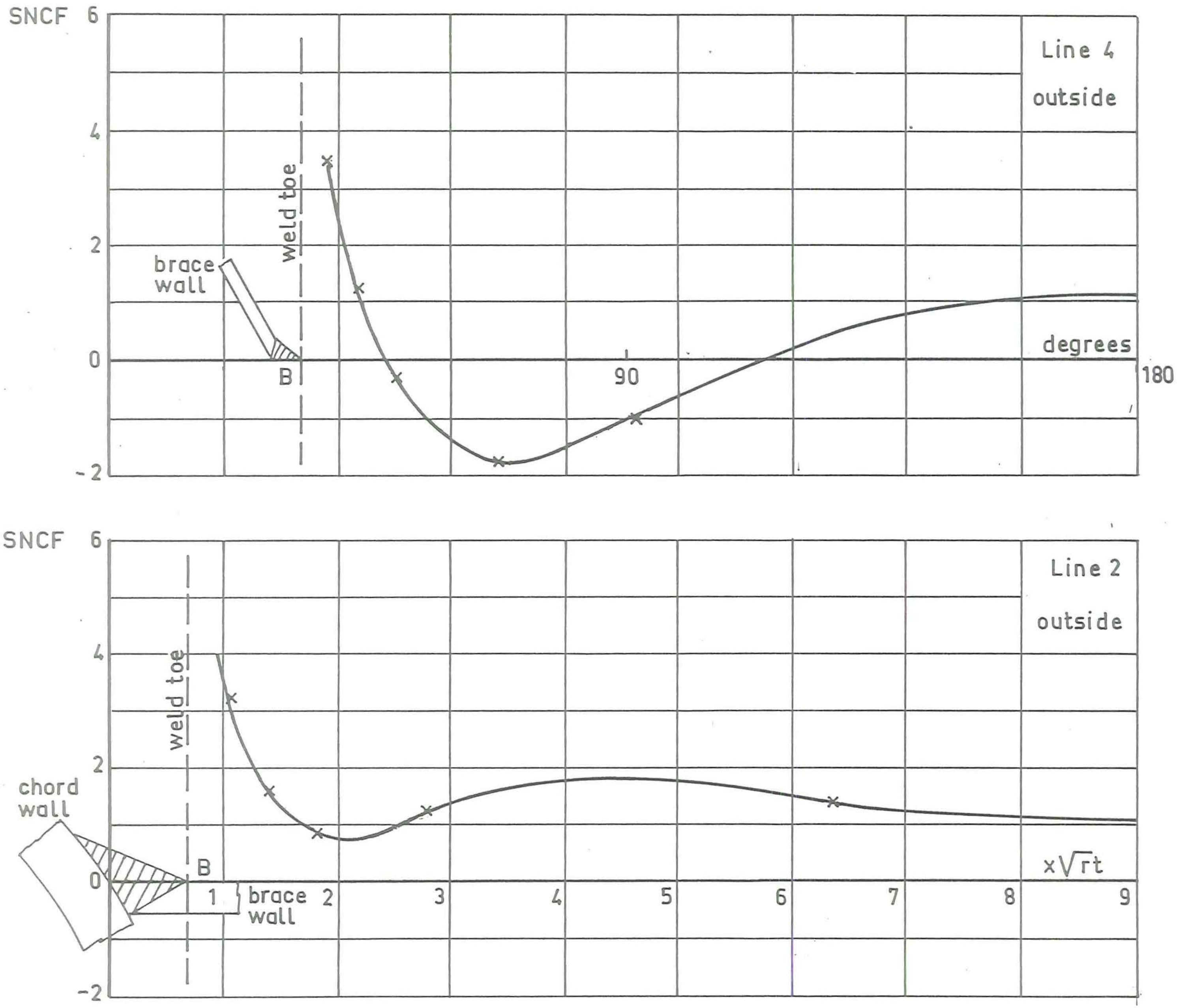

SPECIMEN	1
static load	10 kN
β	0.5
τ	0.5
γ	13.4
chorddim.	ϕ168.3-6.3
$\sqrt{r.t}$	11.9 mm

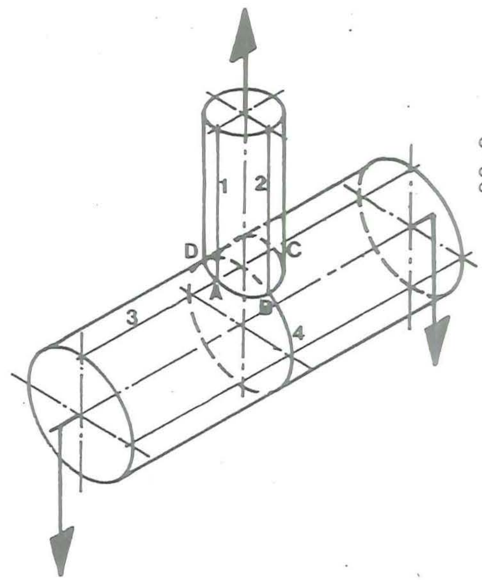

Fig.3.4.1 Specimen 1 : Strain distribution along line 2 and 4

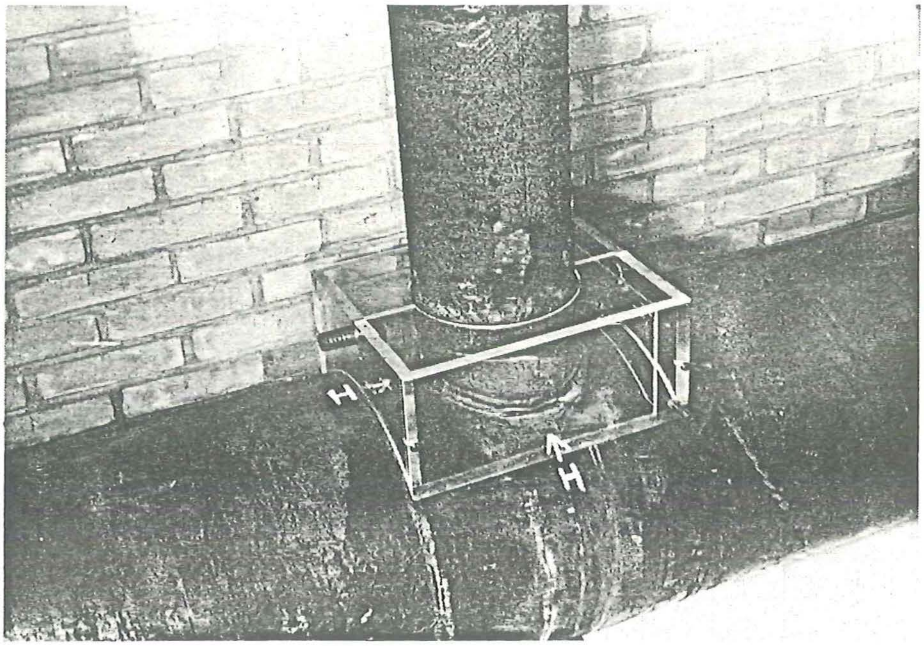

Fig.3.3.8 · Test set up for the corrosion fatigue test on tubular T-joints

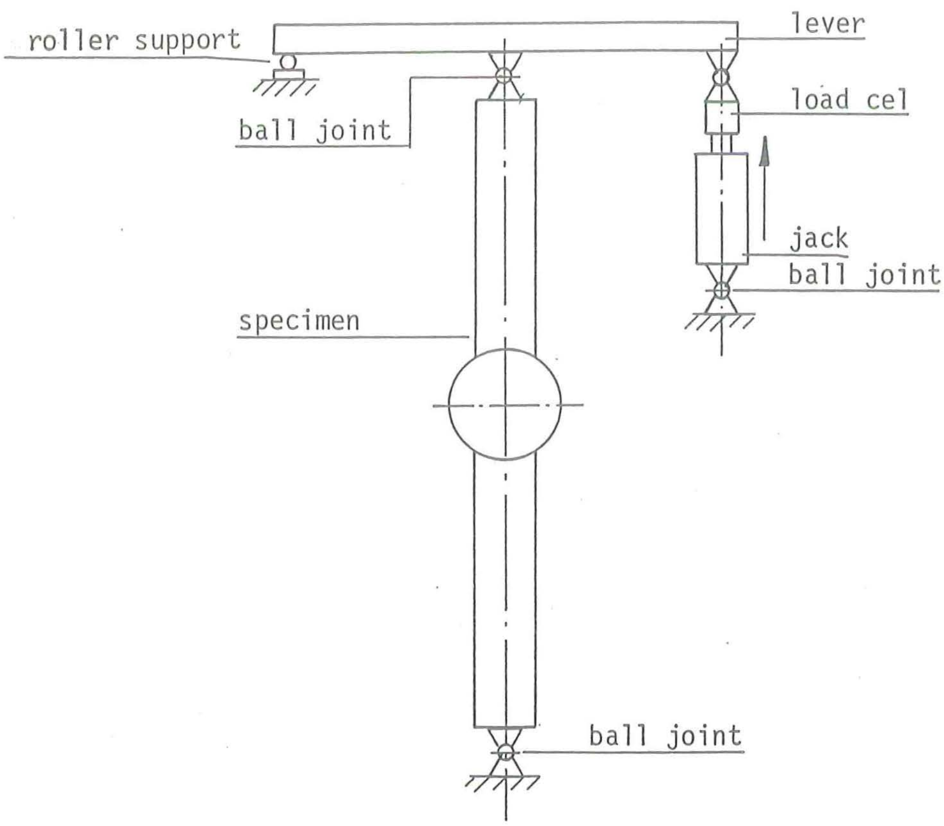

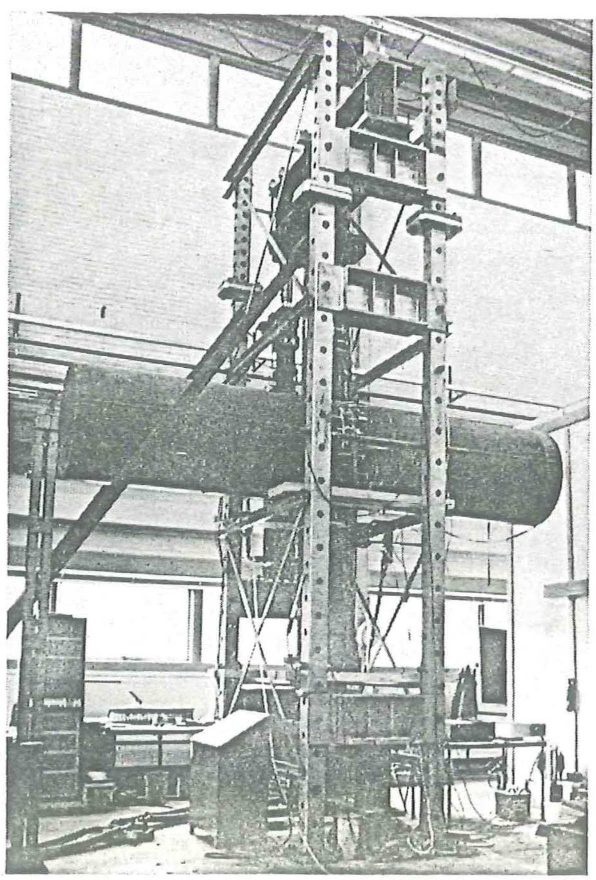

Fig.3.3.7 Test rig for Ø914.4 mm tubular X-joints (axially loaded)
(used for specimen 34 35 39 40)

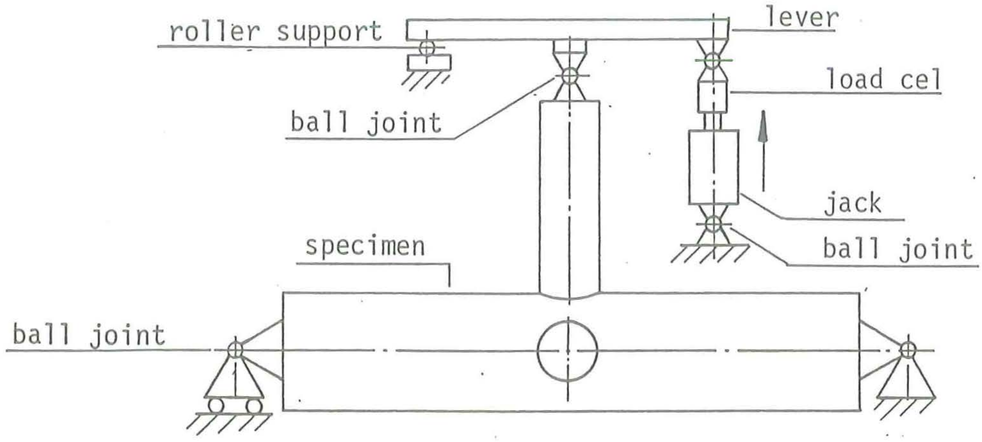

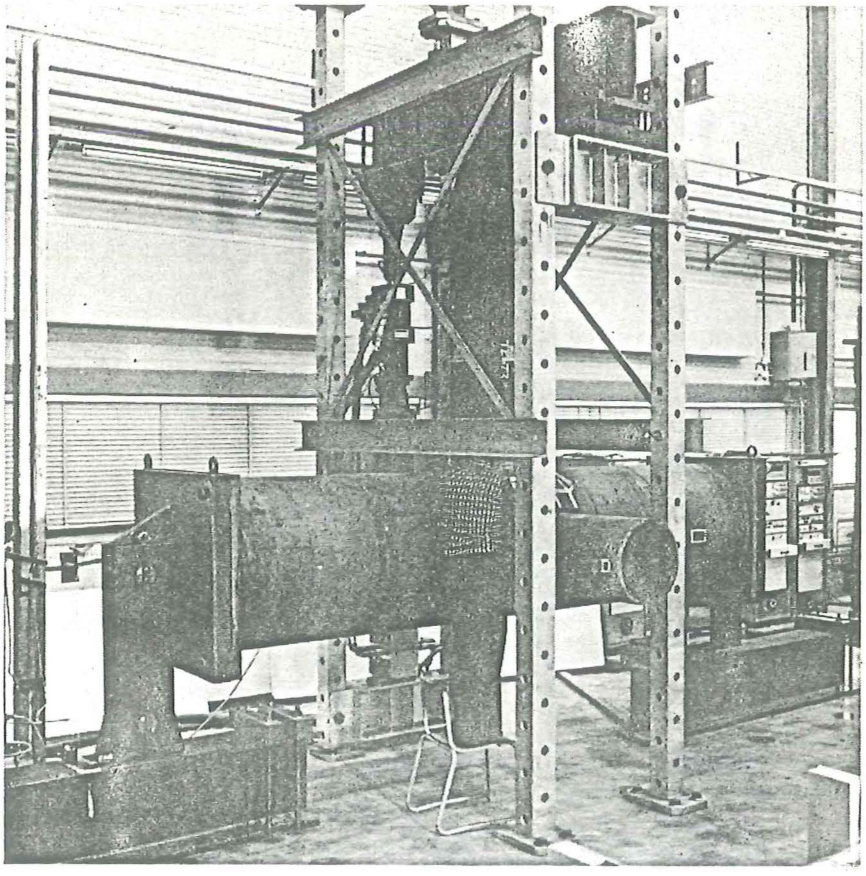

Fig.3.3.6 Test rig for Ø914.4 mm tubular T-joints (axially loaded)
(used for specimen 13 14 15 20 21)

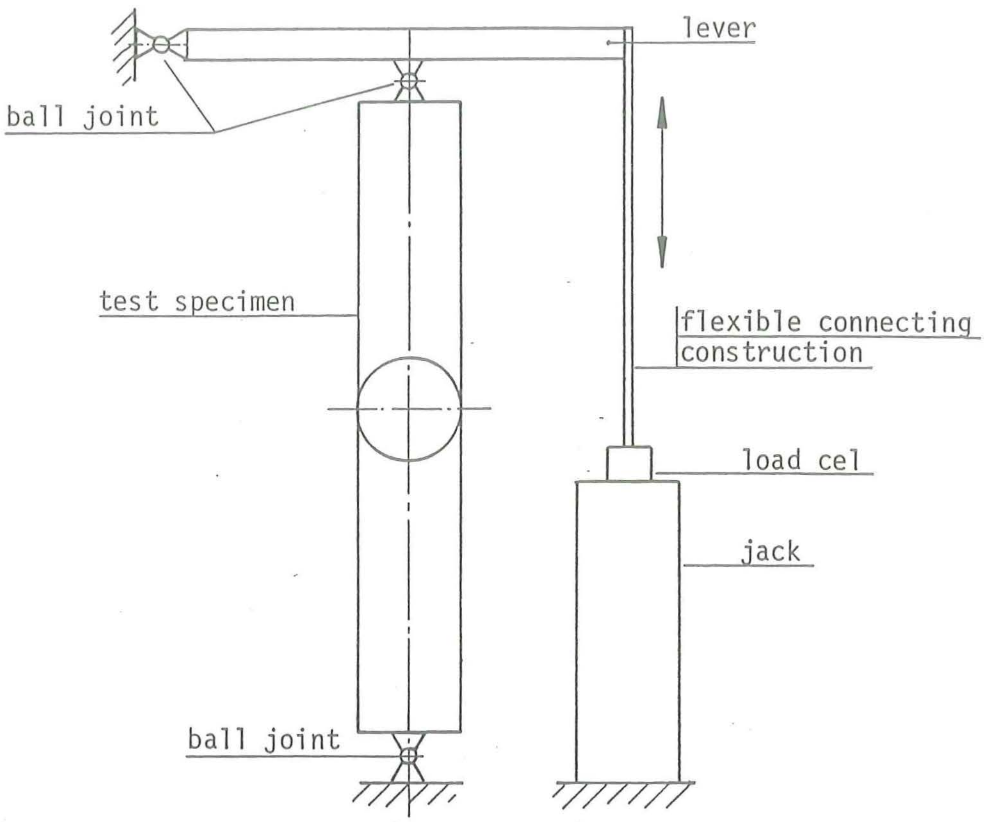

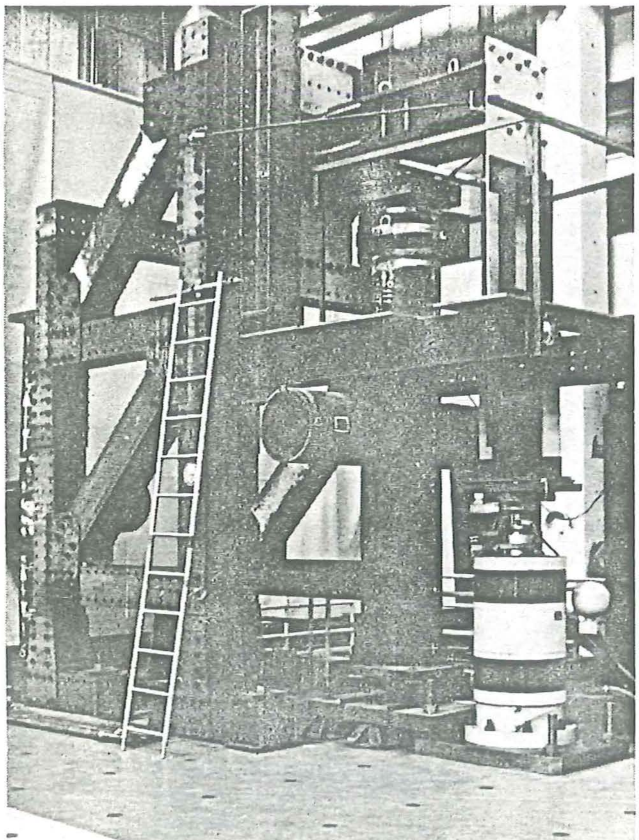

Fig.3.3.5 Test rig for Ø457.2 mm tubular X-joints (axially loaded)
(used for specimen 27 28 29 30 31 32 33 36 37 38)

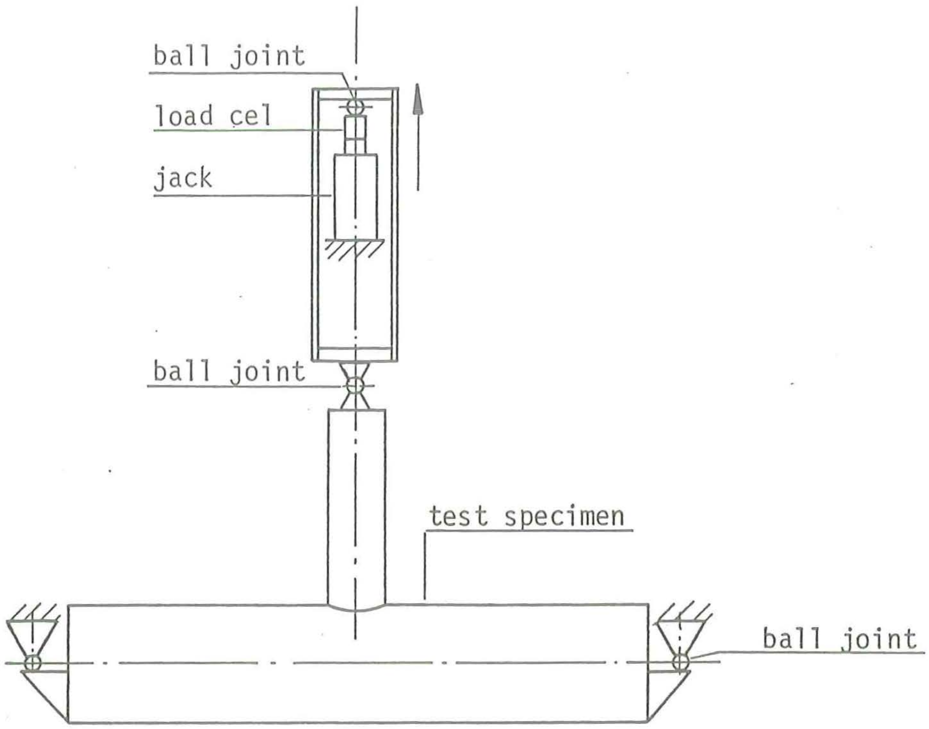

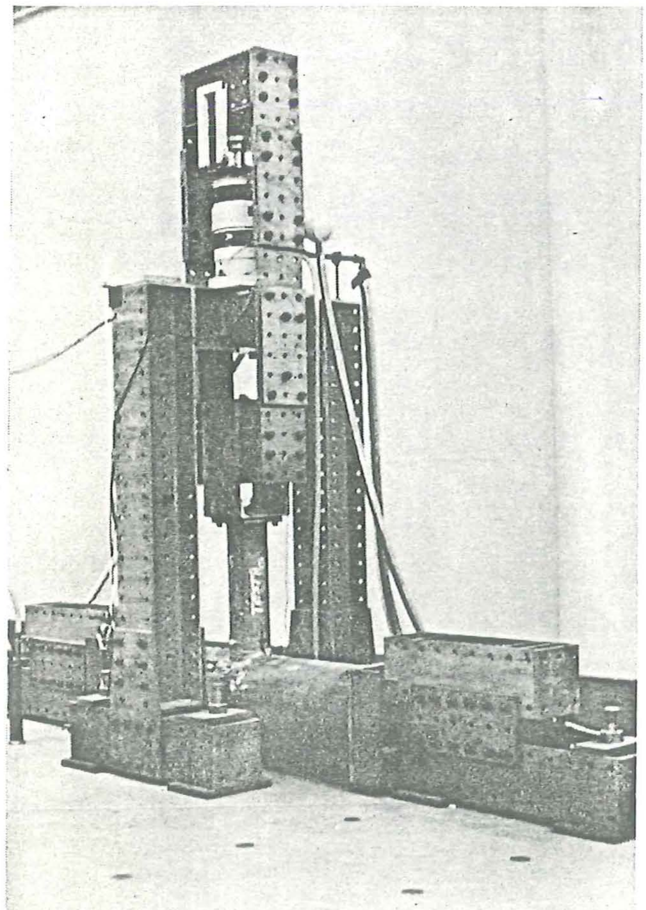

Fig.3.3.4 Test rig for Ø457.2 mm tubular T-joints (axially loaded R=0) (used for specimen 5 6 7 8 9 10)

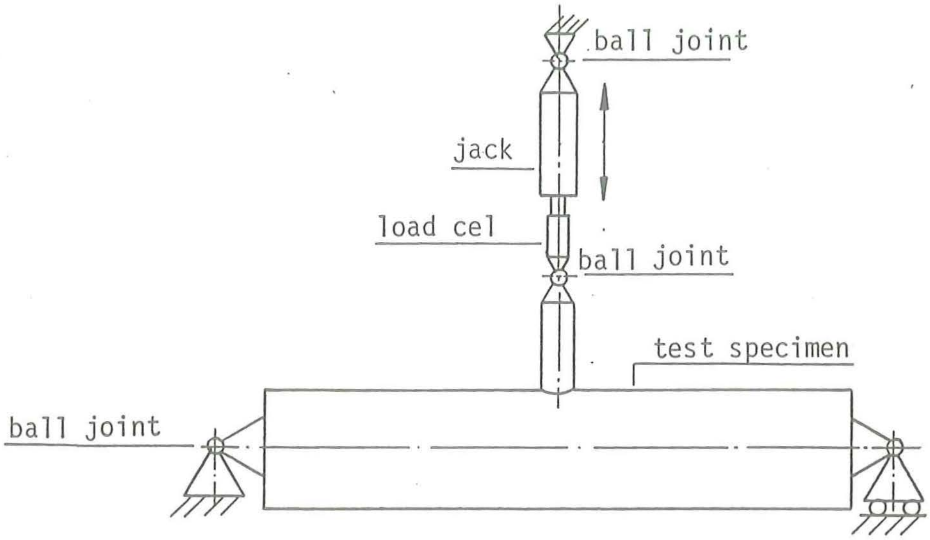

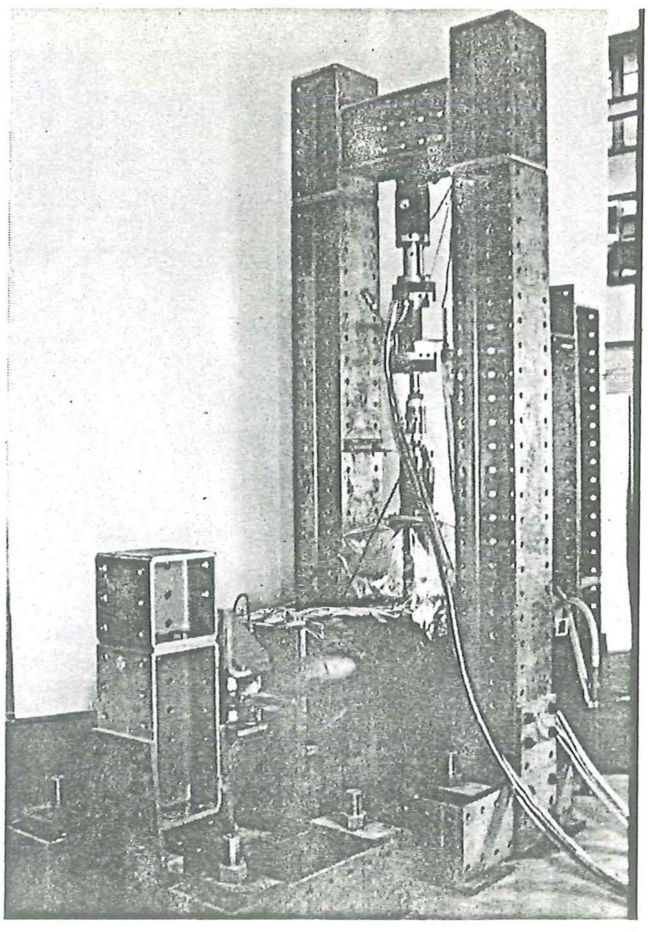

Fig.3.3.3 Test rig for Ø457.2 mm tubular T-joints (axially loaded R=-1)
(used for specimen 4 11 12)

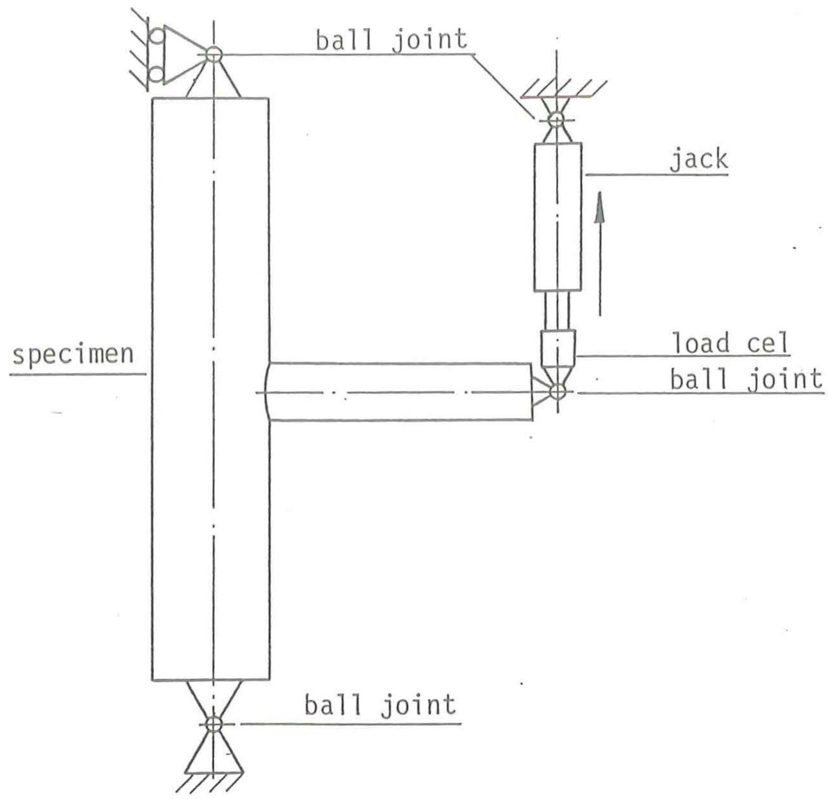

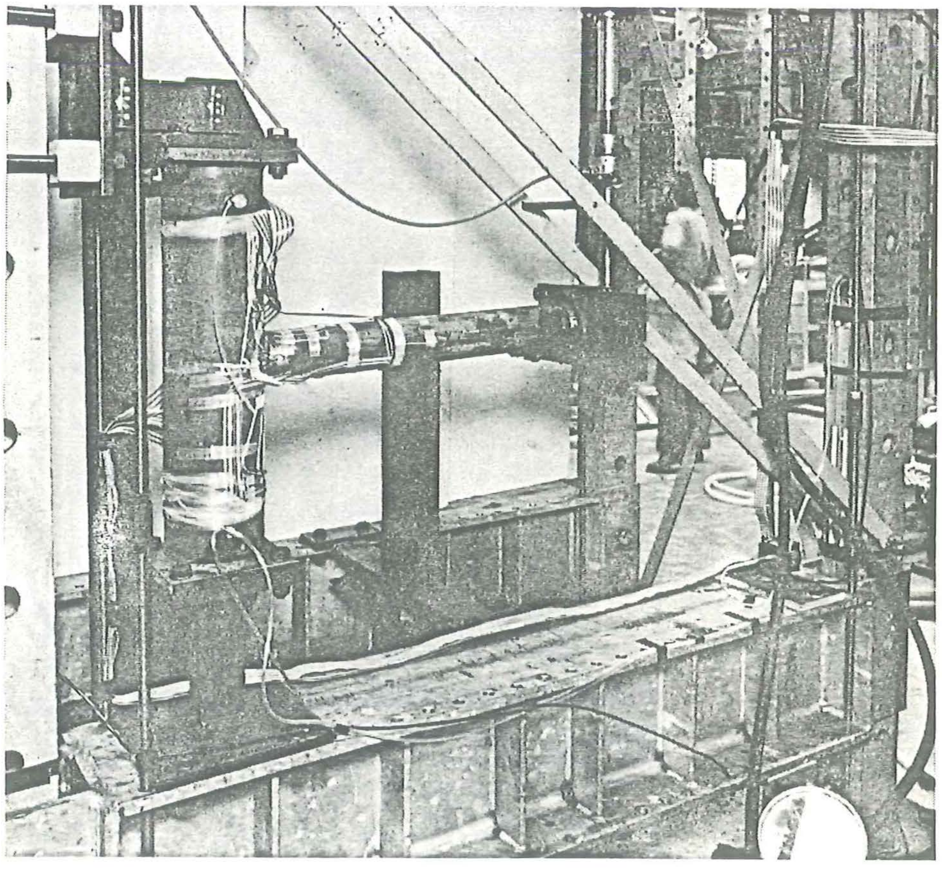

Fig.3.3.2 Test rig for Ø168.3 mm tubular T-joints (in plane bending) (used for specimen 24 25 26)

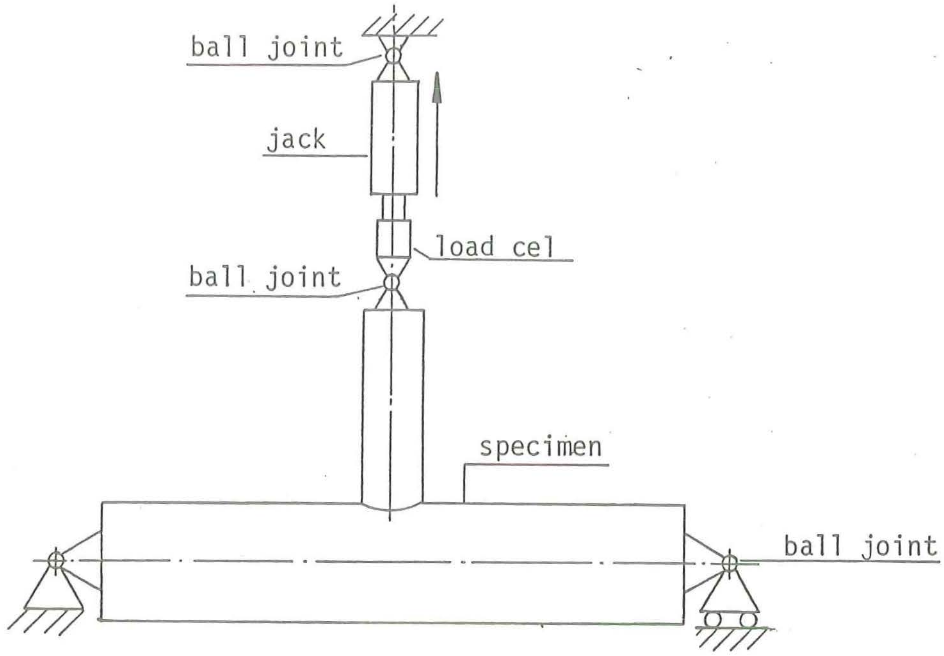

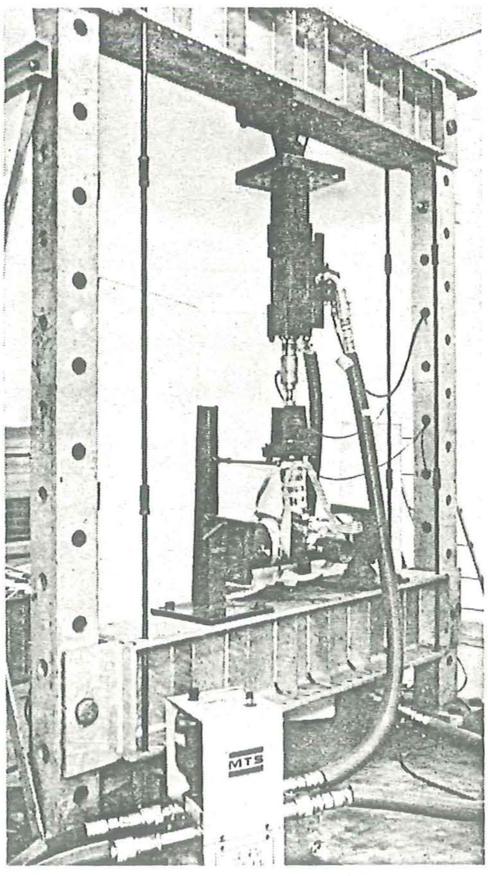

Fig.3.3.1 Test rig for Ø168.3 mm tubular T-joints (axially loaded)
(used for specimen 1 2 3 18 19 22 23)

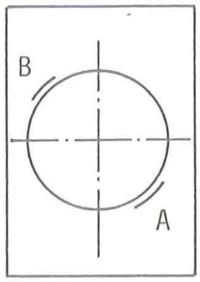

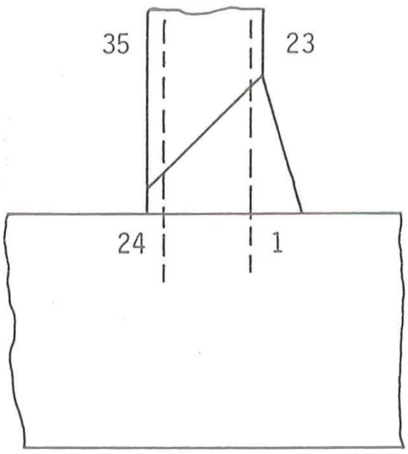

Cross-section A
(position 4-5 'o clock)

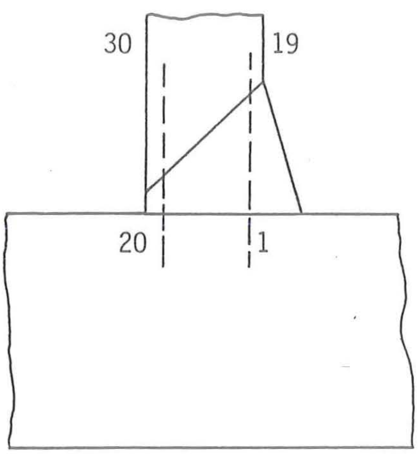

Cross-section B
(position 10-11 'o clock)

Fig.3.2.2 Location of the hardness measurements

0/24509	T.N.O. I.B.B.C.	TUBEPROGRAM EEG-SMOZ	T.H. STEVINLAB	TEST 41 (A)

O.L. = OPLASSEN
H. = HECHT } ZIE PROEF PIJP

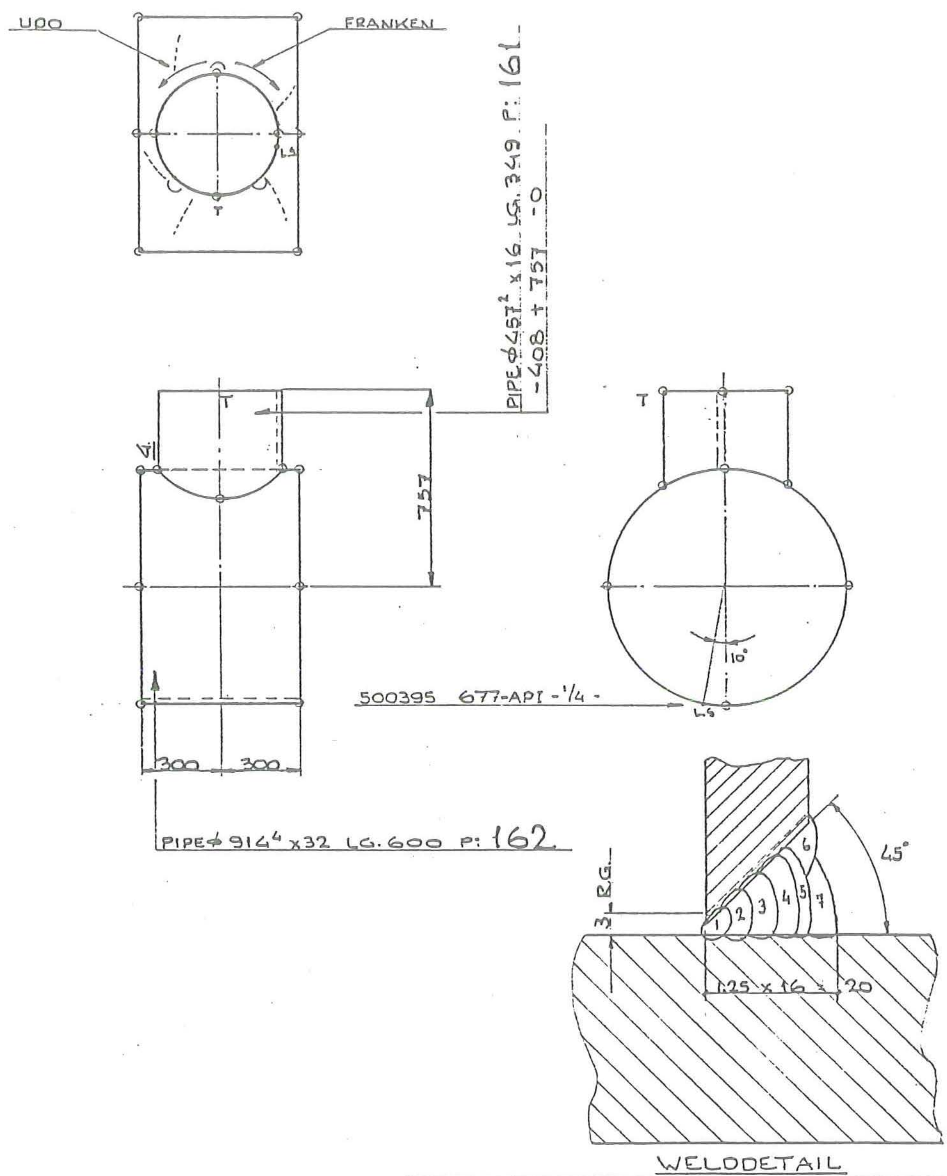

STAMP HEATNR. NEAR L.S. AT THE END OF THE PIPE	
MATERIAL QUALITY: B: C:	
CONNECTION: PIPE $\phi 457^2$ x 16 TO PIPE $\phi 914^4$ x 32	
METHOD OF WELDING: MANUAL	PREHEAT: 100°C

U.S. RESEARCH ACCORDING TO ASME VIII				POSITION 5G	WELDERNAME: FRANKEN / UDO
PASSNUMBER	ELECTRODE	AMP.	TEMP.	REMARKS	SYMBOLS
1	BH 100 2½	90	100°	25 ELECTRODES	o :LOCATION ℄ ON PIPE CIRCUMFERENCE
2	BH 100 3¼	115 - 130	100°	23 "	∩ :LOCATION TACKWELD
3	BH 100 3¼	115 - 130	100°	28 "	__ :LOCATION REPAIRWELD
4	BH 100 4	150 - 175	100°	26 "	... :LOCATION ARCSTRIKE OUTSIDE W. SEAM
5	BH 100 4	130	100°	12 "	L.S. :LONGITUDINAL SEAM (10° BESIDE ℄)
6	BH 100 3¼	115 - 125	100°	22 "	T. :TOP
7	BH 100 3¼	115 - 125	100°	25 "	B : BRACING C: CHORD

DE GROOT CONSTRUCTIE B.V. - ZWIJNDRECHT

Fig.3.2.1 Test specimen 41 : to check the weld procedure

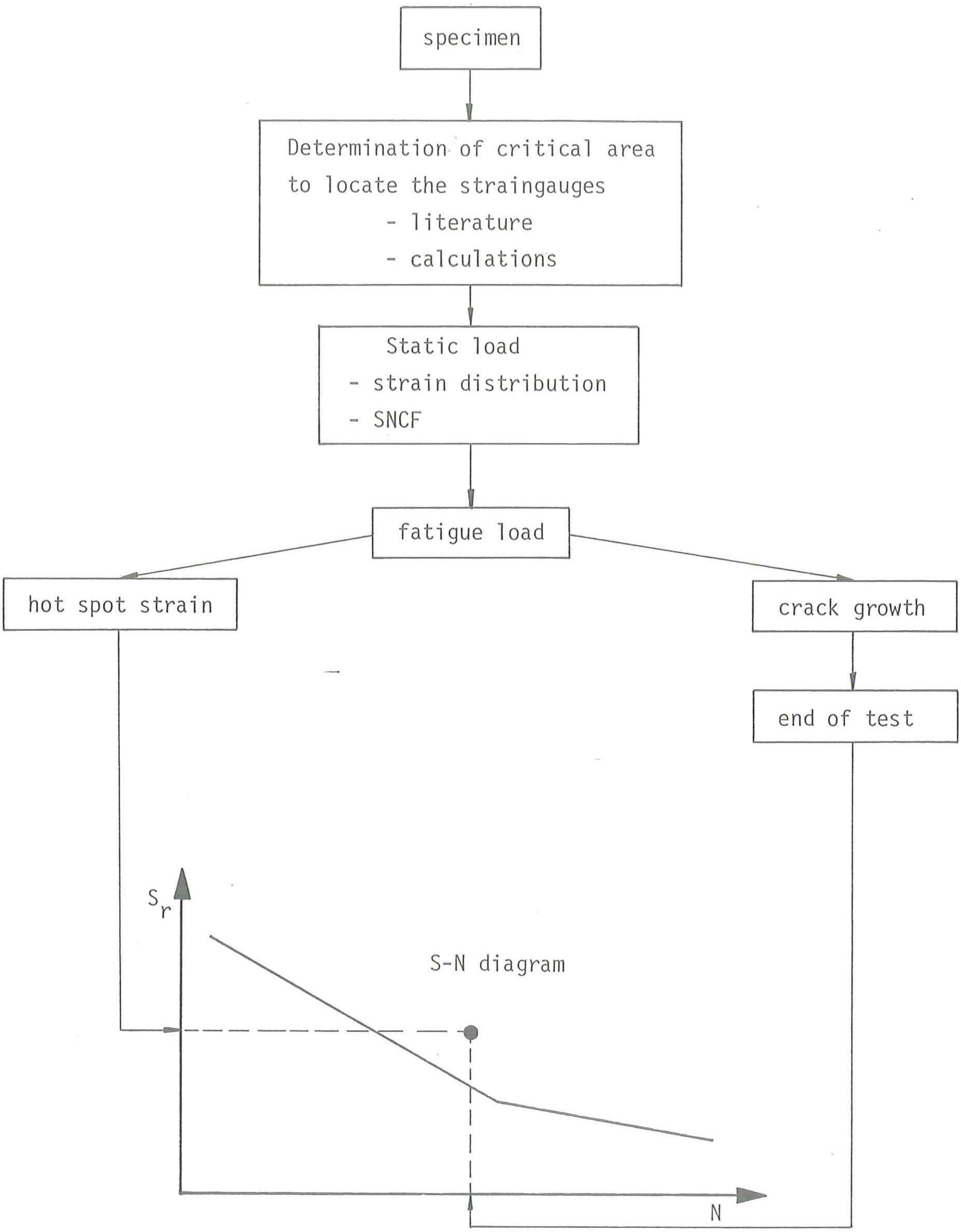

Fig.3.1.1 Test procedure

List of figures page

Table 3.4.5 Review of the test results

chord diam. mm	specimen nr	R	load range kN/Nm	test frequency Hz	nominal strain range 10^{-6}	SNCF extra-polated 1)	hot-spot strain range 10^{-6}	number of cycles to		
								ε_0 - 15% N1 ✱ 10^6	crack through N3 ✱ 10^6	end of test N4 ✱ 10^6
	1	0	84	10	464	4.8	2230	0.0125	0.06	0.063
	2	0	28	10	155	4.8	745	10.0	12.0	13.0
	3	0	50	10	276	4.8	1325	2.9	3.0	3.3
	18	0	35	10	193	4.5	870	1.2	3.0	3.6
168.3	19	0	80	10	442	4.5	1990	0.02	0.06	0.074
	22	0	45	10	249	4.3	1070	0.11	0.88	0.95
	23	0	32	10	177	4.3	760	1.7	2.0	2.4
	24 b	0	4000	10	1069	1.2	1285	0.31	0.33	0.37
	25 b	0	4500	10	1203	1.2	1445	0.43	0.47	0.48
	26 b	0	3150	10	841	1.2	1010	1.53	1.5	1.7
	4 c	-1	85	0.2	75	5.8	435	1.0	2.2	2.7
	5	0	160	4	141	5.8	818	0.35	0.68	0.82
	6	0	144	4	127	5.8	737	0.42	1.0	1.3
	7	0	144	4	127	5.8	737	0.44	0.84	1.1
	8	0	85	5	75	5.8	435	3.6	7.5	8.5
	9	0	160	4	141	5.8	818	0.32	0.76	1.0
	10 c	0	85	0.2	75	5.8	435	1.0	2.3	2.8
	11	-1	56	8	125	3.9	488	2.0	9.0	11.0
457.2	12	-1	110	5	245	3.9	956	0.35	0.7	0.91
	27	-1	600	2	129	3.0	387	3.1	16.0	19.0
	28	-1	1300	1.3	279	3.0	837	0.41	0.66	0.77
	29	-1	880	2	189	3.0	567	1.1	1.8	2.2
	30	-1	880	2	338	2.7	913	-	1.0	1.2
	31 r	-1	~	-	200 2)	2.7	540 2)	3.2 3)	6.5 3)	8.4 3)
	32 r	-1	~	-	254 2)	2.7	686 2)	1.7 3)	2.0 3)	4.0 3)
	33	-1	754	2	290	2.7	783	1.4	2.4	2.9
	36	-1	520	3	199	2.6	517	2,6	10.0	19.0
	37	-1	600	3	230	2.7	621	4.5	6.7	8.1
	38	-1	574	3	220	2.7	594	5.2	7.8	8.5
	13	0	270	2.8	58	6.4	370	1.9	4.1	5.0
	14	0	770	1.5	165	6.4	1055	0.05	0.15	0.17
	15	0	450	2.8	96	6.4	615	0.37	0.95	1.3
	16 cp	0	240	0.2	51	6.4	325	2.4	3.9	4.3
	17 c	0	240	0.2	51	6.4	325	1.2	3.7	4.3
914.4	20	0	600	2.5	129	6.7	865	0.15	0.41	0.68
	21	0	220	4	47	6.7	315	3.3	8.1	16.0
	34	0	160	6	34	9.5	323	3.8	12.0	14.0
	35	0	400	3	86	9.5	817	0.19	0.7	0.85
	39	0	150	6	32	9.8	314	5.5	20.0	26.0
	40	0	390	3	84	9.8	823	0.09	0.5	0.73

1) Average for each geometry

2) Strain of a comparable constant amplitude loading with the same RMS value as the applied random loading

3) Number of positive zero crossings

b = in plane bending   c = seawater test   r = random loading   cp = seawater test with cathodic protection

Specimen number	Joint type and way of loading (*)	D * T (mm)	α L/R	β r/R	γ R/T	τ t/T	measured average values		Calculated SCF		
							SNCF	SCF	Kuang KT Joint EPR (3.11)	Teyler Gibstein DNV (3.9)	Wordsworth Smedley Lloyds (3.12)
1 - 3	T - a	168.3 * 6.3	10	0.5	13.4	0.5	4.8	5.7	6.09	5.88	5.54
18 - 19	T_1- a						4.5	5.4	6.09	5.88	5.54
22 - 23	T_2- a						4.3	5.1	6.09	5.88	5.54
24 - 26	T - b						1.2	1.1	1.60	2.09	1.80
4 - 10	T - a	457.2 * 16	10	0.5	14.3	0.5	5.8	6.7	6.47	6.25	6.66
11 - 12	T - a			0.25		0.39	3.9	4.7	5.45	4.04	3.97
27 - 29	X - a			1		1	3.0	3.0	-	-	3.40
30 - 38	X - a			1		0.55	2.7	-	-	-	2.18
13 - 17	T - a	914.4 * 32	10	0.5	14.3	0.5	6.4	7.7	6.47	6.25	6.57
20 - 21	T_1- a						6.7	8.0	6.47	6.25	6.57
34 - 35	X - a						9.5	10.9	-	-	9.59
39 - 40	X_1- a						9.8	11.2	-	-	9.59

* a = axial load ; b = in plane bending

Table 3.4.4. Comparison of measured SNCF and SCF with SCF calculated from parameter formulae

Table 3.4.2 Various S-values used for design of tubular joints |3.2|

Type of joint	type of stress or strain range	corresponding design S-N curve
simple T, Y or K with complete joint penetration welds	nominal stress range in brace	AWS - D'
simple T, Y or K with partial joint penetration or complex joints with overlap, gussets or ring stiffeners	nominal stress range in brace	AWS - E'
simple K	punching shear range in chord	AWS - K
simple T and Y	punching shear range in chord	AWS - T
Any connection	hot spot stress or strain range at weld toe	AWS - X

Table 3.4.3 Some data of the calculated X-joints

Specimen number	D (mm)	T (mm)	d (mm)	t (mm)	β	τ	Calculated with program
24	914.4	32	457.2	16	0.5	0.5	SATE + ASKA
30	457.2	16	457.2	8.8	1.0	0.55	SATE
27	457.2	16	457.2	16	1.0	1.0	SATE

Table 3.4.1 Comparison of strain distributions

test specimen	Figure number	Interesting parameter	Remarks
1, 5 and 13 18 and 21	3.4.1, 2 and 4 3.4.5 and 6	- scale	In general good correlation; in neighbourhood of weld some difference due to not on scale weldsizes.
1 and 18 13 and 21 35 and 40	3.4.1 and 5 3.4.4 and 6 3.4.11 and 12	-additional unloaded brace	At side without additional brace no difference
18 and 23	3.4.5 and 7	-additional second unloaded brace	At side with first additional brace no difference
5 and 11	3.4.2 and 3	diameter- and wallthickness ratio	
28 and 30	3.4.9 and 10	wallthickness ratio	On line 4 (chord) SNCF proportional with τ

Table 3.2.6 Hardness measurements over two weld cross sections

a) Cross section A (4-5 o clock position)

Position	Hardness HV 70	Average
pipe mat. Ø 914 1-3	181, 190, 181	184
HAZ Ø 914 4-6	187, 187, 187	187
weld material 7-17	184,181,181,184,181,187,181,179 173,179,187	182
HAZ Ø 457 18-20	314, 281, 256	284
pipe mat. Ø 457 21-23	220, 206, 206	211
pipe mat. Ø 914 24-25	183, 181	182
HAZ Ø 914 26	203	203
weld material 27-30	212, 206, 200, 200	205
HAZ Ø 457 31-33	227, 227, 224	226
pipe mat. Ø 457 34-35	200, 207	204

b) cross section B (10-11 o clock position)

Position	Hardness HV 10	Average
pipe mat. Ø 914 1-4	193, 190, 184, 184	188
HAZ Ø 914 5-6	196, 193	195
weld material 7-15	186,184,182,190,196,199,206,213,212	196
HAZ Ø 457 16	274	274
pipe mat. Ø 457 17-19	202, 209, 199	203
pipe mat. Ø 914 20-21	193, 196	195
HAZ Ø 914 22	251	251
weld material 23-24	209, 224	217
HAZ Ø 457 25-27	254, 251, 237	247
pipe mat. Ø 457 28-30	224, 209, 215	216

Table 3.2.4 Chemical composition of tube material

Tube size D - T (mm)	C %	S_i %	M_n %	S %	P %	Al %
88.9 - 3.2	0.16	0.25	1.22	0.014	0.021	0.033
114.3 - 6.3	0.18	0.44	1.26	0.020	0.016	
168.3 - 6.3	0.22	0.30	1.25	0.012	0.019	
219.1 - 8.2	0.20	0.18	1.15	0.020	0.010	
457.2 - 8.7	0.14	0.30	1.29	0.014	0.020	0.041
457.2 - 15.9	0.25	0.37	1.14	0.028	0.015	
914.4 - 31.7	0.15	0.38	1.29	0.010	0.011	0.027

Table 3.2.5 Charpy V test results on test specimen nr. 41

Location of test specimen	average value of three specimens (Joule)
weld metal	77 98
fusion line	31 80
heat effected zone	29 40

Table 3.2.2b Material standard

Tube size D - T (mm)	Standard
88.9 - 3.2	DIN 2457/1629 St 52
114.3 - 6.3	DIN 2448/1629 St 52
168.3 - 6.3	BS 4350 Grade 50 C
219.1 - 8.2	API - 5LX Grade X 52
457.2 - 8.7	API - 5LX Grade X 60
457.2 - 15.9	API - 5LX Grade X 52
914.4 - 31.7	API - 5LX Grade X 52

Table 3.2.3 Mechanical properties of tube material

tube size D - T (mm)	yield stress (N/mm^2)	tensile strength (N/mm^2)	elongation %
88.9 - 3.2	360	518	30.6
114.3 - 6.3	420	590	26.1
168.3 - 6.3	426	563	30.0
219.1 - 8.2	360	520	30.0
457.2 - 8.7	482	580	25.1
457.2 - 15.9	394	603	37.0
914.4 - 31.7	366	532	38.0

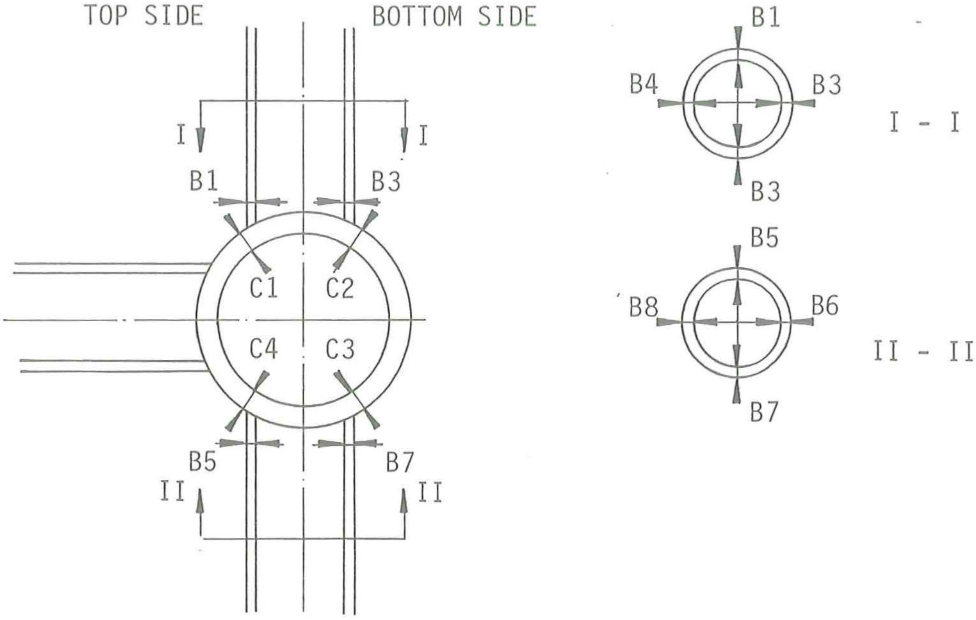

POSITION		TEST SPECIMEN 34	35	39	40
CHORD	C1	31.5	31.8	31.7	
	C2	31.7	31.7	31.9	
	C3	31.6	31.8	31.7	
	C4	31.5	31.5	31.9	
BRACE	B1	15.7	18.3	17.8	
	B2	17.7	18.0	18.4	
	B3	17.5	16.9	17.1	
	B4	18.2	17.4	16.4	
	B5	17.3	18.0	17.1	
	B6	16.6	17.0	17.0	
	B7	18.0	17.6	17.4	
	B8	18.1	17.7	17.2	

Table 3.2.2a Actual dimensions of the wall thickness of the tubes

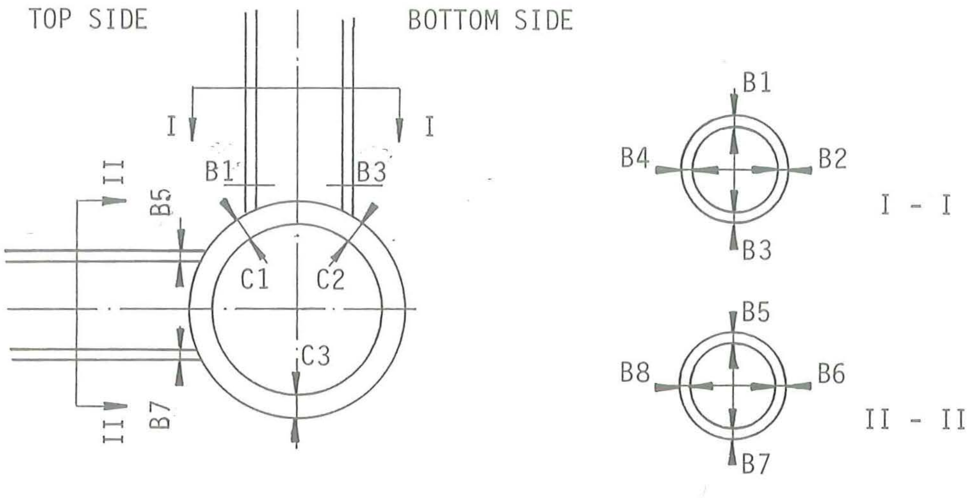

POSITION		TEST SPECIMEN 13	14	15	16	17	20	21
CHORD	C1	32.0		32.0	31.5	31.9	31.7	31.8
	C2	32.0		31.7	31.5	31.8	31.8	31.9
	C3				31.6	31.9		
BRACE	B1	17.4		16.6	16.8	17.0	17.1	16.6
	B2	17.8		17.0	16.8	16.5	17.2	16.9
	B3	16.8		17.3	16.9	16.6	17.4	17.9
	B4	17.6		17.1	16.7	16.7	17.0	17.9
	B5							17.0
	B6							17.1
	B7							
	B8							17.2

Table 3.2.2a Actual dimensions of the wall thickness of the tubes

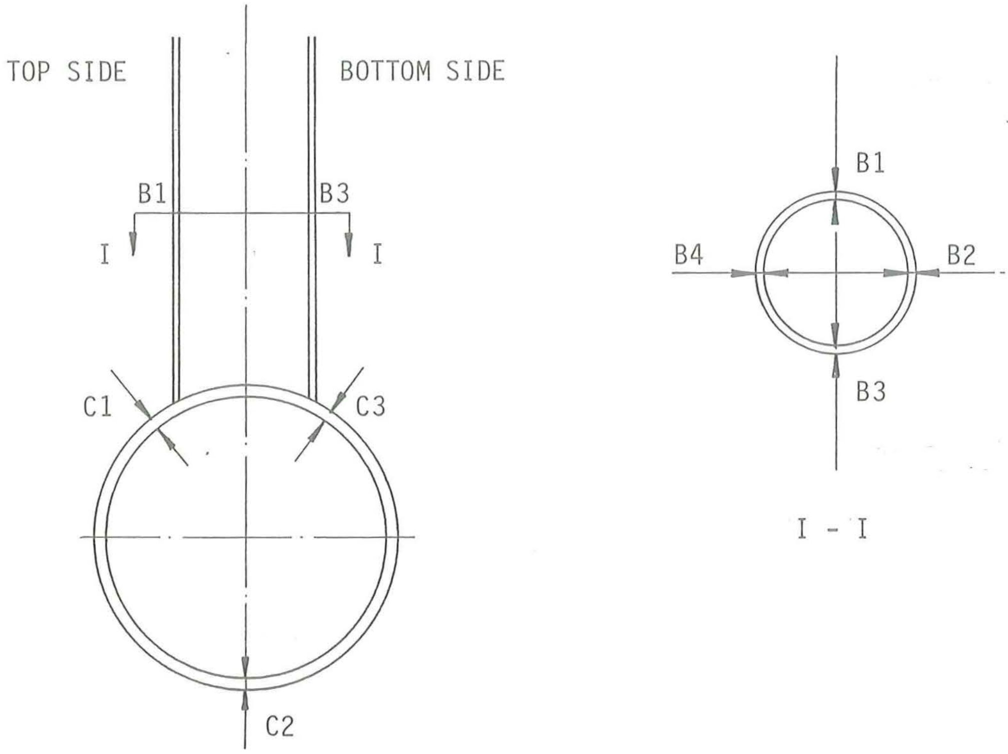

POSITION		TEST SPECIMEN								
		4	5	6	7	8	9	10	11	12
CHORD	C1	16.8	16.6	17.2	16.0	16.0	16.0	16.2	17.8	16.8
	C2	16.4	16.0	16.6	17.2	16.0	18.0	16.8	16.4	16.0
	C3	16.8	16.2	17.7	15.9	17.3	15.8	16.4	16.0	18.0
BRACE	B1	7.6	7.7	8.2	8.8	8.1	8.5	7.6	6.6	6.6
	B2	7.6	7.6	8.2	9.0	8.5	8.6	7.8	6.4	6.2
	B3	7.6	7.6	8.0	8.6	8.6	8.1	7.4	6.4	6.4
	B4	7.2	7.2	7.5	8.6	8.4	8.2	8.0	6.4	6.4

Table 3.2.2a Actual dimensions of the wall thickness of the tubes

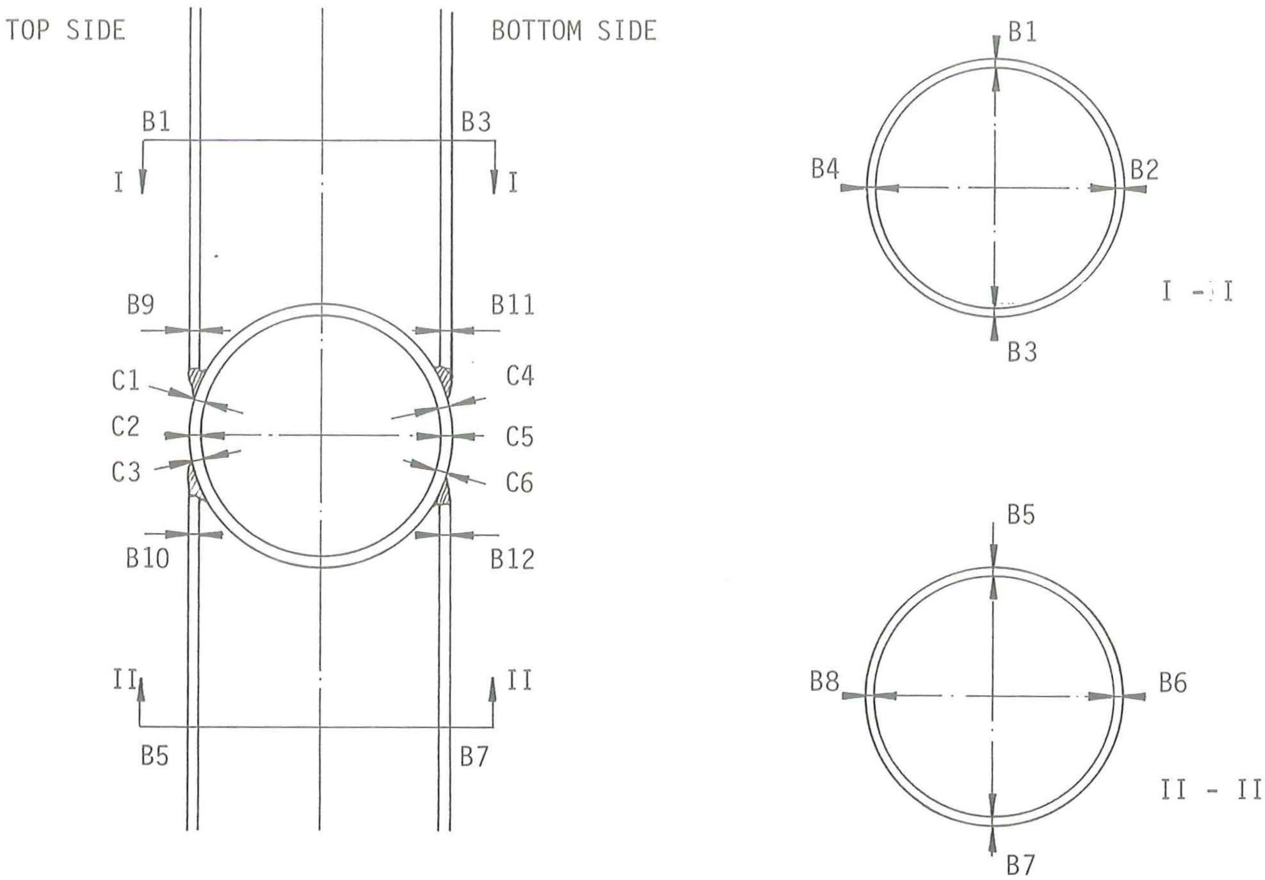

	POSITION	TEST SPECIMEN									
		27	28	29	30	31	32	33	36	37	38
CHORD	C1	16.4	18.0	17.8	17.0	17.2	15.6	18.4	17.2	16.6	17.0
	C2	16.2	18.2	17.8	16.8	18.4	15.6	18.0	17.2	16.6	17.4
	C3	16.4	18.2	18.0	16.8	17.4	16.0	18.0	16.8	16.8	17.2
	C4	16.2	18.4	17.2	16.2	17.2	17.4	16.0	17.0	17.0	17.4
	C5	17.2	18.2	16.8	16.4	16.6	18.0	16.8	16.8	17.2	17.4
	C6	16.4	18.6	17.2	16.4	17.0	18.0	16.0	16.8	17.2	17.2
BRACE	B1	16.8	17.2	18.0	8.4	8.7	8.4	8.2	8.4	8.0	8.6
	B2	17.2	16.4	17.6	8.4	9.2	8.3	8.2	8.2	8.4	8.8
	B3	17.0	16.8	18.8	8.4	8.6	8.4	8.2	8.4	8.4	8.8
	B4	17.0	17.2	18.0	8.4	9.6	8.4	8.4	8.4	8.3	8.8
	B5	16.4	18.2	16.6	8.4	8.6	8.6	8.4	8.4	8.8	8.6
	B6	16.0	16.4	16.4	8.2	8.8	8.4	8.2	8.4	8.7	8.6
	B7	16.4	17.6	16.8	8.2	8.8	8.4	8.4	8.6	8.7	8.8
	B8	16.0	16.0	18.0	8.4	8.8	8.6	8.6	8.4	8.4	8.6
	B9	16.4	17.0	15.6	8.4	8.8	8.4	8.2	8.8	8.6	8.6
	B10	15.8	17.4	17.2	8.8	8.8	8.6	8.4	8.8	8.6	8.4
	B11	17.6	16,8	16.4	8.4	8.4	8.2	8.4	8.4	8.6	9.2
	B12	16.4	18.6	16.4	9.0	8.4	8.4	8.8	8.4	8.3	8.6

Table 3.2.2a Actual dimensions of the wall thickness of the tubes

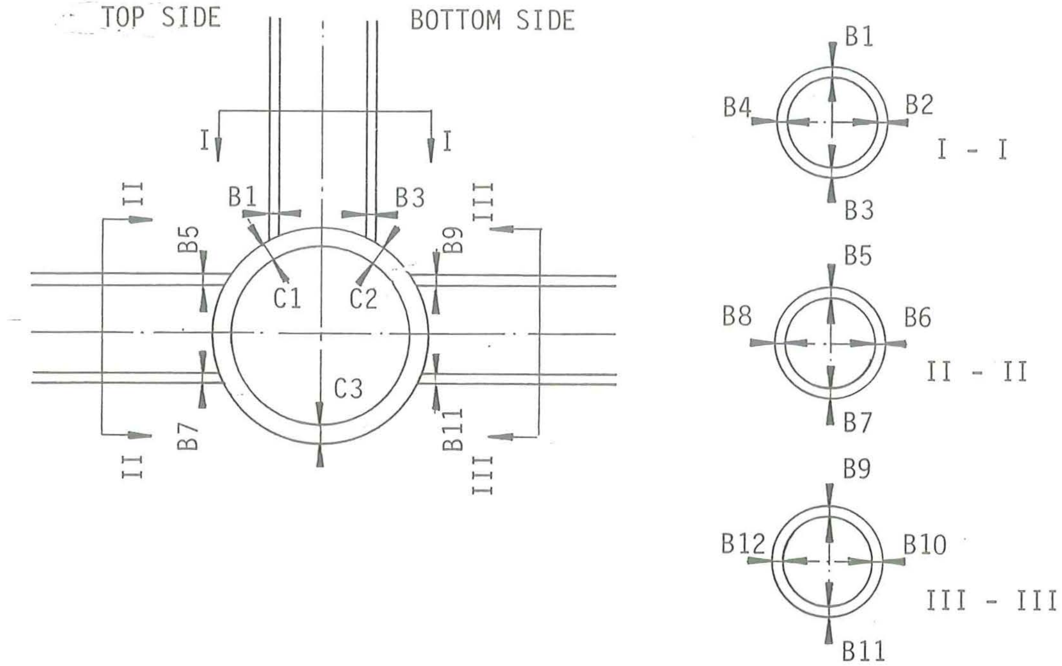

POSITION		TEST SPECIMEN									
		1	2	3	18	19	22	23	24	25	26
CHORD	C1	6.2	6.1	6.1	6.1	6.1	6.1	6.2	6.3	6.2	6.1
	C2	6.1	6.1	6.1	6.1	6.0	6.1	6.3	6.2	6.2	6.2
	C3	6.1	6.2	6.2	6.0	6.1	6.0	6.0	6.3	6.2	6.2
BRACE	B1	3.1	3.2	3.1	3.1	3.1	3.0	3.2	3.3	3.4	3.3
	B2	3.3	3.1	3.1	3.2	3.2	3.2	2.8	3.0	3.2	3.1
	B3	2.9	3.1	3.2	3.1	3.0	3.1	3.1	3.2	3.2	3.4
	B4	3.1	3.2	3.3	3.1	3.3	3.3	3.0	3.1	3.1	3.0
	B5				3.3	3.2	3.3	3.0			
	B6				3.0	3.0	3.2	3.1			
	B7				3.2	3.1	3.2	3.1			
	B8				3.1	3.1	3.2	3.1			
	B9						4.4	3.2			
	B10						3.2	3.1			
	B11						3.2	3.2			
	B12						3.1	3.1			

Table 3.2.2a Actual dimensions of the wall thickness of the tubes

TABLE 3.2.1 Review of test program

joint type	D-T	168-63	457-16					914-32	way of loading
	β	0.5	1	1	0.5		0.25	0.5	
	τ	0.5	1	0.5	0.5		0.39	0.5	
	R	0	−1	−1	0	−1	−1	0	
T		1 2 3			5 6 7 8 9 10^{c}	4^{c}	11 12	13 14 15 16^{cp} 17^{c}	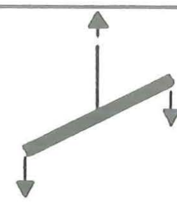
T_1		18 19						20 21	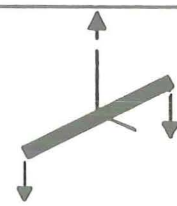
T_2		22 23							
T		24 25 26							
X			27 28 29	30 31^{r} 32^{r} 33 37 38				34 35	
X				36					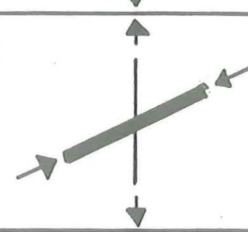
X_1								39 40	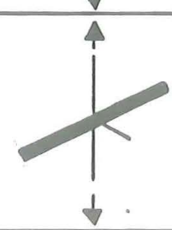

c = seawater tests

r = random tests

cp= cathodic protection

List of tables

3.11 Teyler, R. Gibstein, M., Bjørnstad, H. and Haugan, G.: 'Parametrical stress Analysis of T-joints' Technical report 77-253, Det Norske Veritas, Oslo, November 1977.

3.12 Smedley, G.P.: 'Peak Strains at Tubular Joints'. Ocean Engineering Working Party Seminar on Corrosion and Fatigue in Offshore Installations, Institution of Mechanical Engineering, September 1977

3.13 Kuang, J.G., Potvin, A.B., and Leick, R.D.: 'Stress Concentration in Tubular joints', Paper OTC 2205 presented at Seventh Annual Offshore Technology Conference, Houston, Tex., May 6-8, 1975.

3.14 Gurney, T.R.: 'The influence of thickness on the fatigue strength of welded joints', BOSS Conference 1979, London.

3.15 Kuiper, J.S.: Analyse van het spannings- rekverloop in een X-knooppunt van stalen buizen d.m.v. model onderzoek en computer similatie. Delft University of Technology, Stevinrapport no. 6-81-17

References

3.1 Strain measurements in tubular joints.
StuPOC report (in Dutch, to be published)

3.2 AWS Structural Welding Code, AWS D1.1-80

3.3 Offshore Installations: Guidance on design and construction, U.K. Department of Energy.

3.4 Marshall, P.W.: 'A review of stress concentration factor in tubular connections' CE-32 Report Shell Oil Company, April 1978.

3.5 Van Delft, D.R.V.: "A two dimensional analysis of the stresses at the vicinity of the weld toes of welded tubular joints". Stevin Report nr. 6-81-8, Delft University of Technology.

3.6 Wordsworth, A.C. and Smedley, G.P. 'Stress Concentration at unstiffened Tubular Joints' Paper 31 of the 'European Offshore Steel Research' Select seminar, November 1978, Cambridge.

3.7 Bovendeur W., 'Finite-element analysis of three unstiffened tubular X-joints for TNO-IBBC' KSEPL, Technical Service Report RKTR 0086.78, june 1978.

3.8 Janssen, G.T.M. and Meyer, G.J.: 'Marien Technological Research regarding Investigations in the Field of the Lifetime of Offshore structures (MaTS 21-2) - Finite Element Calculations - first phase 'TNO-IWECO report nr. 5061031-79-1, October 1979 (in Dutch).

3.9 Dijkstra, O.D., Hartog, J. and Wardenier, J. 'Stress Concentration factors in Tubular Joints', Stevin report nr. 6-77-10, IBBC-TNO report nr. BI-77-58/05.3.31315, Delft, The Netherlands.

3.10 Dijkstra, O.D., and Hartog, J. 'Dutch part of the large scale tubular joint fatigue test program' Paper 35 of the 'European Offshore Steel Research' Select Seminar, November 1978, Cambridge.

3.5 General conclusions of the tubular joint tests

The conclusions of these tests are:

a) There is a scale effect. The fatigue life decreases with increasing joint size.

b) Some results of the large specimens (Ø 914 mm) fall below the AWS-X curve.

c) The hot spot strain range is a better parameter for fatigue than the punching shear range

d) Seawater has a detrimental effect on the lifetime. It reduces the lifetime by a factor of 2.5-3. Cathodic protection had no favourable effect on the lifetime of one tested large T-joint.

e) Finite element calculations give a good prediction of the strain distribution in the tested joint.

f) The SCF determined with recent published parameter formulas give a good correlation with the measured SCF in the tested joints, except for X-joints with $\beta = 1$ and $\tau = 0.5$.

3.4.10 General discussion of the fatigue results

Scale effect

As mentioned before, the influence of the joint size can be seen in fig. 3.4.40 and 3.4.44. The decreasing fatigue strength with increasing joint dimensions are not only noticeable in tubular joints, but also in flat plate specimens |3.14|. With fracture mechanics it can be shown that a crack in a thin plate will grow slower than in a thick plate. This faster crack growth results in a shorter fatigue life for the thicker plate. It seems reasonable to expect a similar phenomenon for tubular joints. But a fracture mechanics crack growth model for tubular joints is not available at the moment.

Joint geometry and loading effect

In the S-N diagrams based on punching shear, there is a clear geometry and a clear loading effect. Compare e.g. the ø 168 T-a and T-b specimens (fig. 3.4.37); ø 457 T and X specimens (fig. 3.4.38); or the ø 914 T and X specimens (fig. 3.4.40). This difference is understandable, because of the very approximate parameter used for the stress range. The calculated punching shear stress does not take the complete behaviour of the joint (stress or strain distribution) into account.
In the hot spot strain determination, the joint geometry and the loading condition is taken into account. The difference in fatigue strength between the small specimen in bending and the axial loaded specimen disappeared. The difference between the large T- and X-joints disappeared also and the difference between the medium size T- and X-joints diminished. The remaining difference in the fatigue strength with the X-joints is proba- probably due to the more complex crack growth pattern in the X-joints.

Scatter

Each of the three joint sizes has a different scatter. For the small ones the difference between the 95 % and 50 % survival line is about a factor of 5. For the medium and large ones this is 3.5 and 2 respectively.

3.4.9.2 Random tests

Two joints are tested with a random loading (nr. 31 and 32) The random loading was achieved in a digital way, using a pseudo random binary sequence generator.
A digital filter technique was used to shape a narrow band power spectrum, with a freguency of 3 ± 1/8 Hz.
The generator and filter were implemented as programmes in a computer.
The signal had a Gaussian probability density-function and the distribution function of the amplitude was a Rayleigh distribution.
The crest factor for these tests was 4.35.
The random test results are plotted on the strain level of a constant amplitude test with the same RMS-value.
Therefore: $\varepsilon_{range} = \frac{2\,\varepsilon\,(RMS)}{0.707}$

For the number of cycles N the number of positive zero crossings has been used.
The results of the tests fit well into into the test results of the constant amplitude test.

3.4.9.3 Biaxial test

Test specimen 36 (X-joint, $\beta = 1.0$ and $\tau = 0.55$) was tested with both chord and brace loaded. The chord loading was out of phase with the brace loading Although the crack growth started relatively early, the number of cycles to end of test was significantly higher than those for other joints of the same geometry (see fig. 3.4.48).
During the last part of the testing, the crack growth rate diminished. At that moment a very large crack had already developed in the joint.

N_1 = 15 % change in strain range
N_2 = first visible crack
N_3 = through crack
N_4 = end of test.
See also fig. 3.4.36.

From fig. 3.4.45 to 48, the results are plotted with N_1, N_3 and N_4 on the vertical axis. In these figures the ratio's between N_1, N_3 and N_4 as mentioned in 3.4.6.1 are indicated.

3.4.9 Influence of special test conditions

3.4.9.1 Corrosion tests

Four tests were carried out in artificial seawater (nr. 4, 10, 16 and 17). One of them was cathodically protected (nr. 16). The seawater conditions are mentioned in 3.3.2. The test frequency was o.2 Hz.
The fatigue life of the medium sized specimens, tested in seawater (nr. 4 and 10) was only 30 % of the life of the same specimens tested in air. The fatigue life of the large specimens tested in seawater was 40 % of the life of the same specimens tested in air. There was no difference in fatigue life between the cathodically protected specimen and the unprotected one.
But there was a different in behaviour of the protected specimen compared to the unprotected one. This can be illustrated in fig. 3.4.49. In this figure the drop in strain range of a specimen tested in air (nr. 13), the cathodically protected specimen (nr. 16) and the specimen with free corrosion (nr. 17) are given. On the horizontal axis the ratio of the number of cycles to end of test for an air test is given. The free corrosion specimen compared with the air test gives a similar behaviour in a shorter time. The cathodically protected specimen gives a later start of the crack growth, but the crack grows faster. So in the end there is no difference in lifetime.

- All results of tests in air fall above the AWS-X curve
- The seawater tests fall just on the AWS-X-MODIFIED curves.
- The geometry has an influence. The T-joints with $\beta = \tau = 0.5$ and the X-joints with $\beta = \tau = 1$ fall in one scatter band and the T-joints with $\beta = 0.25$ and $\tau = 0.39$ and the X-joints with $\beta = 1$ and $\tau = 0.5$ fall in another, higher, scatter band.

Comparing this figure with fig. 3.4.38 we come to the following additional conclusions:
- The 'margin of safety' between test results and design curve is greater by the punching shear presentation compared with the hot spot strain presentation.
- Less scatter in all the results in the hot spot strain presentation indicates that the hot spot strain range is a better parameter for fatigue than the punching shear range.

The results from the <u>large sized joints</u> are plotted in fig. 3.4.43. The conclusions are:
- One result of the air tests falls below the AWS-X-MODIFIED curve and some results fall below the AWS-X curve.
- The seawater tests fall below the AWS-X curve
- The X-and T-joints fall in one scatter band.

Comparing this figure with fig. 3.4.39 we come to the following additional conclusion:
- less scatter in all the results in the hot spot strain presentation indicates that the hot spot strain range is a better parameter for fatigue than the punching shear range.

The results of the <u>simple T-joints</u> with the same geometry ($\beta = 0.5$ and $\tau = 0.5$) but different sizes are given in fig. 3.4.44. This figure again shows the size effect as in fig. 3.4.40. Due to a somewhat lower SNCF for a smaller joint (see table 3.4.4) the size effect is slightly reduced but it is still very significant.

3.4.8.4 S-N plots to various failure criteria

The WG III has decided to distinguish four different criteria viz:

The results of the large joints are plotted in fig. 3.4.39 Again the X-joints are also plotted.
The conclusions are:

- Some results of the X-joints fall below the AWS-T curve.
- The life-time of the seawater tests is 40 % of the life-time of the same specimens in air.
- There is no difference in life-time in the cathodic protected specimen (nr. 16) and the non protected one (nr. 17).
- The geometry has an influence. The results of the T-joints fall above the results of the X-joints.

The results of the simple T-joints with a comparable geometry $\beta = 0.5$ and $\tau = 0.5$ but different sizes are given in fig. 3.4.40. This figure clearly shows the influence of the joint size. The life-time decreases with increasing joint size,

3.4.8.3 S-N plots based on hot spot strain range

The hot spot strain range is calculated according to 3.4.3. The results of the small joints are plotted in fig. 3.4.41. The corresponding AWS-X curve is also given in the same figure. The conclusions are:

- All results fall above the AWS-X curve.
- The specimens loaded with in plane bending fall in the scatter band of the axially loaded specimens.

Comparing this figure with fig. 3.4.37 we come to the following additional conclusions:

- The 'margin of safety' between test results and design curve is greater by the punching shear presentation compared with the hot spot strain presentation.
- The different location of the bending moment results relative to the axially loaded results indicates that the hot spot strain range is a better parameter for fatigue than the punching shear range.

The results of the medium sized joints are plotted in fig. 3.4.42 The conclusions are:

3.4.8 S-N plots of the results

3.4.8.1 General

In 3.4.3 and 3.4.7 some general remarks were made about the possible value on the axis of an S-N curve. In the next chapter, we are showing S-N curves with punching shear- or hot spot strain range on the vertical axis. On the horizontal axis, one of the following failure criteria is used: 15% change in strain range, through crack or end of test.
Table 3.4.5. gives a review of the test results.

3.4.8.2 S-N plots based on punching shear range

The punching shear range is calculated according to the Structural Welding Code of the American Welding Society|3.2|.
The results of the small joints are plotted in fig. 3.4.37. The corresponding A.W.S.-T curve is also given in the same figure. The conclusions from this figure are:
- All results fall above the AWS-T curve
- The specimens loaded with in plane bending fall above the scatter band of the axially loaded specimens.

The results of the medium sized joints are plotted in fig. 3.4.38. The X-joints are also plotted, although they are not mentioned in the AWS code as joints which can be plotted with punching shear.
The conclusions form this figure are:
- All results fall above the AWS-T curve
- The life-time of the two seawater tests is 30 % of the life-time of the same specimens in air.
- There is no significant influence of the R-ratio on the seawater tests (one was tested with R = 0 and the other with R = -1).
- Geometry has an influence. The T-joint with β and τ ratio of 0.5 give the lowest results. The results of the T-joints with β = 0.25 and τ = 0.39 are somewhat higher, while the X-joints give the highest results.

b) A drop in strain range at the hot spot

This failure criterion can be used by laboratory specimens which are gauged. The use of this in practice is not so easy. In the WG III discussions a 15 % drop in strain range was mentioned.

c) A specified crack length or depth

Taking something like this as failure criterion looks reasonable. However the difficulty is to decide on the specified dimension.

d) A through crack

After a through crack the behaviour of the joint changes relatively rapid. A through crack occurs in a late stage of the test and is unambiguous to determine. Therefore this looks like a reasonable criterion.

e) A decrease in stiffness

When its stiffness decreases, a joint in a redundent structure will not carry its load anymore. So the joint is not performing its function anymore. Therefore this looks like a reasonable criterion.

f) A total seperation of brace and chord

Total separation of chord and brace was never reached in the tests. This was done for practical reasons, because when a long crack was in the joints the displacements increases and therefore the frequency has to be slowed down to maintain the load. So it is expected that from a large crack to a complete separation takes a lot of time. But this criterion does not look reasonable, because long before one would say that a joint with such a large crack has already failed long before.

We consider our tests are carried out far enough to cover any reasonable failure criterion. And the description of the tests is sufficient to determine any failure criteria chosen. In the next chapter we will plot the results against various failure criteria on the horizontal axis.